Characterising mutant Cyclin F in the development of Amyotrophic Lateral Sclerosis

Stephanie Rayner

Department of Chemistry and Biomolecular Sciences,

Macquarie University

A thesis in partial fulfilment of the Master of Research degree

Supervisor: *Associate Professor Mark Molloy*

Associate Supervisor: *Professor Roger Chung*

10th of October 2014

Abstract

Amyotrophic lateral sclerosis is a relentless neurodegenerative disease typically leading to death of patients within 5 years from onset. Recently, several ALS-causing gene mutations in *CCNF*, the gene encoding Cyclin F have been identified. We have focused on the substitution from serine to glycine at amino acid 621 and show that the mutation affects the functionality of the ubiquitin ligase, $SCF^{Cyclin\ F}$. Specifically, the mutation impacts proteostasis of a known substrate, RRM2 (ribonucleotide reductase family member 2). Although the abundance of RRM2 is not affected, there is increasing abundance of ubiquitinated RRM2 in transfected Neuro-2A cells after 24 hours post-transfection. Using a label-free proteomic workflow, a total of 60 differentially expressed proteins were associated with mutant Cyclin F-mCherry expressing cells after 8 and 24 hours post-transfection. Many changes are functionally involved in protein translation and RNA processing, which is consistent with ALS pathogenesis. Using a workflow consisting of SDS-PAGE and LC-MS/MS we also obtained protein aggregate profiles that are linked to the mutation in Neuro-2A cells under heat-stress. Notably, Septin 2 was increasingly insoluble in association with mutant Cyclin F. This is a strong candidate for validation studies, as it is known to form insoluble aggregates within Parkinsonism models.

Declaration

The content of this thesis is original and does not contain material written by another individual, unless a reference to another work has been cited. Effort has also been taken to acknowledge the contribution of others to this work.

Stephanie Rayner

Acknowledgements

Firstly, I would like to thank my supervisors, Associate Professor Mark Molloy and Professor Roger Chung. I am thankful for the opportunity to have worked with both of these great supervisors and I appreciate all the guidance, patience and support they have given me through another challenging but worthwhile year.

I consider myself lucky to have worked within the Molloy and Chung research groups and am so grateful for the mentoring I have received from Dr. Albert Lee this year. I would not have learned so much without his guidance.

I would also like to thank everyone in the Molloy and Chung research groups as they have all given me constant support and great advice along the way. I enjoyed working in CBMS and ASAM laboratories, as they were such different environments. Both provided a unique and comfortable environment to work in.

Finally, I would like to thank my family and friends. I am grateful for all the support and encouragement I have received from my parents and I am lucky to have friends and family who supported me each step of the way.

Table of Contents

1 Introduction 1
1.1 Amyotrophic lateral sclerosis and Frontotemporal dementia 1
1.2 Causes of ALS and FTD 1
1.3 Converging mechanisms leading to aggregation 2
1.4 Impairments to RNA processing 2
1.5 Protein quality control systems 4
1.5.1 Degradation machinery 4
1.5.2 Ubiquitin-conjugation systems 5
1.6 Linking ALS pathology to neurodegeneration and dysfunction 8
1.7 Prion-like spread of neurodegenerative diseases 9
1.8 Proteomic studies of co-aggregating proteins in ALS 10
1.9 Aims 12
1.10 Significance 12
2 Methods 13
2.1 Cell culture 13
2.2 DNA purification and cell transfections 13
2.3 Flow cytometry 13
2.4 Cell Harvesting and preparation for analysis 13
2.4.1 Preparing whole cell lysates 14
2.4.2 Subcellular fractionation 14
2.4.3 Isolating aggregates 14
2.5 Western blot analysis 15
2.6 Preparing samples for mass spectrometry 15
2.7 Trypsin digestion 15
2.7.1 In-solution digestion for total cell lysates 15
2.7.2 In-gel digestion for urea-soluble lysate fractions 16
2.8 Sample Purification after in-solution digestion 16
2.9 Mass Spectrometry 16
2.10 Database searching 17
2.11 Criteria for protein identification 17
2.12 Statistical analysis 17
3 Results 18
3.1 Cyclin F-mCherry expression in neuron-like cells 18

3.2 The ratio of Cyclin F to RRM2 was altered in mutant Cyclin F cells 19
3.3 Cyclin F abundance correlated with changes in RRM2 and TDP-43 20
3.3.1 Mutant Cyclin F was processed differently to wild type Cylin F 20
3.3.2 TDP-43 and RRM2 levels were constant in the nucleus but not in the cytoplasm .. 22
3.3.3 RRM2 levels decreased with expression of Cyclin F 22
3.3.4 TDP-43 abundance increased with the expression of Cyclin F 22
3.4 Proteomic characterisation of mutant Cyclin F 23
3.4.1 Differentially expressed proteins in association with mutant Cyclin F 25
3.4.2 Functional annotations and enrichments 28
3.4.3 Urea-soluble fractions of lysates contained TDP-43 29
3.4.4 Functional analysis of enriched urea-soluble proteins 33
4 Discussion 38
4.1 Implications of Cyclin F-mCherry expression 38
4.2 Cyclin F expression only correlated with RRM2 expression in the cytoplasm 39
4.3 TDP-43 did not translocate into the nucleus or become increasingly insoluble in mutant Cyclin F expressing cells 41
4.4 Investigating the proteome associated with wild type and mutant Cyclin F expression 42
4.5 RNA processing and protein translation were affected in mutant Cyclin F transfected cells 43
4.5.1 Insight into RNA processing and protein translation provided by differential expression studies 43
4.5.2 Insight into translational control provided by proteins enriched in urea-soluble fractions 44
4.6 Several components of the ubiquitin-proteasome pathway are regulated by mutant Cyclin F 45
4.6.1 Insight into altered proteostasis networks provided by differential expression studies 45
4.6.2 Insight into altered proteostasis networks provided by proteins enriched in urea-soluble fractions 45
4.7 Chaperones were not enriched in mutant Cyclin F expressing cells 47
4.7.1 Insight into chaperone function provided by differential expression studies 48
4.7.2 Insight into chaperone function provided by proteins enriched in urea-soluble fractions 48
4.7.3 Proteasome and chaperone function in urea-soluble fractions 48

4.8 Changes to mitochondrial energy metabolism 49
4.8.1 Insight into altered energy metabolism provided by differential expression studies 49
4.8.2 Insight into altered energy metabolism provided by proteins enriched in urea-soluble fractions 49
4.9 A closer look at aggregating proteins 50
4.9.1 Septins may be involved in ALS pathogenesis 51
4.9.2 Cross-over with aggregating proteins identified in similar studies 52
4.10 Limitations 52
4.11 Future Directions 53
4.12 Concluding remarks 54

List of Tables

Table 1. Experiments used to identify aggregating proteins in ALS. 10
Table 2. Number of proteins and peptides identified in empty vector, $CCNF^{WT}$ and $CCNF^{S621G}$ transfected cells over 8 and 24 hours post-transfection. 24
Table 3. Proteins that significantly changed in expression between $CCNF^{WT}$ and $CCNF^{S621G}$ transfected cells after 8 hours post-transfection. 25
Table 4. Proteins that significantly changed in expression between $CCNF^{WT}$ and $CCNF^{S621G}$ transfected cells after 24 hours post-transfection 26
Table 5. Gene Ontology categories that were over-represented at 8h post-transfection 28
Table 6. Gene Ontology categories that were over-represented at 24h post-transfection 28
Table 7. $CCNF^{S621G}$-associated urea-soluble proteins that play key roles in the ubiquitin-proteasome pathway. 31
Table 8. $CCNF^{WT}$-associated urea-soluble proteins that play key roles in the ubiquitin-proteasome pathway. 31
Table 9. Functional summary of E3-ligases found in urea-soluble fractions with increased association with mutant Cyclin F. 32

List of Figures

Figure 1. Domains and mutations in TDP-43 and FUS. 3
Figure 2. Domain composition of Cyclin F and interacting partners. 6
Figure 3. Plasmid map of Cyclin F expression construct 12
Figure 4. Transgenic CCNF-mCherry was expressed in Neuro-2A cells. 18
Figure 5. Transgenic CCNF and RRM2 ratios are altered in mutant cells. 19
Figure 6. Nuclear and cytoplasmic fractionation of transfected Neuro-2A cells over 8, 24 and 48 hours post-transfection. 21
Figure 7. Proteomic analysis of Cyclin F transfection over time. 23
Figure 8. TDP-43 became more insoluble upon heat-stress 29
Figure 9. LC3-I increased in urea-soluble fractions in association with mutant Cyclin F. 32
Figure 10. Ingenuity pathway analysis of the 190 urea-soluble proteins enriched in Cyclin F (S621G) expressing cells. 34
Figure 11. Ingenuity pathway analysis of the 30 urea-soluble proteins enriched in Cyclin F (WT) expressing cells. 35
Figure 12. Ingenuity pathway analysis of the 65 urea-soluble proteins enriched in Cyclin F (S621G) expressing cells also subject to heat-stress 36
Figure 13. Ingenuity pathway analysis of the 121 urea-soluble proteins enriched in Cyclin F (WT) expressing cells also subject to heat-stress. 37

This thesis has been presented in the style of: *Proteomics*

Abbreviations

ACN	acetonitrile
ALS	amyotrophic lateral sclerosis
BCA	bicinchoninic acid
BSA	bovine serum albumin
Bis-Tris	1,3-bis(tris(hydroxymethyl)methylamino)propane
CO_2	carbon dioxide
DTT	dithiothreitol
FA	formic acid
FBS	fetal bovine serum
FDA	food and drug administration
FDR	false discovery rate
FTD	frontotemporal dementia
FTLD	frontotemporal lobar degeneration
FUS	(protein) fused in sarcoma
GO	gene ontology
HBSS	hank's balanced salt solution
IMAC	immobilized metal ion affinity chromatography
IAA	iodoacetamide
MND	motor neuron disease
MOPS	3-(N-morpholino)propanesulfonic acid
MS	mass spectrometry
MS/MS	tandem mass spectrometry
nanoESI	nanoelectrospray ionization
NLS	nuclear localisation signal
PBS	phosphate buffered saline
PBST	phosphate buffered saline + tween 20
PTM	post translational modification
RRM	RNA recognition motif
SCX	strong cation exchange
SD	standard deviation
SDS-PAGE	sodium dodecyl sulphate polyacrylamide gel electrophoresis
SpC	spectral count

SRM	selected reaction monitoring
TARDBP	(gene name) transactive response DNA binding protein 43
TDP-43	(protein name) transactive response DNA binding protein 43
TEAB	triethylammonium bicarbonate
TFA	trifluoroaceticacid

1 Introduction

1.1 Amyotrophic lateral sclerosis and Frontotemporal dementia

Amyotrophic lateral sclerosis (ALS), also known as Lou Gehrig's disease, is the most common form of Motor Neuron Disease (MND) and refers to the selective degeneration of upper and lower motor neurons of the cerebral cortex and spinal cord respectively [1]. Upon onset, patients are subject to muscular weakness, which then progresses to muscular dystrophy and eventual respiratory failure [2]. Life expectancy after disease onset is still typically less than 5 years and the only available FDA approved drug for ALS treatment, Riluzole, may add about 3 months to a patient's life [3]. Approximately 20% of ALS patients also develop Frontotemporal Lobar Degeneration (FTLD), which leads to Frontotemporal Dementia (FTD). In these cases the patients exhibit, to different degrees, additional symptoms such as declined cognitive functions, personality changes and difficulty controlling emotions [4].

1.2 Causes of ALS and FTD

ALS-causing mutations can be inherited in an X-linked dominant, autosomal dominant or autosomal recessive pattern [5]. This form of ALS is known as familial ALS (fALS) and accounts for ~5-10% of all ALS cases. In other cases, ALS is not inherited and occurs randomly. This is known as sporadic ALS (sALS) and accounts for 90-95% of all ALS cases [6]. One feature that unifies fALS and sALS is the formation of insoluble protein inclusions within affected cells, and these are indistinguishable between familial and sporadic patients. Although fALS-causing mutations only account for a small proportion of ALS, proteins encoded by these genes can be present in the aggregates of both fALS and sALS patients. Notably, *TARDBP* mutations are responsible for ~5% of fALS cases but the aggregated protein is present in 97% of ALS cases whether familial or sporadic [7]. This makes continual identification of ALS-causing genes important to advance our understanding of ALS and FTD as it highlights key protein players in disease progression. Conversely, the identification of novel aggregating proteins may lead to the identification of gene mutations responsible for ALS.

Recently our collaborators at Macquarie University, led by Associate Professor Ian Blair, have identified novel mutations in *CCNF*, a gene encoding Cyclin F (unpublished). These mutations lead to ALS and FTD phenotypes in populations around the world. At the cellular level, characteristic TDP-43 positive inclusions are observed. In addition, zebrafish

expressing transgenic mutant Cyclin F show a higher percentage of aberrant neurons compared to wild type controls. The altered neuron phenotype is particularly noticeable in zebrafish expressing transgenic Cyclin F (S621G). This missense mutation substitutes serine for glycine at amino acid 621 and will be the subject of this thesis.

1.3 Mechanisms leading to aggregation

There are several mechanisms leading to ALS pathogy. Two that are relevant to the study of Cyclin F are aggregating proteins [8] and dysfunctional protein quality control systems [9]. These mechanisms help to explain protein aggregation and neurodegeneration. However, there is still debate over the exact role of the aggregates and how they spread throughout the central nervous system.

1.4 Aggregate-prone proteins promote ALS pathology

Our understanding of ALS and FTD pathology took a turn in 2006 when Transactive Response DNA binding protein of 43 kDa (TDP-43) was identified as the main component of tau-negative, ubiquitin immunoreactive aggregates found in both ALS and FTLD post-mortem tissue [10]. This landmark discovery solidified the connections between ALS and FTD (which showed a cross-over of patient symptoms) and led to the identification of >30 mutations in *TARDBP,* the gene encoding TDP-43 [11]. The majority of these mutations in TDP-43 proteins are located in the prion-like, glycine rich region, which has been shown to make TDP-43 more aggregate prone (Figure 1). TDP-43 consists of 414 amino acids and although mainly situated in the nucleus, its nuclear localisation signal (NLS) and nuclear export signal (NES) enable it to continuously shuttle between the cytoplasm and nucleus [12]. TDP-43 also contains two RNA-recognition motifs, also known as RNA-binding domains, which enable TDP-43 to bind to a diverse set of RNA molecules [13]. Studies focused on the quaternary structure of TDP-43 reveal that TDP-43 exists as a homodimer where all 4 RRM domains are involved in binding to substrates. Interaction studies between dimeric TDP-43 with DNA or RNA revealed that this homodimer has preference for TG-rich DNA sequences and UG-rich sequences of RNA [13]. In terms of protein interactions, FLAG-immunoprecipitations of TDP-43 and co-interactors identified binding partners that play roles in several aspects of RNA metabolism as well as translation [14]. Together these data reflect the diverse set of roles TDP-43 plays in transcription and translation. It is therefore not difficult to see how potential impairment of TDP-43 activity during nuclear clearance and aggregation would alter diverse processes within the cell.

A year after mutant TDP-43 was discovered, attention was drawn to mutations found in *FUS*. In pathological inclusions, Fused in Sarcoma or Translocation in Liposarcoma (FUS/TLS) accounts for approximately 9% of FTD and an even smaller percentage in ALS [7]. The identification of FUS mutations was important to our understanding of ALS as it reiterated the idea that altered RNA processing is central to ALS and FTD pathogenesis [15]. An important aspect of FUS primary structure is that it is very similar to TDP-43 (Figure 1). Both of these proteins contain RRM domains, a prion-like domain, a glycine rich region, nuclear localisation signal (NLS) and nuclear export signal (NES). Unlike TDP-43 however, FUS binds to RNA with limited sequence preference and as a result, there is limited crossover between the RNA transcripts regulated by FUS and TDP-43 [16].

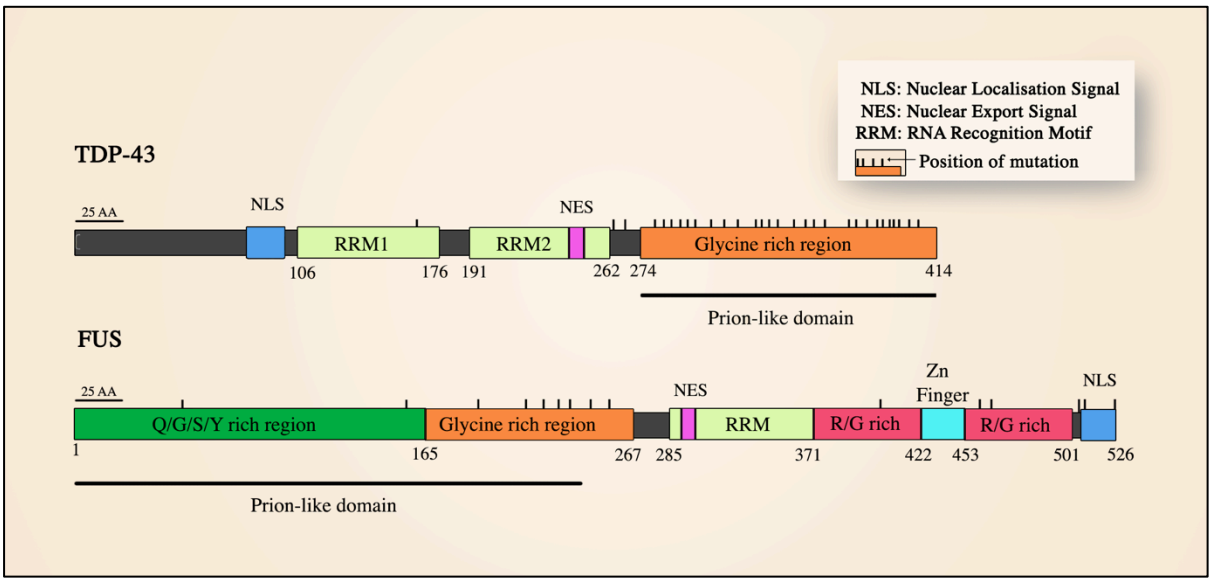

Figure 1. Domains and mutations in TDP-43 and FUS. Adapted from reference [15].

The prion-like domains of both of these proteins are highly relevant to protein aggregation through the formation of stress granules (SGs) [17]. When under stress, SGs temporarily store mRNA and repress translation [7]. As a result, these macromolecular complexes are known to contain an array of RNA-binding proteins (many containing a prion-like domain) and mRNA transcripts [18]. Prion-like domains enable proteins to form self-templated amyloid fibrils [19]. In ALS, these domains assist in the quick formation of P-bodies and SGs in response to stress. Given that many of these aggregating proteins also contain RRM binding domains, it becomes possible to quickly recruit proteins like TDP-43 and FUS along with bound RNA or protein molecules in order to stall translation [18].

Usually, cell stress leads to TDP-43 association with stress granules until the stress subsides. Once the cell is no longer under stress, TDP-43 is released and may return back to the nucleus. In pathological conditions however, the process is not completely reversible, given that the proteins do not return to the nucleus and remain partially associated with SGs in the cytoplasm [20]. Granule composition reveals that a large proportion of proteins within SGs are post-translationally modified and that this aspect may affect the assembly and disassembly of the granules themselves [21].

Besides the fact that TDP-43 and FUS become misfolded and aggregated along with other proteins, TDP-43 is also known to translocate out from the nucleus into the cytoplasm, where it is found highly ubiquitinated. This has been noted by the lack of diffuse TDP-43 nuclear staining and increased staining within ubiquitin-positive inclusion bodies in the cytoplasm [22]. Subcellular localisation is essential for optimal protein and cell function and mislocalisation may be a contributing factor to ALS pathogenesis. In one notable study, TDP-43 mislocalisation was found to be toxic to neurons regardless of inclusion body formation [23]. Furthermore, protein translocation can occur prior to or during aggregation, as the mislocalised proteins would be shuttled out of the nucleus and into the cytoplasm, where they are found to aggregate.

1.5 Protein quality control systems

Proteostasis networks are also implicated in the initial formation and spread of these misfolded aggregates. The ubiquitin-proteasome and autophagy-lysosome systems are the two main degradation systems involved in proteostasis and are responsible for degrading aggregating proteins such as mutant TPD-43 and SOD1 [24, 25].

1.5.1 Degradation machinery

Neurons are long-lived and post-mitotic which makes efficient cellular clearance mechanisms highly important for cell function [26]. The proteasome is a well characterised multi-subunit complex known to degrade ubiquitinated proteins [27]. Normally, misfolded proteins are targeted to the proteasome where they are rapidly degraded [27]. In contrast, macroautophagy is a bulk catabolic degradation system that makes use of lysosomal machinery that works alongside the ubiquitin-proteasome system [28]. Rather than degrade single proteins, autophagy can degrade bulk cytoplasmic material such as protein aggregates, excess organelles and damaged cellular components [29]. A pathological hallmark of ALS is the accumulation of ubiquitinated, aggregated proteins indicating inefficient or defective

clearance of many misfolded proteins. Mutations found in p62, an adaptor protein for sequestering components into autophagosomes leads to its accumulation and enhanced formation of aggregates [30] highlighting the importance of bulk degradation systems in the efficient clearance of aggregates.

1.5.2 Ubiquitin-conjugation systems

Ubiquitin consists of 76 amino acids and contains 7 internal lysine residues that can each be ubiquitinated to form polyubiquitin chains on substrates. Protein ubiquitination is best known to target the protein for degradation by the proteasome however differences in polyubiquitin chain topology can determine the fate of the protein [31].

For example, K48 or K11-linked polyubiquitin chains usually target the substrate for proteasome degradation [32], whereas K63 chains may target the protein to aggresomes [33], which can be degraded through autophagy-mediated lysosomal degradation [34]. Ubiquitin conjugation to substrates requires a cascade of enzymatic reactions where E1 enzymes activate ubiquitin, E2 act as a ubiquitin-conjugating enzyme and E3-ligases specify the substrates to be ubiquitinated [31]. Overall, the interactions between ubiquitin-conjugation systems and protein degradation machinery are intricate and interconnected with many biological functions of the cell. As a result, a small change, such as a missense mutation, could potentially alter the function or interaction between Cyclin F and its binding partners thereby initiating a cascade of events causing biological processes to deviate from the norm. This creates the need to understand how the missense mutation (S621G) affects the activity of Cyclin F.

To date, Cyclin F is known to interact with Cyclin B1 [35] as well as within a multi-protein E3-ligase complex [36] in order to regulate the nuclear localisation of Cyclin B1 or to ubiquitinate substrate proteins respectively (Figure 2).

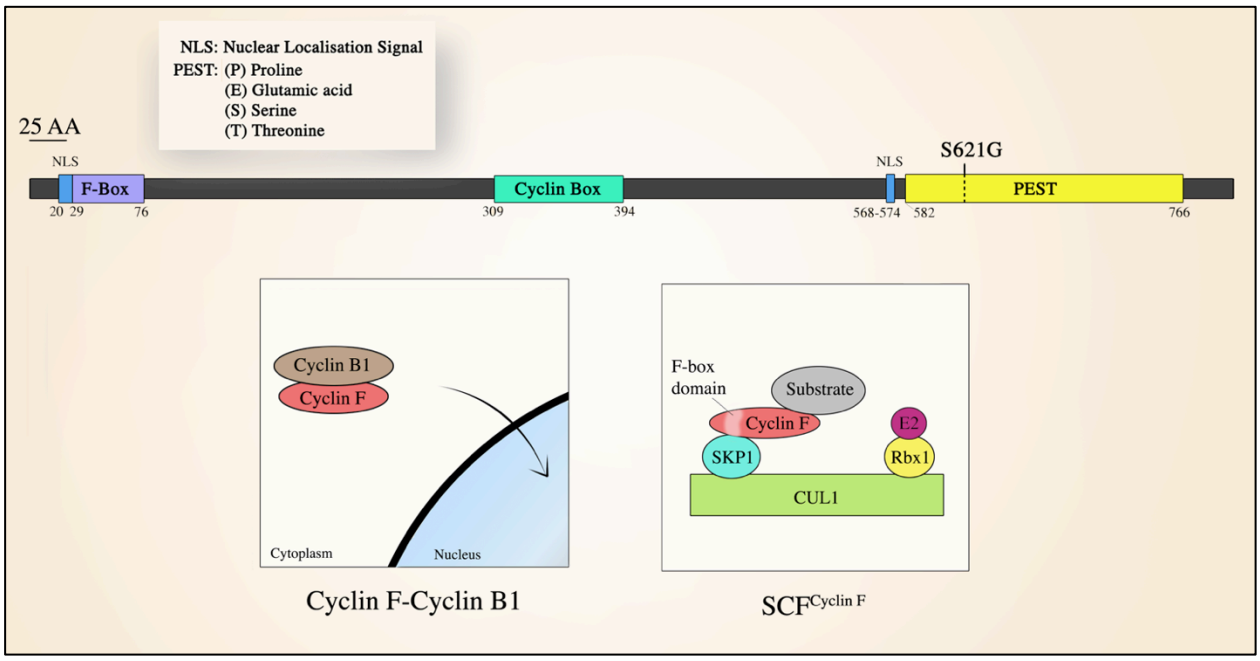

Figure 2. Domain composition of Cyclin F and interacting partners. Cyclin F translocates Cyclin B1 to the nucleus. Cyclin F also forms part of a SCF complex and attaches substrates to other components of the complex. Adapted from reference [35].

Cyclins are known to interact with S-phase kinase-associated protein 1 (SKP1) and Cullin-1 (CUL1) to form an SKP1-CUL1-F-box protein complex (SCF complex) [36] which selectively recruits substrates and modifies them with a ubiquitin or ubiquitin-like protein. SCF complexes are the largest family of E3-ubiquitin ligases and have been evolutionarily conserved from yeast to mammals. These account for approximately 20% of ubiquitinated proteins degraded by the proteasome [37]. The core scaffold of this complex is made up of SKP1, CUL1, RING box protein 1 (RBX1) and an F-box protein. SKP1 is an elongated, globular scaffolding protein on which other SCF components assemble. The N-terminus of CUL1 binds SKP1, which attaches to an F-box protein through the F-box motif composed of 40 amino acids [38]. At the C-terminus, Rbx1 attaches to CUL1 through the cullin consensus domain [39] and binds to an E2 ligase. This interaction is essential for ubiquitination of substrates. Within this scaffold, the F-box protein is responsible for recruiting substrates. To date there are sixty-nine putative F-box proteins in mammals which play roles in diverse cellular processes [40]. Substrate recruitment by Cyclin F makes use of the hydrophobic patch situated within the cyclin box domain to bind substrates containing a Cy (RxL) motif [41]. Due to the spatial restraint imposed by the tertiary structure of the SCF complex, the substrate's ε-amino groups on lysine residues are positioned in close proximity to the E2 active site in order to facilitate transfer of activated ubiquitin onto the substrate lysine [42].

Insights into the processes that could be affected by altered mutant $SCF^{Cyclin\ F}$ may be found by looking at its protein substrates. The function of $SCF^{Cyclin\ F}$ and its substrates are best characterized in dividing cells and to date, there are only three known $SCF^{Cyclin\ F}$ complex targets which are: ribonucleotide reductase family member 2 (RRM2) [43], centriolar coiled-coil protein of 110 kDa (CP110) [38] and nucleolar and spindle associated protein 1 (NuSAP1) [44].

Ribonucleotide reductase (RNR) is an enzyme that converts ribonucleotides to deoxyribonucleotides (dNTPs); precursors of DNA. Structurally, RNR consists of two RRM1 units and two RRM2 units. As RNR essentially regulates dNTP pools, its activity directly impacts DNA damage and repair (DDR) mechanisms as well as DNA replication [41]. In dividing cells, RNR activity is coordinated with cell cycle progression and the subunit, RRM2, is known to oscillate with the cell cycle, suggesting a link between RRM2 abundance and enzyme activity [45]. During genotoxic stress, RNR has been shown to translocate from the cytoplasm to the nucleus in order to manage local dNTP pools near the damaged site [41]. DNA damaging agents have also been reported to induce a reduction in Cyclin F abundance, which correlates with increased RRM2 levels [45].

CP110 and Cyclin F are known to interact on centrioles during G2, during which CP110 is ubiquitinated by the $SCF^{Cyclin\ F}$ complex for degradation. This process is used to finely tune centrosome duplication. *CCNF* gene silencing using siRNA during G2 results in abnormalities during mitosis such as multipolar or asymmetric spindle formation [46].

NuSAP1 is another protein that has been implicated in cell cycle progression with protein levels peaking between the G2 stage of the cell cycle and mitosis. NuSAP is known to localize with and organize mitotic spindles. Depletion of NuSAP in dividing cells using RNAi results in deformed nuclei as well as impaired cell proliferation [47].

1.6 Linking ALS pathology to neurodegeneration and dysfunction

The widespread presence of TDP-43 and other aggregating proteins in ALS/FTD has led to numerous studies that explore the relationship between these aggregates and neurodegeneration itself. There are a couple of hypotheses that could explain the effect of TDP-43 aggregates and these are highly controversial.

The first hypothesis is based on the observation of partial TDP-43 nuclear clearance and the aggregation of misfolded, insoluble TDP-43 in the cytoplasm. The sequestering of TDP-43 within condensed granules would result in a non-functional protein whereas its depletion in the nucleus means that a lower amount of functional TDP-43 is available to form TDP-43 protein/RNA complexes (which require a specific stoichiometric ratio to be functional). In turn this adversely affects TDP-43 protein/RNA complex function, subsequently altering RNA metabolism. In models where TDP-43 is overexpressed, there is below optimal stoichiometric ratios between TDP-43 proteins and RNA complexes leading to incomplete and dysfunctional complexes [48]. Other evidence to support the loss-of-function hypothesis has been in the form of *in vivo* studies. The critical function of TDP-43 in the development and functioning of the nervous system is suggested by TDP-43 knock-out studies in zebrafish during embryonic development. This leads to impaired growth of motor neuron axons and swimming deficits [49]. Another *in vivo* study shows that the partial loss of TDP-43 in mouse models, using RNAi, recapitulates several ALS phenotypes and leads to neurodegeneration [50].

The second hypothesis is that protein inclusions induce neurotoxicity. Many studies which support this hypothesis have been based on the overexpression of TDP-43. These have shown that overexpression of full-length TDP-43 results in phenotypes common to ALS and FTD patients, at least in terms of neuron dysfunction and degeneration. Furthermore, the toxicity correlates with the amount of TDP-43 expressed [51].

1.7 Prion-like spread of neurodegenerative diseases

An interesting emerging concept that applies to several neurodegenerative diseases is that aggregates can spread from cell to cell, from one brain region to another during the progression of the disease. This cell to cell spreading is thought to occur in a *prion-like* manner [52]. Prions, or infectious proteins, cause a series of neurodegenerative diseases through modification of the prion protein. Cellular, unaffected versions of the prion protein are converted to the pathological form through post-translational processing with the assistance of other proteins [53]. Similarly, many proteins involved in neurodegenerative diseases are thought to change into this pathological form. When transmitted to neighbouring cells, these pathological 'seeds' sequester and convert endogenous protein into this pathological form, creating a chain reaction and a growing proteinaceous inclusion [52]. Proteomic studies have also revealed that TDP-43 and several TDP-43 co-aggregating proteins contain a prion-like domain which makes them intrinsically prone to aggregate [54].

The most convincing forms of evidence to support this mode of transmission has come from isolating the pathogenic form of the protein from affected ALS models and introducing them into a healthy model [52]. Several reports have shown that the pathogenic proteinaceous seeds cause further aggregation of proteins in previously unaffected systems. The result is the subsequent spreading of the disease throughout the cell population [55]. In post-mortem tissue, these aggregates are seen scattered throughout the central nervous system and in some cases these seeds may form in disparate regions of the brain, thus cell to cell spreading may not have one originating site of infection [56]. Due to the fact that these aggregates may be involved in the seeding and spreading of ALS pathology it is necessary to identify the protein components that make up these aggregates.

1.8 Proteomic studies of co-aggregating proteins in ALS

Discovery-oriented proteomic techniques are useful to provide non-biased protein related insight into disease pathogenesis. As seen in Table 1 below, ALS protein mutations may give rise to a unique protein profile and this could give clues into pathogenesis in each unique case. It also demonstrates that the protein aggregates associated with ALS-causing mutations are poorly characterised. The most comprehensive study that revealed several TDP-43 co-interacting proteins was conducted by Dammer *et al*, where the authors implemented a quantitative mass spectrometry analysis using SILAC labelling of samples and LC-MS/MS using an Orbitrap instrument. Using this workflow they identified 35 co-aggregating proteins within urea-soluble fractions of HEK-293 cell lysates. This study revealed many TDP-43 co-aggregators that were functionally involved with RNA-binding and mRNA splicing. Another subset of identified proteins were associated with cytoplasmic stress granules. This study also looked at the ubiquitination status of aggregated TDP-43. Four sites of ubiquitin were found on or near the RNA-recognition motif of TDP-43. Furthermore, a quadruple TDP-43 ubiquitin site mutant (which could not be ubiquitinated) was not susceptible to aggregation upon stress. Overall the study points out that specific ubiquitination events can play a role in ALS pathogenesis as ubiquitination is suspected to be a contributing factor to protein misfolding and sequestration.

Table 1. Experiments used to identify aggregating proteins in ALS.

sALS/mutated fALS-causing gene	**Sample analysed**	**Technique/s used to identify aggregating proteins**	**Aggregating proteins identified in experiment**	**Cross-over with sporadic ALS?**	**Ref.**
sALS	Post-mortem tissue	Immunoblotting, 2D-PAGE gels, LC-MS/MS.	TDP-43 was identified as the main component of ubiquitin-positive aggregates.	N/A	[57]
fALS (*mt*FUS)	NSC-32 cells, post-mortem tissue	Immunoblotting, immunofluorescence, Co-immunoprecipitation, Immunostaining.	FUS co-aggregates with PDI- an important ER chaperone protein. In some cases, calreticulin also co-aggregated.	Yes	[58]
fALS (*mt*SOD)	ALS post-mortem tissue	Immunoblotting, 2D-gels, LC-MS/MS.	GFAP was the dominant component in protein clusters and was heavily acetylated at 6 lysine residues.	N/A	[59]
fALS (*mt*SOD)	SOD-YFP transgenic mice motor neurons and spinal cord at different ages.	MudPIT, LC-MS/MS, Label-free.	*mt*SOD became increasingly insoluble around 6 month of age. Hsc70 was associated with mutant SOD at all ages. Several intermediate filaments were increasingly associated with *mt*SOD1 aggregates at later stages.	Yes	[60]
fALS (C9ORF72 expansion)	Post-mortem tissue, HEK293	Immunohistochemistry, Immunoblotting.	Most inclusions contain poly-(Gly-Ala), poly-(Gly-Pro) and poly-(Gly-Arg).	No	[61]
FTD (*mt*VCP)	Post-mortem tissue from patients with FTD and Paget disease	Immunohistochemistry, Immunoblotting.	Phosphorylated TDP-43 aggregates formed however VCP did not co-localise with these aggregates.	No	[62]
fALS (*mt*ATXN2)	HEK293T, lymphoblast cells, M17 cells	Immunoblotting.	Phosphorylated TDP-43 aggregated. In some cases Ataxin 2 co-aggregates.	Yes	[63]
fALS (*mt*UBQLN2)	Post-mortem tissue	Immunostaining.	Ubiquilin 2 regulates ubiquitinated protein degradation and accumulates alongside ubiquitinated proteins, TDP-43 and FUS.	Yes	[64]

1.9 Aims

There are 3 main aims to this study:

1. Assess changes in cytoplasmic and nuclear abundance of RRM2 and TDP-43 in Cyclin F (S621G) expressing cells, compared to Cyclin F (Wild type) expressing cells.
2. Identify early changes in protein abundance in Cyclin F (S621G) expressing cells compared to Cyclin F (Wild type) expressing cells.
3. Use mass spectrometry to characterise detergent insoluble proteins enriched in Cyclin F (S621G) expressing cells compared to Cyclin F (Wild type) expressing cells.

1.10 Significance

In the first part of this study the effect of the *CCNF* mutation on the $SCF^{Cyclin\ F}$ complex will be investigated. This will provide insights into the biological processes that are affected due to altered E3-ligase activity or proteostasis dysfunction. The second part of this study may identify components of insoluble protein aggregates that are forming in mutant Cyclin F expressing cells. This will provide insight into key protein players involved in initiating protein inclusions and which could be involved in cell-to-cell spreading of the inclusions. This could inform experiments for future therapeutic applications.

2 Methods

2.1 Cell culture

NSC-34 and Neuro-2A murine cell lines were used. NSC-34 is a hybrid cell line produced by fusion of motor neuron enriched, embryonic mouse spinal cord cells with mouse neuroblastoma. Neuro-2A cells are mouse neuroblastomas. They were grown and maintained in Dulbecco's modified Eagle's medium (DMEM; Sigma Aldrich) supplemented with 10% heat-inactivated fetal bovine serum (FBS; Sigma Aldrich) and 1% antibiotics (100 mg/mL streptomycin and 100 U/mL penicillin; Sigma Aldrich) in a 37°C incubator with 5% CO_2 and 95% humidity. When the cells reached 60-80% confluence, media was removed and cells were washed with pre-warmed phosphate buffered saline (PBS). Cells were detached from flasks using trypsin (Sigma Aldrich) before seeding cells into new flasks or plates.

2.2 Plasmids preparation, purification and cell transfections

Expression constructs comprising wild type and mutant human CCNF cDNA fused with an N-terminal mCherry were a gift from A/Prof. Ian Blair's research group. A plasmid map is shown in Figure 3.

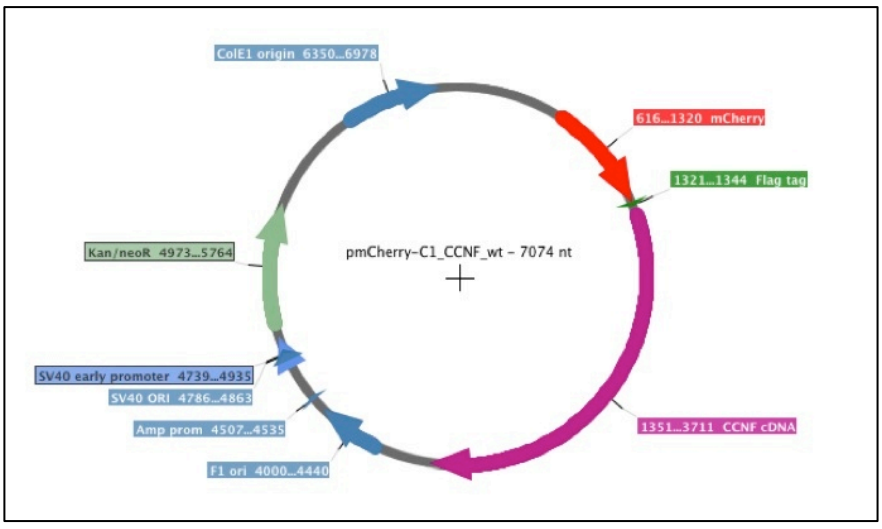

Figure 3. Plasmid map of Cyclin F expression construct.

Plasmid purification from transformed *E. coli* was done using a QIAGEN Plasmid Midi Kit according to the manufacturer's instructions. Transfections were carried out using Lipofectamine 2000 (Life Technologies) and opti-MEM media (Life Technologies) according to manufacturer's protocol. Transfections made use of 10 μg of DNA for each T75 flask.

Expression constructs were composed of wild type or mutant cDNA fused to mCherry at the N-terminus. Empty vectors expressing mCherry were also used as a control.

2.3 Flow cytometry

Neuro-2A cells were transfected with empty vector constructs and maintained for 24 hours. Negative control cells were not transfected. Cell suspensions were obtained by washing cells in PBS before detaching cells from flasks using trypsin and resuspending them in growth media. Cell numbers were equalised between the cell populations prior to analysis using an Influx flow cytometer (BD Biosciences). The population corresponding to cells was resolved from the background using a Forward- versus Side-Scatter plot. Fluorescent mCherry expressing cells were then distinguished from non-mCherry expressing cells using a 200 mW 488 nm laser source on biplots of Forward-Scatter versus mCherry fluorescence detected using a 610/30 nm bandpass filter.

2.4 Cell Harvesting and preparation for analysis

NSC-34 and Neuro-2A cells were harvested at 80% confluence by scraping cells from the surface of the flask into ice cold phosphate buffered saline (PBS). Cells were pelleted by centrifugation and either stored at -80°C or lysed immediately. Three biological replicates were obtained.

2.4.1 Preparing whole cell lysates

Pellets were resuspended in sodium deoxycholate lysis buffer (1% sodium deoxycholate, 0.1M triethylammonium bicarbonate (TEAB), 1.5 mM magnesium chloride, pH 8.0) and immediately boiled for 2 minutes at 95° C. Samples were cooled to room temperature and 1 μL of Benzonase Nuclease (Novagen, 70746) was added to cell lysates for 30 minutes at room temperature to degrade DNA.

2.4.2 Subcellular fractionation

Neuro-2A cells were transfected and harvested at 8, 24 and 48 hours post-transfection. Three biological replicates were obtained. To obtain nuclear and cytoplasmic fractions, cell pellets were resuspended in low salt extraction buffer (20 mM HEPES pH 7.3, 1mM EDTA, 1 mM EGTA and protease inhibitor cocktail (Roche)) at 4 °C for 20 minutes with occasional pipetting. Intact nuclear pellets were then separated from cytoplasmic material by centrifuging lysates at 4°C for 1 minute at 14,000 × *g*. Crude cytoplasmic fractions (supernatant) were

transferred to a new tube and nuclear fractions were washed thrice with low salt extraction buffer. Washed nuclear fractions were resuspended in high salt buffer (20 mM HEPES pH 7.3, 1 mM EDTA, 1 mM EGTA, 420 mM NaCl, 20% v/v glycerol and protease inhibitor cocktail (Roche)) and mixed gently on a rotating device for 20 min at 4 °C. Nuclear fractions were then lysed using a probe sonicator (10 s, Setting 3, Branson Sonifier 450). Cytoplasm and nuclear fractions were both cleared of cellular debris through centrifugation at 15, 000 g (30 min, 4°C) prior to analysis.

2.4.3 Isolating aggregates

Protein aggregation was induced in transfected cells by subjecting them to heat shock (42°C for 1 hour) or 10 μM hydrogen peroxide for 2 hours. Control cells were not subject to any stress after transfection. Cells were harvested at 24 hours post-transfection and lysed in pre-chilled radioimmunoprecipitation assay (RIPA) buffer (1% (v/v) Triton-X-100, 150mM NaCl, 1% (w/v) sodium deoxycholate, 1% SDS, 50mM Tris-HCl, pH 8 and protease inhibitor cocktail (Roche)). RIPA-insoluble proteins aggregates were isolated by centrifugation at 10000 x *g* for 30 minutes at 4°C, after which a pellet containing insoluble protein aggregates, cell debris and DNA could be seen clearly at the bottom of the tube. Supernatants, containing soluble proteins were removed and the insoluble pellet was resuspended in 8M urea in RIPA buffer. To degrade the DNA, Benzonase Nuclease (Novagen, 70746) was added to cell lysates for 30 minutes at room temperature with occasional vortexing until a homogenous solution was observed. Lysates were analysed using western blotting or mass spectrometry. One biological sample was analysed due to time constraints.

2.5 Western blot analysis

Protein concentrations were determined using a Pierce® BCA Protein assay kit. Equal amounts of protein were separated by electrophoresis using 12% Bis-Tris SDS-PAGE gel (NuPAGE®, Life Technologies). Proteins were transferred onto a nitrocellulose membrane (BioRad, 1620115) using a semi-dry transfer method using the Trans-blot® Turbo™ transfer system (BioRad). After protein transfer, membranes were blocked for up to 1 hour in 3% bovine serum albumin in PBS containing 0.05% v/v Tween (3% BSA in PBS-T). Primary antibodies were applied at 4°C over night or for 1 hour at room temperature. After incubation, membranes were washed in PBS-T three times for 10 minutes before fluorescently labelled IRDye 800CW *Goat Anti-Rabbit IgG* (1:15,000; cat# 926-32211, LI-COR) secondary antibody was applied for 45 minutes at room temperature. Proteins were imaged using a Li-

Cor Odyssey imaging system at the appropriate wavelength. Densitometry analysis was conducted using ImageJ software (v1.47; National Institute of Health) [65] and statistics were conducted using Microsoft Excel. Graphs were made using GraphPad Prism 5 and Microsoft Excel. Antibodies used in this study were: rabbit polyclonal anti-Cyclin F (1:300; cat# sc-952, Santa Cruz Biotechnology), mouse monoclonal anti-mCherry (1:300; cat# 632543, Clonetech) mouse monoclonal anti-TDP-43 (1:1000; cat# H00023435-M01, Abnova), rabbit polyclonal anti-ubiquitin (1:300, cat# Z0458, Dako), mouse monoclonal anti-RRM2 (1:2500; cat# ab57653, Abcam), mouse monoclonal anti-β-actin (1:12,000; cat# ab6276-101, Abcam), rabbit polyclonal anti-Lamin A/C (1:1000; cat# 2032, Cell Signaling), mouse monoclonal α-tubulin (1:1000; cat# T5168, Sigma).

2.6 Preparing samples for mass spectrometry

Mass spectrometry was used to analyse whole cell lysates and urea-soluble fractions. In-solution digests were used to prepare whole cell lysates whereas in-gel digests were used to ensure urea was removed from urea-solubilised proteins.

2.7 Trypsin digestion

2.7.1 In-solution digestion for total cell lysates

Aliquots of 500 µg of whole cell lysate were reduced using 10 mM dithiothreitol for 30 min at 50°C. For alkylation, 25 mM of iodoacetamide was added to cell lysates at room temperature. Samples were kept in the dark for 30 min. Once alkylated, samples were subject to trypsin (sequencing grade modified trypsin; cat# V5111, Promega) digestion, using 1:50 µg trypsin:protein, and left to digest overnight at 37°C.

2.7.2 In-gel digestion for urea-soluble lysate fractions

Prior to in-gel digestion, equal amounts of urea-soluble lysate fractions were run on SDS-PAGE. Gels were stained with Coomassie blue G-250 (Sigma) for 2 hours and destained overnight in 25% methanol or until the background was clear. Each lane was then excised into 5 pieces based on mass. In-gel digestions were then carried out using the procedure established by Shevchenko *et al*, 2006 [66].

2.8 Sample Purification after in-solution digestion

C18 OMIX tips (Agilent) were used to desalt samples prior to analysis. The filter was washed

with methanol, followed by sample buffer 2 (2% (v/v) ACN, 1% (v/v) TFA). Peptide samples were run through the filter and washed with sample buffer 2. Peptides were eluted using 70% (v/v) ACN, 0.1% (v/v) TFA. Eluted peptides were acidified to 1% (v/v) TFA, then dried down in a SpeedVac. Samples were stored at -20°C. Upon analysis, samples were resuspended in a solution of 2% (v/v) ACN and 0.1% (v/v) formic acid.

2.9 Mass Spectrometry

Samples were analysed using on-line C18 reverse phase nanoscale liquid chromatography tandem mass spectrometry. A 10 µL aliquot containing 20 µg of sample was injected using an Eksigent nano-LC system with cHiPLC® system coupled to the 5600 TripleTOF™ mass spectrometer (AB SCIEX) equipped with a nanoelectrospray ionisation emitter (PicoTip Emitter, New Objective). Samples were first loaded onto a 0.5 mm C-18 reverse phase chip trap (200 µm inner diameter, 3 µm particle size, Eksigent, part of AB SCIEX) and desalted at a flow rate of 10 µL/min using Buffer A (2% (v/v) ACN, 0.1% (v/v) formic acid) for 5 min. Desalted peptides were separated by a 15 cm C18 analytical reverse-phase chip column (200 um inner diameter, 3 um particle size, Eksigent, part of AB SCIEX) using Buffer B (90% (v/v) ACN, 0.1% (v/v) formic acid) over a 140 min, 5-40% gradient for analysis of total cell lysates. A 2 hour gradient was used for urea-soluble fraction analysis. The 5600 TripleTOF™ was operated in an information-dependant acquisition mode involving 1 full MS scan between 350-1500 m/z, and 20 MS/MS scans generating approximately 15-20 points per peak. Monoisotopic precursor selection, charge state screening and dynamic exclusion were chosen parameters. Charge states that were unassigned, >4 or +1 were not selected for MS/MS fragmentation.

2.10 Database searching

ProteinPilot™ (v4.2, AB SCIEX) was used to generate peaklists (Mascot Generic Files (MGF)) from raw data files (wiff files) for protein database searches with Mascot [67]. A Mascot search (v2.4.0, Matrix Science London, UK) was conducted for each sample using the Swissprot_2014_04 database (selected for Mus musculus; 16676 entries). The following search parameters were chosen: carbamidomethylcysteine as a fixed modification and methionine oxidation, protein amino-terminal acetylation as variable modifications. Enzyme specificity was set to trypsin and allowed for 2 missed cleavages. Parent ion tolerance had to be within ±50 ppm whilst MS/MS fragment ion tolerance was within ±0.1 Da. Peptide charges were set to 2+, 3+ and 4+. A target-decoy search strategy using a reversed database

was used. For urea-soluble lysate fractions, raw data files were grouped prior to database searching so that all peptides and proteins found in each lane were pooled.

2.11 Criteria for protein identification

MASCOT was used to generate DAT files that were further processed using Scaffold (v4.0.5, Proteome software). Peptide and protein false discovery rate was set at less than 1%. Protein identifications were accepted if there were at least two unique peptides.

2.12 Statistical analysis

Spectral counts were converted to normalised spectral abundance factors (NSAF) which takes into account the length of a given protein as well as the total amount of protein in a given sample [68]. Adding 0.5 to all spectral counts prior to normalisation accounted for missing values and total spectral counts for at least one condition was equal to 6. NSAF values were calculated using the following equation as was conducted by Zybailov *et al*, [68] :

$$(\mathrm{NSAF})_k = \frac{(\frac{SpC}{L})k}{\sum_{i=1}^{N}(\frac{SpC}{L})i}$$

In this equation 'k' is the protein of interest; 'SpC' refers to the number of spectral counts, 'L' is the amino acid length, 'N' refers to the sum of all proteins in a given sample (*i*). NSAF values were $\log_2$-transformed and Student's *t*-tests were used to identify significant ($p < 0.05$) changes in protein abundance between any two samples. Determining fold-changes made use of non-transformed NSAF values and changes of ≥ 1.5 or ≤ 0.67 were of interest. Statistical data preparation and tests were done using Microsoft Excel. Enriched GO annotations and signaling pathways were identified using the Database for Annotation, Visualization and Integrated Discovery (DAVID) [69] and QIAGEN's Ingenuity® Pathway Analysis (IPA®, QIAGEN Redwood City, www.qiagen.com/ingenuity).

3 Results

3.1 Human cyclin F-mCherry expression in neuron-like cells

Neuro-2A cells were transfected with *CCNF*(S621G)-mCherry, *CCNF*(WT)-mCherry or an empty vector control. To evaluate the efficiency of *CCNF*-mCherry transfections, flow cytometry and immunoblotting were utilised. The expected size of mCherry is 28.8 kDa whilst the expected size of Cyclin F-mCherry is 115.8 kDa).

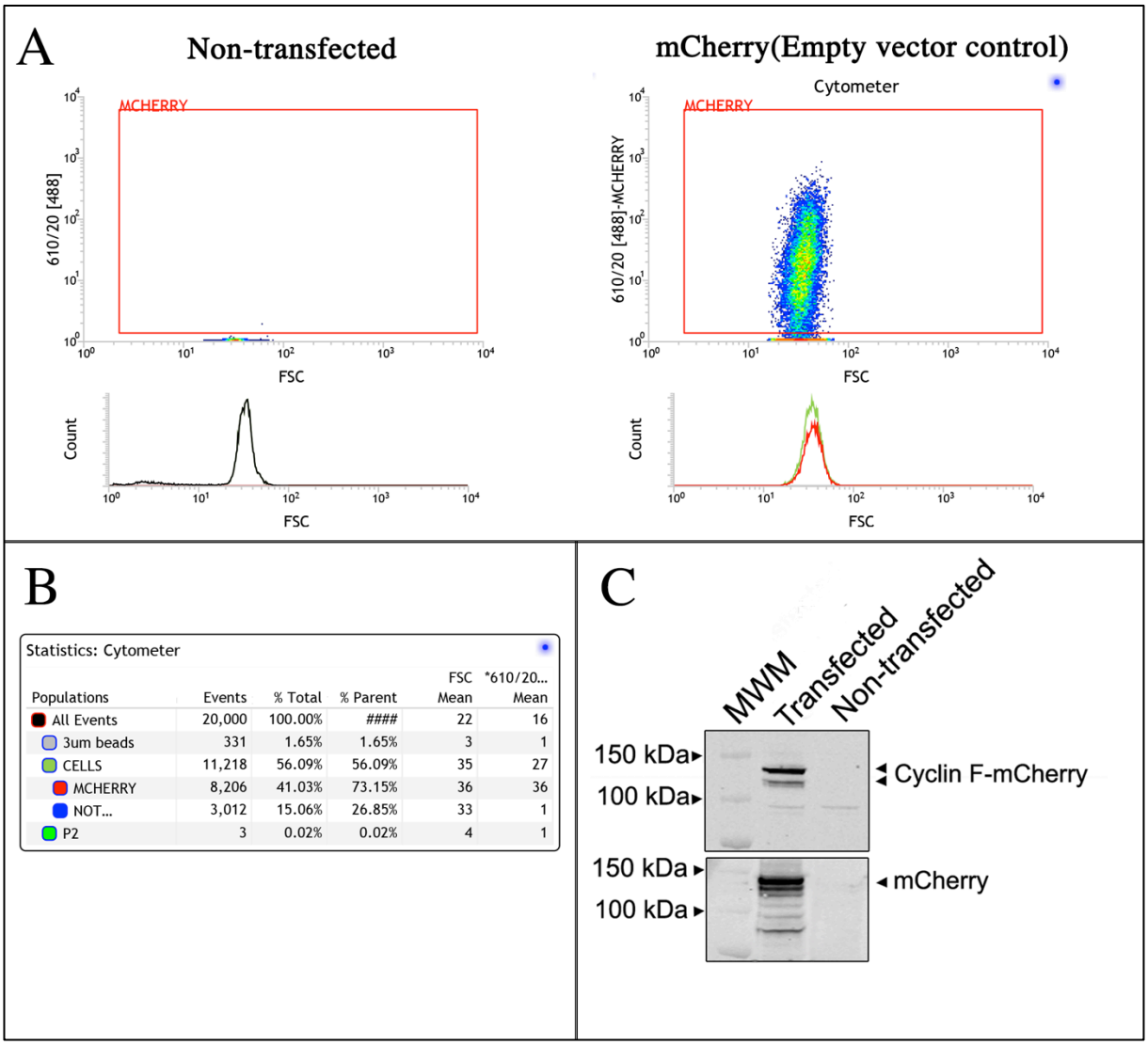

Figure 4. Transgenic CCNF-mCherry was expressed in Neuro-2A cells. **A.** Flow cytometry revealed clear expression of mCherry constructs **B.** Transfection efficiency was 73.15% **C.** Immunoblotting for CCNF-mCherry and mCherry reveals overlap above100 kDa. MWM; Molecular weight marker.

Flow cytometry revealed that non-transfected cells were clearly distinguished from transfected cells despite similar cell counts and density (Figure 4A). In total, 56.09% of all events were considered cells and within this population, 73.15% of cells expressed mCherry-

constructs whereas 26.85% of cells did not fluoresce (Figure 4B). Immunoblotting for Cyclin F and mCherry revealed Cyclin F-mCherry expression in transfected Neuro-2A cells but not in non-transfected control cells (Figure 4C). In addition, the position of mCherry and Cyclin F-mCherry bands overlap above 100 kDa (Figure 4C). Upper and lower bands of Cyclin F-mCherry may be due to post-translationally modified protein or truncation.

3.2 The ratio of human cyclin F-mCherry to RRM2 was altered in mutant Cyclin F-mCherry cells

To gain insight into the functional implications of the $CCNF^{S621G}$ mutation, we specifically probed for a known target of the $SCF^{Cyclin\ F}$ complex; RRM2 (Figure 5A). Neuro-2A and NSC-34 cells were both used to confirm the consistency of the experiment (Figure 5). In further experiments, NSC-34cells were no longer used due to time constraints.

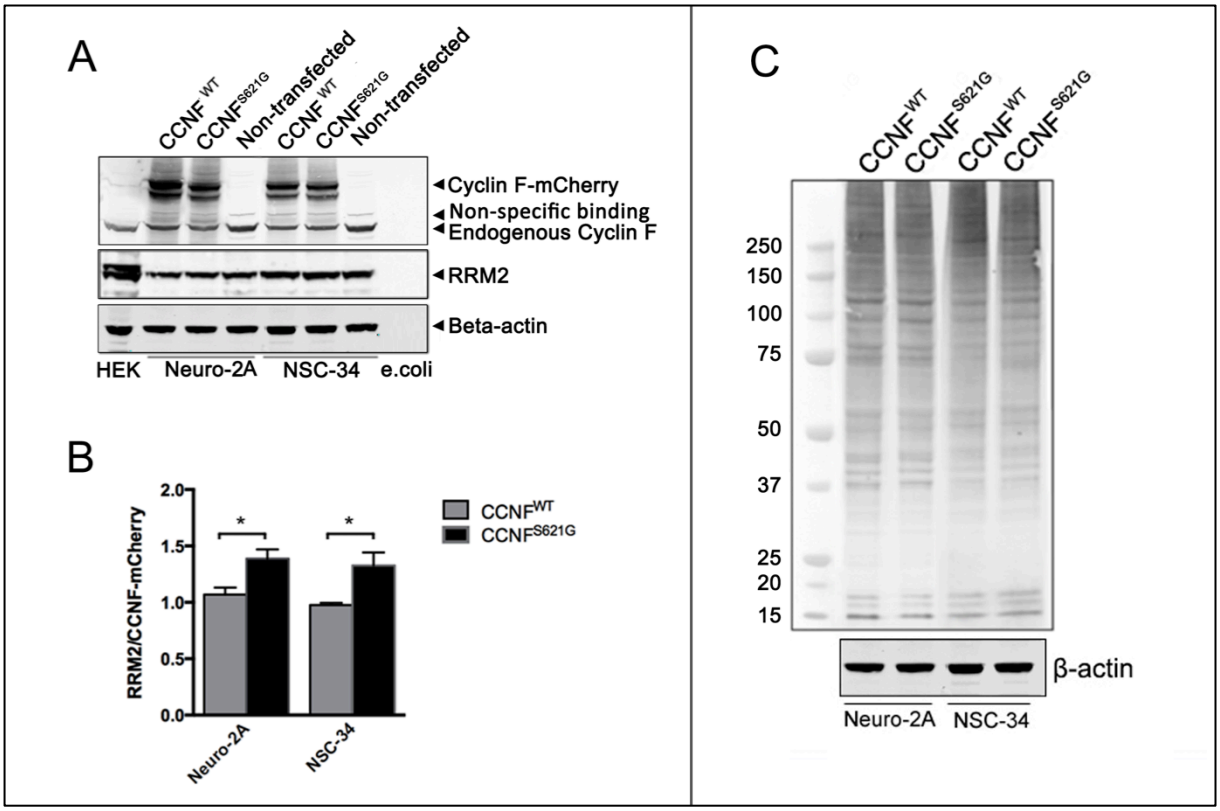

Figure 5. Cyclin F-mCherry to RRM2 ratios are altered in mutant cells. **A.** Neuro-2A and NSC-34 cells were transfected to express wild type or mutant Cyclin F tagged with mCherry. Whole cell lysates were subject to immunoblotting using antibodies as indicated **B.** Densitometry analysis using ImageJ revealed significantly different ratios of RRM2 to Cyclin F-mCherry in Neuro-2A and NSC-34 cells. *$p < 0.05$ **C.** Immunoblotting using an antibody recognising pan-ubiquitin comparing wild type and mutant whole cell lysates from transfected Neuro-2A and NSC34 cells. Results shown are representative of three independent experiments ± SEM.

No differences in RRM2 expression were found in transfected Neuro-2A or NSC-32 cell lines at 24h, however we did note differences in the abundance of wild type and mutant Cyclin F-mCherry. Densitometry analyses followed by comparing the ratio of RRM2 to Cyclin F-mCherry revealed a statistically significant ratio increase of RRM2 to mutant Cyclin F-mCherry (Figure 5B). This could have implications on SCF complex formation and interactions with its substrates.

Given that Cyclin F forms part of an E3 ubiquitin ligase complex, changes to global ubiquitination in mutant Cyclin F expressing cells was investigated. To do this, a pan-ubiquitin antibody was used to visualise ubiquitinated proteins from whole cell lysates of wild type and mutant Cyclin F-mCherry expressing cells. Densitometry showed that there were no significant differences in pan-ubiquitinated proteins between wild type and mutant Cyclin F-mCherry in Neuro-2A and NSC-34 cell lines at 24h (Figure 5C). This suggests that mutant Cyclin F-mCherry does not cause clear changes in protein ubiquitination and degradation at 24h.

3.3 Human cyclin F-mCherry abundance correlated with changes in RRM2 and TDP-43

In order to observe spatial and temporal changes of Cyclin F, RRM2 and TDP-43 (which translocates during ALS pathogenesis) transfected cells were harvested after 8, 24 and 48h post-transfection. The extent of cellular fractionation was determined by the presence or absence of the nuclear protein, Lamin A/C, and predominantly cytoplasmic protein, β-tubulin. Immunoblotting revealed that Lamin A/C was only found in nuclear fractions with no contamination in the cytoplasmic fraction. In addition, β-tubulin was clearly found in the cytoplasm and not in the nucleus (Figure 6A).

3.3.1 Human mutant cyclin F-mCherry was processed differently to human wild type Cyclin F-mCherry

Consistent with results shown in Figure 5A, wild type and mutant forms of Cyclin F-mCherry differ in abundance at 24h (Figure 6A). In addition, this trend is also clearly seen in the cytoplasm and nucleus of Neuro-2A cells. Spatial and temporal studies of Cyclin F-mCherry draw attention to the regulation of the upper and lower isoforms of Cyclin F (Figure 6B). At 8h, there is little difference in both isoforms of Cyclin F-mCherry. However, after 24h, the abundance of *cytoplasmic* Cyclin F-mCherry, especially the lower band, was significantly

lower in mutant Cyclin F-mCherry expressing cells when compared to the wild type control. A similar trend was also seen in the nuclear fraction, however the quantitation failed to be statistically significant. At 48h, both isoforms of Cyclin F-mCherry clearly drop in abundance. A drop in transgenic protein expression is expected due to the nature of transient transfections. Immunoblotting for Cyclin F-mCherry expression over time reveals that transgenic Cyclin F-mCherry is highly expressed at 8 and 24h.

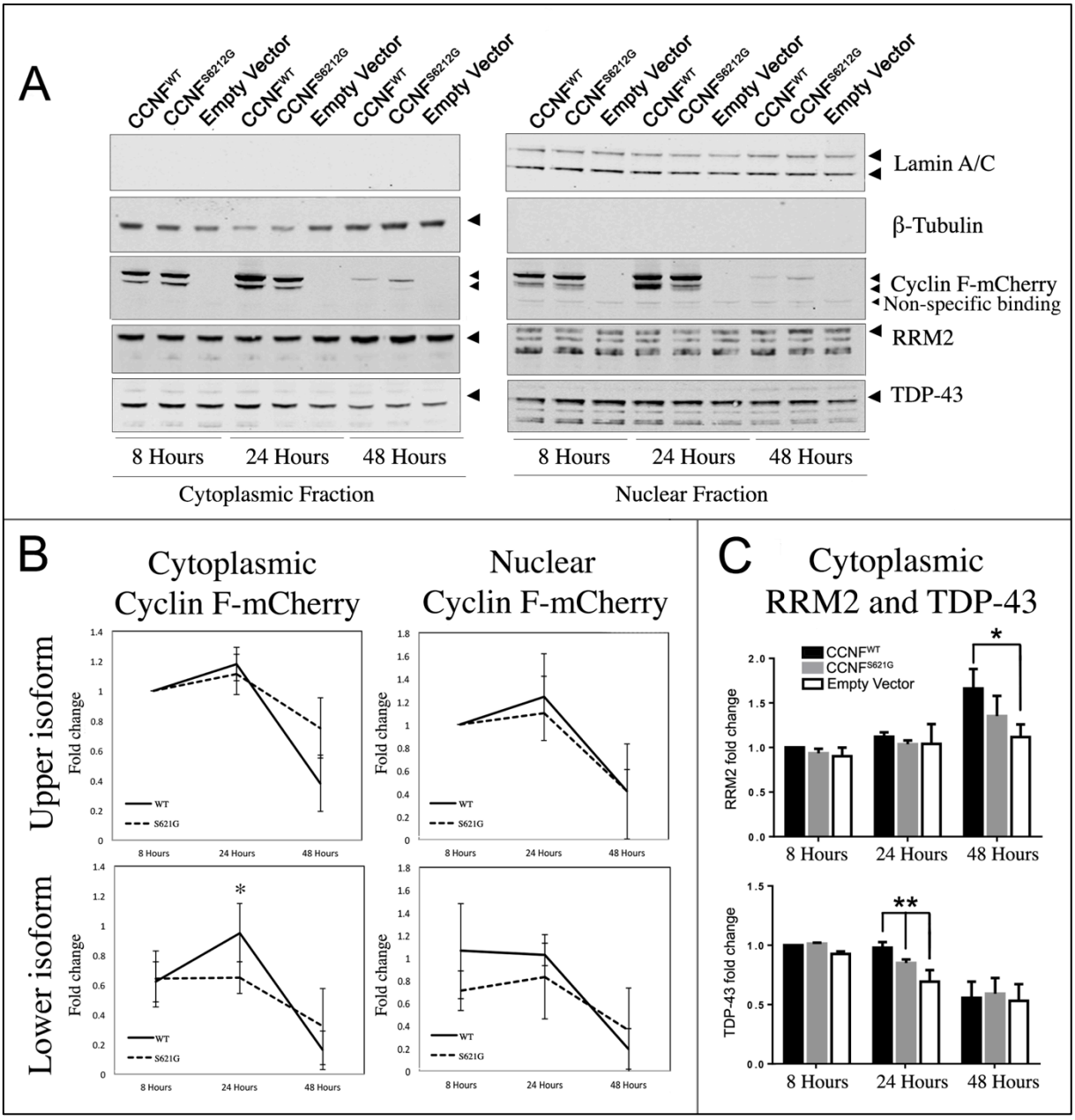

Figure 6. Nuclear and cytoplasmic fractionation of transfected Neuro-2A cells over 8, 24 and 48 hours post-transfection. **A.** Immunoblotting for Cyclin F, RRM2 and TDP-43 revealed protein abundance in the nucleus and cytoplasm of transfected Neuro-2A cells. **B.** Abundance of upper and lower transgenic Cyclin F isoforms in the cytoplasm and nucleus. **C.** ImageJ was used to determine TDP-43 and RRM2 fold changes in the cytoplasm of transfected cells. All images and statistics are representative of 3 independent experiments. Values depicted show mean ± SD.

3.3.2 TDP-43 and RRM2 levels were constant in the nucleus but not in the cytoplasm.

When observing the expression of TDP-43 and RRM2 in the nucleus and cytoplasm, there was an interesting difference in the number of bands representing each of these proteins. In the cytoplasm, there was a clear band representing both TDP-43 and RRM2 and the density of these bands varied over the time-course. In contrast, in the nuclear fraction, both TDP-43 and RRM2 had triplicate bands and the levels were consistent over the time-course (Figure 6A and C). The differences between the number of bands in the nucleus and cytoplasm may be due to differences in post-translational modifications in each location.

3.3.3 RRM2 levels decreased with expression of Cyclin F

When Cyclin F (WT)-mCherry protein abundance dropped at 48h, densitometry revealed a statistically significant increase in *cytoplasmic* RRM2, when compared to cells expressing the empty vector control (Figure 6C). A similar trend is seen in cells expressing Cyclin F (S621G)-mCherry, however these results are not statistically significant. Here, the abundance of Cyclin F (WT)-mCherry correlates with *cytoplasmic* RRM2 and may be due to interactions.

3.3.4 TDP-43 abundance increased with the expression of Cyclin F

As mentioned earlier, translocation of TDP-43 from the nucleus into the cytoplasm is a pathological feature of ALS. To identify any changes in TDP-43 translocation, TDP-43 was monitored by immunoblot in the cytoplasmic and nuclear fractions of transfected cell lysates (Figure 6A). There was no evidence to suggest the translocation of TDP-43 under the given conditions.

3.4 Proteomic characterisation of mutant Cyclin F

A label-free quantitative mass spectrometry study was used to identify changes in protein abundance that occurs alongside mutant Cyclin F-mCherry expression. Given that Cyclin F-mCherry was most clearly expressed at 8 and 24h, Neuro-2A cells were harvested at these time points and subjected to a to mass spectrometry work flow using biological triplicates as shown in Figure 7. Tryptic peptides were separated by nanoLC/MS using a 5600 TripleTOF mass spectrometer operated in IDA mode.

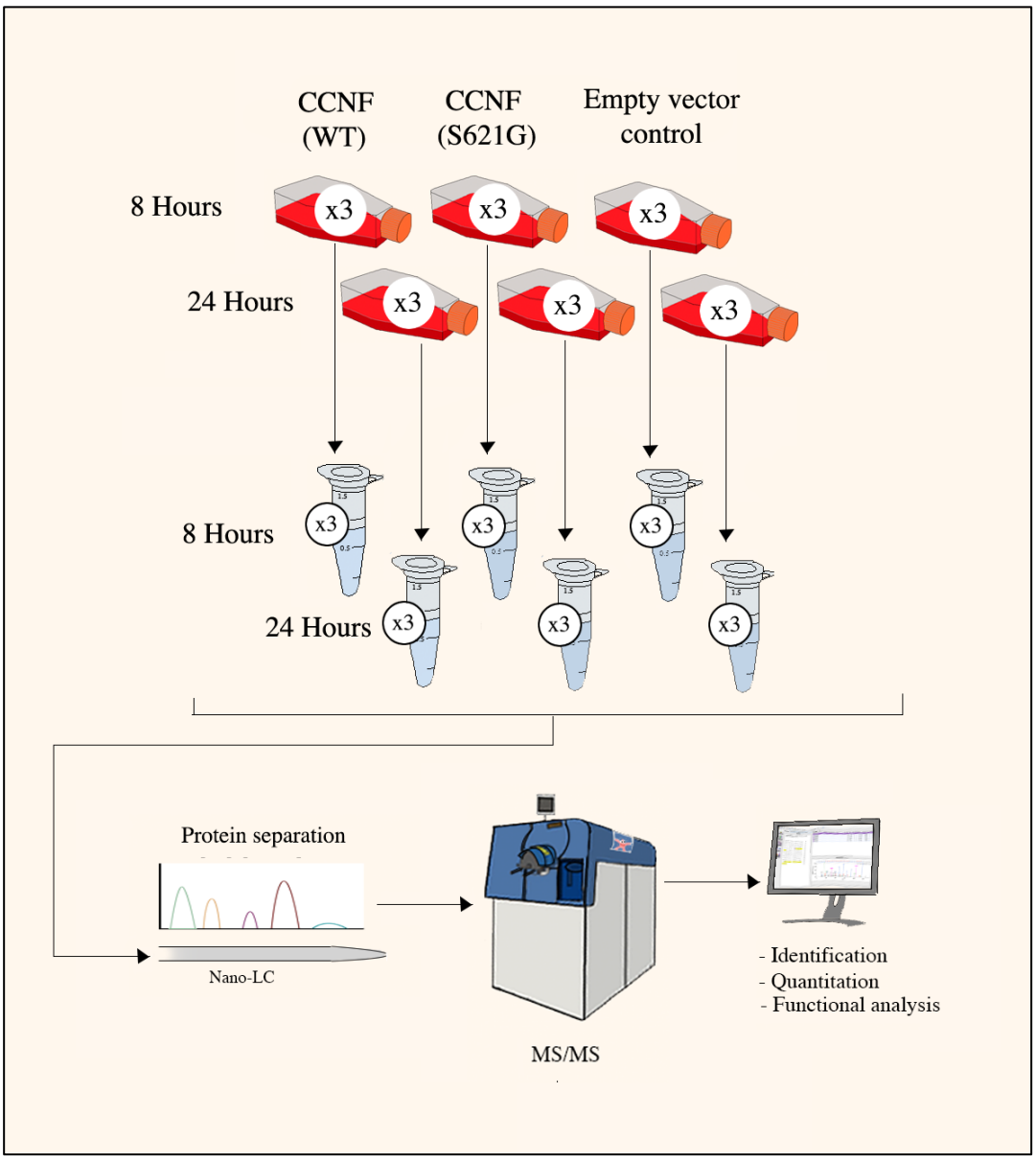

Figure 7. Proteomic workflow used to characterise Cyclin F-mCherry expression over time. Neuro-2A cells were transfected with *CCNF* (S621G)-mCherry, CCNF (WT)-mCherry or an empty vector control. Cells were harvested at 8 and 24 hours post-transfection. Whole cell lysates were obtained and subject to in-solution digests. Tryptic peptides were separated by nano-LC before analysing samples using a 5600 TripleTOF mass spectrometer (MS/MS). Spectra were used to identify peptides and proteins in each sample. Finally bioinformatics software, including DAVID and Ingenuity, were used to gain biological insight in to the effect of mutant Cyclin F-mCherry expression at each time point.

Table 2 shows that the average number of proteins and peptides found in all samples and triplicates was consistent. In total there were 1673 unique proteins at 1% FDR at the protein and peptide level.

Table 2. Number of proteins and peptides identified in empty vector, $CCNF^{WT}$ and $CCNF^{S621G}$ transfected cells over 8 and 24 hours post-transfection.

	Sample	Number of unique proteins	SD	Unique peptides above ion score cut off	SD	Number of proteins common to all three replicates
t=8h	Empty 1	1541		13089		
	Empty 2	1549		12465		
	Empty 3	1729		12437		
	Average	1606	± 106.3	12663	± 368.6	1385
	Wild Type 1	1753		13408		
	Wild Type 2	1619		12384		
	Wild Type 3	1606		11835		
	Average	1659	± 81.4	12542	± 798.4	1367
	Mutant 1	1685		12581		
	Mutant 2	1541		11299		
	Mutant 3	1602		11760		
	Average	1609	± 72.2	11880	± 649.4	1347
t=24h	Empty 1	1599		11832		
	Empty 2	1536		11725		
	Empty 3	1561		12034		
	Average	1565	± 31.7	11863	± 156.9	1349
	Wild Type 1	1560		11840		
	Wild Type 2	1714		12893		
	Wild Type 3	1752		13329		
	Average	1675	± 101.7	12687	± 765.5	1389
	Mutant 1	1719		12845		
	Mutant 2	1723		12636		
	Mutant 3	1716		12620		
	Average	1719	± 3.5	12700	± 125.5	1418

Spectral counting of peptides was used for quantitative comparisons. To identify proteins that were differentially expressed between wild type and mutant Cyclin F-mCherry expressing cells, a Students *t*-test was employed. Proteins were considered differentially expressed if spectral counts increased/decreased by at least 1.5-fold. Differences in protein abundance were considered significant if $p < 0.05$. At 8h, 29 proteins were differentially expressed between wild type and mutant Cyclin F expressing cells (Table 3). At 24h, 31 proteins were differentially expressed (Table 4). Empty vector transfected cells were also subject to this workflow to distinguish between expression changes due to transfections and changes due to Cyclin F-mCherry expression.

3.4.1 Differentially expressed proteins in mutant Cyclin F expressing cells

Table 3. Proteins that significantly changed in expression between $CCNF^{WT}$ and $CCNF^{S621G}$ transfected cells after 8h post-transfection. *Significantly different at 8 and 24 hours post-transfection.

Differentially expressed protein at 8 hours post-transfection	Accession number	Wild Type Average SpC + SD	Mutant Average SpC + SD	*p*-value (using lnNSAF)	Fold change (using NSAF)
Tropomodulin-3	TMOD3_MOUSE	0 ± 0.6	2 ± 0.6	0.048	↑ 2.8
Vesicle transport protein USE1	USE1_MOUSE	0 ± 0.6	2 ± 0.6	0.048	↑ 2.8
Integrin alpha-V	ITAV_MOUSE	0 ± 0.6	2 ± 0.6	0.047	↑ 2.7
PRA1 family protein 3	PRAF3_MOUSE	1 ± 0.6	4 ± 0	0.004	↑ 2.6
Ragulator complex protein LAMTOR1	LTOR1_MOUSE	1 ± 0.6	3 ± 1	0.036	↑ 2.0
Nipped-B-like protein	NIPBL_MOUSE	1 ± 0.6	3 ± 1	0.04	↑ 2.0
Sphingomyelin phosphodiesterase 4	NSMA3_MOUSE	1 ± 0.6	3 ± 0	0.026	↑ 2.0
Casein kinase II subunit beta	CSK2B_MOUSE	1 ± 0.6	3 ± 0.6	0.036	↑ 1.8
mRNA export factor 1	RAE1L_MOUSE	1 ± 0.6	3 ± 0.6	0.036	↑ 1.8
*Plasminogen activator inhibitor 1 RNA-binding protein	PAIRB_MOUSE	2 ± 0.6	4 ± 0	0.007	↑ 1.7
Mitochondrial import inner membrane translocase subunit Tim8 B	TIM8B_MOUSE	1 ± 0	2 ± 0	0	↑ 1.7
Calcium/calmodulin-dependent protein kinase type II subunit delta	KCC2D_MOUSE	2 ± 0	3 ± 0.6	0.014	↑ 1.6
39S ribosomal protein L46, mitochondrial	RM46_MOUSE	4 ± 0.6	6 ± 0.6	0.025	↑ 1.5
Multifunctional protein ADE2	PUR6_MOUSE	2 ± 1	0 ± 0	0.006	↓ 5.0
Eukaryotic translation initiation factor 1A, X-chromosomal	IF1AX_MOUSE	3 ± 1.2	0 ± 0.6	0.024	↓ 3.3
Casein kinase I isoform epsilon	KC1E_MOUSE	2 ± 0.6	0 ± 0.6	0.028	↓ 3.3
Synaptic vesicle membrane protein VAT-1 homolog-like	VAT1L_MOUSE	4 ± 1	1 ± 0.6	0.023	↓ 3.3
Protein arginine N-methyltransferase 1	ANM1_MOUSE	4 ± 1.2	1 ± 0	0.002	↓ 2.5

Apoptosis inhibitor 5	API5_MOUSE	5 ± 1	2 ± 1.2	0.029	↓ 2.5
Chloride intracellular channel protein 1	CLIC1_MOUSE	3 ± 1.2	1 ± 0	0.006	↓ 2.5
Eukaryotic translation initiation factor 3 subunit L	EIF3L_MOUSE	3 ± 1	1 ± 0	0.018	↓ 2.5
Peptidyl-prolyl cis-trans isomerase FKBP4	FKBP4_MOUSE	6 ± 1.2	3 ± 0.6	0.009	↓ 2.0
Proteasome subunit alpha type-6	PSA6_MOUSE	2 ± 0.6	1 ± 0	0.018	↓ 2.0
26S proteasome non-ATPase regulatory subunit 2	PSMD2_MOUSE	3 ± 1.2	1 ± 0.6	0.049	↓ 2.0
Threonine--tRNA ligase, cytoplasmic	SYTC_MOUSE	3 ± 1	1 ± 0.6	0.048	↓ 2.0
F-actin-capping protein subunit alpha-2	CAZA2_MOUSE	3 ± 0.6	2 ± 0.6	0.045	↓ 1.7
Eukaryotic translation initiation factor 2 subunit 2	IF2B_MOUSE	5 ± 0.6	2 ± 0.6	0.005	↓ 1.7
Lupus La protein homolog	LA_MOUSE	8 ± 1	4 ± 1.2	0.044	↓ 1.7
S-phase kinase-associated protein 1	SKP1_MOUSE	2 ± 0.6	1 ± 0	0.004	↓ 1.7

Table 4. Proteins that significantly changed in expression between $CCNF^{WT}$ and $CCNF^{S621G}$ transfected cells after 24h post-transfection. *Significantly different at 8 and 24 hours post-transfection.

Differentially expressed protein at 24 hours post-transfection	**Accession number**	**Wild Type Average SpC + SD**	**Mutant Average SpC + SD**	***p*-value (using lnNSAF)**	**Fold change (using NSAF)**
DnaJ homolog subfamily B member 1	DNJB1_MOUSE	0 ± 0	2 ± 0.6	0.001	↑ 4.3
WD repeat-containing protein 74	WDR74_MOUSE	0 ± 0	2 ± 1.2	0.01	↑ 4.3
Phenylalanine—tRNA ligase alpha subunit	SYFA_MOUSE	1 ± 0.6	3 ± 1	0.043	↑ 3.0
Inorganic pyrophosphatase 2	IPYR2_MOUSE	1 ± 0.6	4 ± 0	0.005	↑ 2.5
60S ribosomal protein L31	RL31_MOUSE	1 ± 0.6	4 ± 0.6	0.011	↑ 2.3
Ferrochelatase, mitochondrial	HEMH_MOUSE	1 ± 0	3 ± 1.2	0.031	↑ 2.1
Alpha-soluble NSF attachment protein	SNAA_MOUSE	3 ± 1.2	7 ± 1	0.027	↑ 2.0
Peptidyl-prolyl cis-trans isomerase FKBP9	FKBP9_MOUSE	2 ± 0.6	3 ± 0.6	0.045	↑ 1.8

SWI/SNF complex subunit SMARCC1	SMRC1_MOUSE	2 ± 0.6	3 ± 0.6	0.039	↑ 1.8
GPI-anchor transamidase	GPI8_MOUSE	1 ± 0	2 ± 0	0	↑ 1.7
Up-regulated during skeletal muscle growth protein 5	USMG5_MOUSE	2 ± 0.6	4 ± 1.2	0.047	↑ 1.7
Procollagen-lysine,2-oxoglutarate 5-dioxygenase 3	PLOD3_MOUSE	10 ± 1.5	17 ± 2.1	0.012	↑ 1.6
Histone deacetylase 2	HDAC2_MOUSE	3 ± 0.6	4 ± 0.6	0.034	↑ 1.5
ER membrane protein complex subunit 7	EMC7_MOUSE	2 ± 1	0 ± 0	0.004	↓ 5.0
Galectin-3-binding protein	LG3BP_MOUSE	2 ± 0.6	0 ± 0	0.001	↓ 5.0
UPF0556 protein C19orf10 homolog	CS010_MOUSE	2 ± 1.2	0 ± 0.6	0.046	↓ 3.3
Polynucleotide 5'-hydroxyl-kinase NOL9	NOL9_MOUSE	2 ± 0	0 ± 0.6	0.031	↓ 3.3
Src substrate cortactin	SRC8_MOUSE	3 ± 1.2	0 ± 0.6	0.025	↓ 3.3
Aladin OS=Mus musculus	AAAS_MOUSE	2 ± 0.6	1 ± 0	0.004	↓ 2.0
*Plasminogen activator inhibitor 1 RNA-binding protein	PAIRB_MOUSE	4 ± 1	2 ± 0.6	0.025	↓ 2.0
Paralemmin-1	PALM_MOUSE	3 ± 0.6	1 ± 0	0.004	↓ 2.0
26S proteasome non-ATPase regulatory subunit 8	PSMD8_MOUSE	2 ± 0.6	1 ± 0	0.005	↓ 2.0
Protein QIL1	QIL1_MOUSE	4 ± 1.5	2 ± 0	0.023	↓ 2.0
Syntaxin-binding protein 1	STXB1_MOUSE	4 ± 1.2	2 ± 0	0.015	↓ 2.0
Pinin	PININ_MOUSE	8 ± 2	5 ± 1.2	0.034	↓ 1.7
Polypyrimidine tract-binding protein 1	PTBP1_MOUSE	10 ± 1.2	6 ± 1	0.018	↓ 1.7
Protein transport protein Sec61 subunit gamma	SC61G_MOUSE	6 ± 0.6	3 ± 0.6	0.006	↓ 1.7
Nuclease-sensitive element-binding protein 1	YBOX1_MOUSE	8 ± 1.7	5 ± 1.2	0.04	↓ 1.7
Ribosome biogenesis protein BOP1	BOP1_MOUSE	4 ± 0.6	3 ± 0.6	0.027	↓ 1.4
NADH dehydrogenase [ubiquinone] 1 alpha subcomplex subunit 8	NDUA8_MOUSE	3 ± 0.6	2 ± 0	0.005	↓ 1.4
RuvB-like 2	RUVB2_MOUSE	8 ± 1.2	5 ± 0.6	0.011	↓ 1.4

3.4.2 Functional annotations and enrichments

Due to the limited data set, there was an under-representation of proteins involved in canonical pathways. To observe any biological functions representative of this data-set, DAVID statistical tools were used to identify over-represented gene ontology (GO) terms. Of the 60 differentially expressed proteins, 55 fell under one or more gene ontology (GO) term. Tables 5 and 6 show over-represented GO annotations for differentially expressed proteins at 8 and 24h.

Table 5. Gene Ontology categories that were over-represented at 8h post-transfection

Gene Ontology Term	Number of proteins	Percentage of total proteins	*p*-value
Translational initiation	3	11	0.002
Translation initiation factor activity	3	11	0.004
Translation factor activity, nucleic acid binding	3	11	0.010
Translation	4	14	0.018

Table 6. Gene Ontology categories that were over-represented at 24h post-transfection

Gene Ontology Term	Number of proteins	Percentage of total proteins	*p*-value
Intracellular organelle lumen	8	27	0.007
Organelle lumen	8	27	0.007
Nuclear lumen	7	23	0.008
Membrane-enclosed lumen	8	27	0.008
Nucleolus	4	13	0.026
Non-membrane-bounded organelle	8	27	0.092
RNA processing	4	13	0.041
RNA splicing	3	10	0.049

3.4.3 Urea-soluble fractions of lysates contained TDP-43

It was of interest to observe how mutant Cyclin F may affect proteins that are aggregating within the cell. Previous studies had used hydrogen peroxide and heat stress to induce TDP-43 positive aggregates within stress granules or the nucleus [70].

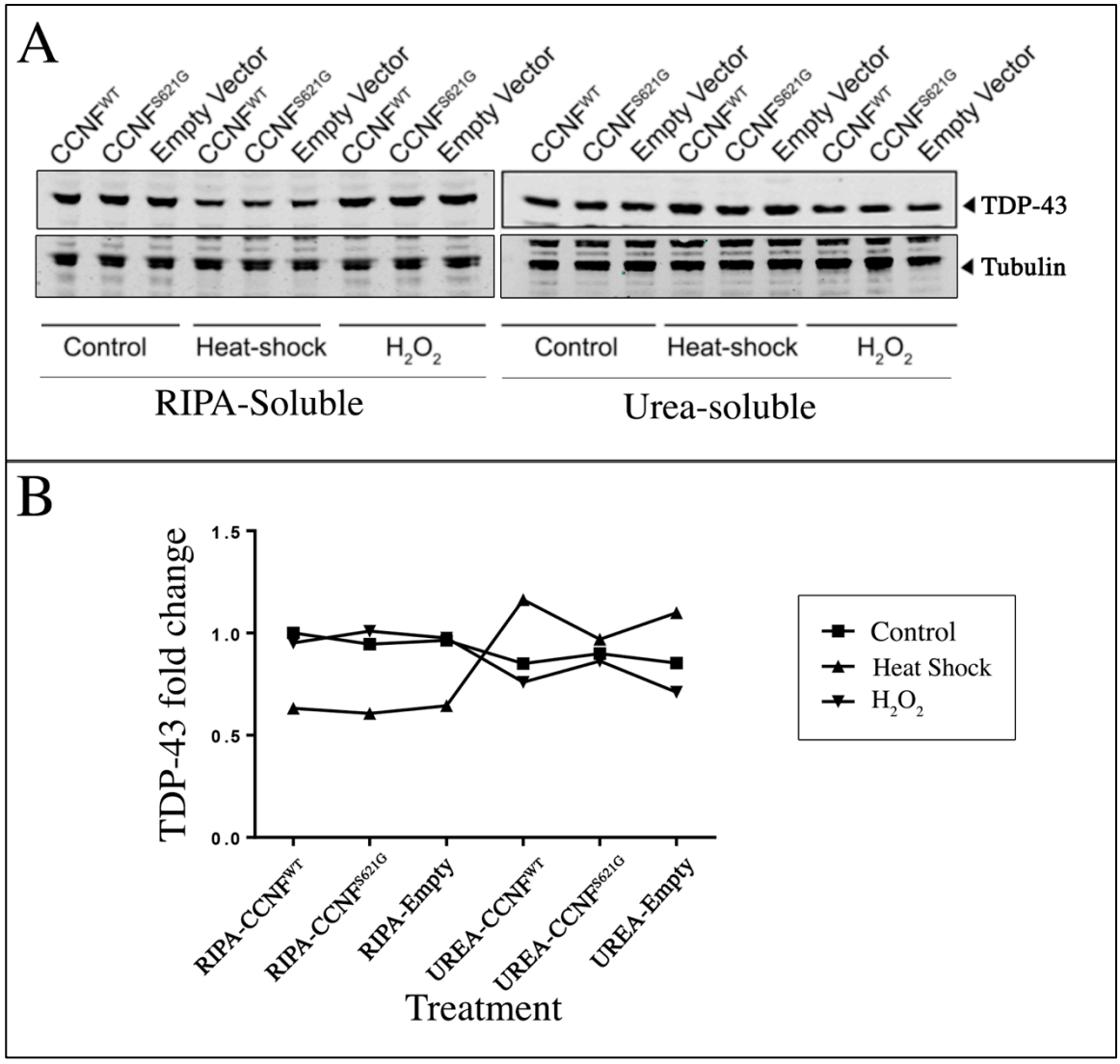

Figure 8. TDP-43 became more insoluble upon heat-stress **A.** Distribution of RIPA and Urea-soluble proteins in Cyclin F-mCherry transfected cells subject to heat shock and hydrogen peroxide stress at 24 hours post-transfection. As a control cells were not subject to stress at 24 hours post-transfection. Heat-shock; transfected cells were subject to 42°C for 1 hour. H_2O_2; transfected cells were subject to hydrogen peroxide for 2 hours. Cells were lysed and detergent-insoluble proteins were separated using centrifugation. Detergent-soluble (RIPA-soluble) and detergent-insoluble (Urea-soluble) fractions were subject to immunoblotting using the antibodies indicated. **B.** Densitometry using ImageJ was used to measure band density on immunoblots. Fold changes of TDP-43 abundance are plotted against TDP-43 levels in lane 1 of Fig. 8A.

Figure 8 shows that heat shock, at 24 hours post-transfection, leads to a change in TDP-43 solubility as it increases in the urea-soluble fractions. Immunoblotting also shows that after heat shock, slightly less TDP-43 became insoluble in mutant Cyclin F expressing cells compared to the control and empty vector expressing cells. In response to hydrogen peroxide however there was no increase in the abundance of TDP-43 compared to the untreated cells. Oxidative stress did not increase the amount of TDP-43 in these samples as expected, therefore heat shock conditions were chosen for further analysis. Urea-soluble proteins were examined using MS. In order to remove contaminating substances (ie. urea) lysates were separated by SDS-PAGE gel before cutting out each lane into 5 size-based fractions. In total, 30 fractions were analysed using a 2 hour LC-column gradient. After LC-MS/MS analysis, a total of 2882 unique proteins were discovered at 1% FDR at the protein and peptide level. This experiment was done only once due to time restrictions. In the future it would be useful to obtain additional biological replicates to conduct statistical analyses.

To identify proteins enriched in mutant Cyclin F-mCherry expressing cells, protein abundance was first normalised to account for protein length and total sample loaded. This was achieved by converting spectral counts to NSAF values. Proteins were considered enriched based on two criteria. Firstly, they had to increase at least 2-fold when comparing mutant and wild type Cyclin F-mCherry expressing cells. Secondly, they had to increase at least 2-fold when comparing mutant and empty vector Cyclin F-mCherry expressing cells. Using this process, 190 proteins were considered enriched in mutant Cyclin F-mCherry transfected cells. Another 64 were enriched in mutant Cyclin F-mCherry transfected cells also subject to heat-shock. A full list of proteins enriched in control and heat-stressed conditions are available in the supplementary section (Supplementary Tables 1 and 2). Proteins enriched in wild type Cyclin F-mCherry transfected cells were also identified (Supplementary Tables 3 and 4).

Notably, a subset of proteins enriched in mutant Cyclin F expressing cells are involved in proteostasis pathways. Tables 7 and 8 lists the identified proteins and shows that after heat shock there were fewer proteins enriched in mutant Cyclin F expressing cells that are involved with the ubiquitin-proteasome system.

Table 7. Urea-soluble proteins enriched in mutant Cyclin F-mCherry expressing cells that play key roles in the ubiquitin-proteasome pathway. **W:** Wild Type Cyclin F; **M:** Mutant Cyclin F, **SpC:** Spectral Count/s

GENE	PROTEIN	SpC (WT)	SpC (S621G)	RATIO: M/W	RATIO : M/E
PSMD9	26S proteasome non-ATPase regulatory subunit 9	1	3	2.26	3.05
CUL5	Cullin-5	1	8	6.79	4.57
CAND2	Cullin-associated NEDD8-dissociated protein 2	1	6	4.54	3.06
RBP2	E3 SUMO-protein ligase RanBP2	5	21	4.55	8.15
ARI1	E3 ubiquitin-protein ligase ARIH1	1	5	4.54	3.06
HUWE1	E3 ubiquitin-protein ligase HUWE1	3	11	4.53	12.23
UBR4	E3 ubiquitin-protein ligase UBR4	5	23	4.92	26.55
PSME2	Proteasome activator complex subunit 2	1	62	5.28	7.12
PSME3	Proteasome activator complex subunit 3	3	12	4.92	6.62
PSB3	Proteasome subunit beta type-3	1	4	3.02	4.06
ECM29	Proteasome-associated protein ECM29 homolog	1	8	6.81	2.30
LTOR1	'Ragulator' complex protein LAMTOR1	1	4	3.03	4.08
SAE2	SUMO-activating enzyme subunit 2	3	12	4.91	4.40
UBP7	Ubiquitin carboxyl-terminal hydrolase 7	1	4	3.79	5.09
UCHL3	Ubiquitin carboxyl-terminal hydrolase isozyme L3	1	5	4.54	2.03
UBP2L	Ubiquitin-associated protein 2-like	3	9	3.78	5.10
UBE2N	Ubiquitin-conjugating enzyme E2 N	1	6	5.30	2.38
UBE2O	Ubiquitin-conjugating enzyme E2 O	3	5	2.26	6.11

Table 8. Urea-soluble proteins enriched in mutant Cyclin F-mCherry expressing cells exposed to heat shock. These proteins play key roles in the ubiquitin-proteasome pathway. **W:** Wild Type Cyclin F; **M:** Mutant Cyclin F. **SpC:** Spectral Count/s

GENE	PROTEIN	SpC (WT)	SpC (S621G)	RATIO: M/W	RATIO: M/E
PSB3	Proteasome subunit beta type-3	5	20	3.75	2.56
PSMD9	26S proteasome non-ATPase regulatory subunit 9	1	3	2.24	3.44

Functional analysis was conducted for E3-ligases that were increasingly insoluble in mutant Cyclin F-mCherry expressing cells (Table 9). These proteins were found to play roles in several diverse cellular functions from base excision repair to transcriptional control.

Table 9. Functional summary of E3-ligases enriched in urea-soluble fractions of mutant Cyclin F expressing cells.

E3-ligase identified	Function	Known Substrates	Reference
E3 SUMO-protein ligase RanBP2	Transcriptional control.	HDAC4	[71]
E3 ubiquitin-protein ligase ARIH1	Protein translation.	EIF4E2	[72]
E3 ubiquitin-protein ligase HUWE1	Base excision repair, neural differentiation and proliferation.	MCL1, POLB (monoubiquitnation), p53, MYCN, CDC6	[73], [74]
E3 ubiquitin-protein ligase UBR4	Membrane and cytoskeletal organisation.	ACLY, STAT2	[75]

Given that several components of the ubiquitin-proteasome system increased after transfection, it was of interest to establish whether another major protein degradation system- the autophagy-lysosome system - was also affected in mutant cells. Immunoblotting for LC3-I and LC3-II which are classical markers of autophagy (Figure 9) revealed a slight increase of LC3-I in the mutant cells compared to control and wild type cells after transfection. In heat-shocked cells however there was an equal increase in LC3 isoforms in wild type and mutant cells but not in empty vectors suggesting added stress due to the overexpression of transgenic Cyclin F during heat-stress.

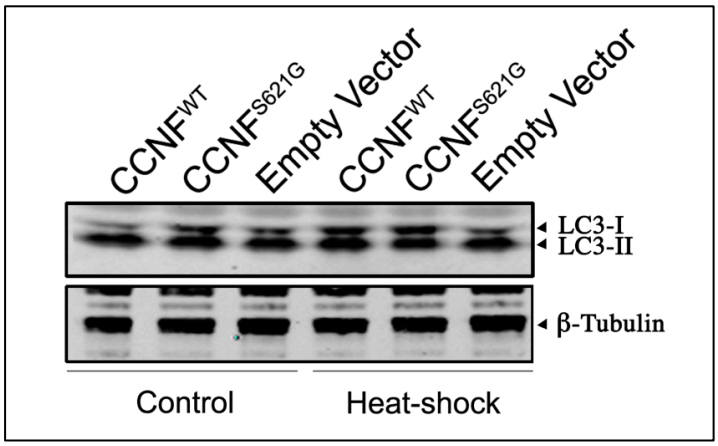

Figure 9. LC3-I increased in urea-soluble fractions of mutant Cyclin F expressing cells. Cells were transfected with $CCNF^{WT}$, $CCNF^{S621G}$ or empty vector controls. In control conditions, transfected cells were harvested at 24h post-transfection before cells were lysed in RIPA buffer and urea-soluble fractions were obtained. Western blots show an increase in LC3-I and II levels in mutant Cyclin F expressing cells under control conditions. In heat shock conditions, transfected cells were subject to heat shock for 1 hour at 42 °C before cell lysis and immunoblotting for LC3 isoforms. This reveals an increase in insoluble LC3-I in wild type and mutant Cyclin F expressing cells after heat shock.

3.4.4 Functional analysis of enriched urea-soluble proteins

Ingenuity pathway analysis (IPA) was used to identify canonical pathways represented by proteins enriched in urea-soluble fractions (Figures 10-13). Using this application, a Fisher exact test is used to determine over-represented pathways ($p < 0.05$) using proteins that have known functions. The pathways are ranked according to their *p*-value. The vertical orange line shows the significance threshold ($p = 0.05$) used. Ratios (orange boxes) represent the number of proteins from the data set over the number of proteins within the canonical pathway. Thus, the higher the ratio, the greater the representation of the data set in a canonical pathway. In most cases, enriched urea-soluble proteins represent a small ratio of canonical pathways. However, increasing insolubility could affect the involvement of these proteins within each pathway.

Analysis of the 190 proteins that were enriched in mutant Cyclin F-mCherry expressing cells in control conditions revealed 26 over-represented canonical pathways (Figure 10). Overall these pathways were involved in glucose and fatty acid metabolism and mitochondrial function hinting at the insolubility of components involved in energy production. The ubiquitin-proteasome pathway was also represented in mutant Cyclin F-mCherry expressing cells. In contrast, only 7 canonical pathways represented wild type Cyclin F-mCherry urea-soluble fractions. These pathways did not overlap with those seen in mutant Cyclin F-mCherry expressing cells and included heme degradation, endocytosis signaling and transcriptional repression signaling (Figure 11).

Analysis of the 64 proteins enriched in mutant Cyclin F-mCherry expressing cells subject to heat shock revealed 23 over-represented canonical pathways (Figure 12). The most significant pathway was EIF2 signalling which was complemented by regulation of eIF4 signalling and a few pathways involved in amino acid metabolism. When comparing these pathways to those represented in wild type Cyclin F-mCherry expressing cells, amino acid metabolism was implicated in both (Figure 13). Interestingly, the ubiquitin proteasome system was implicated in wild type Cyclin F-mCherry expressing cells but not in mutant Cyclin F-mCherry expressing cells subject to heat shock. Overall comparison between these pathways suggests that amino acid metabolism is affected during heat shock however, translation initiation proteins are increasingly insoluble in mutant Cyclin F-mCherry cells subject to heat shock.

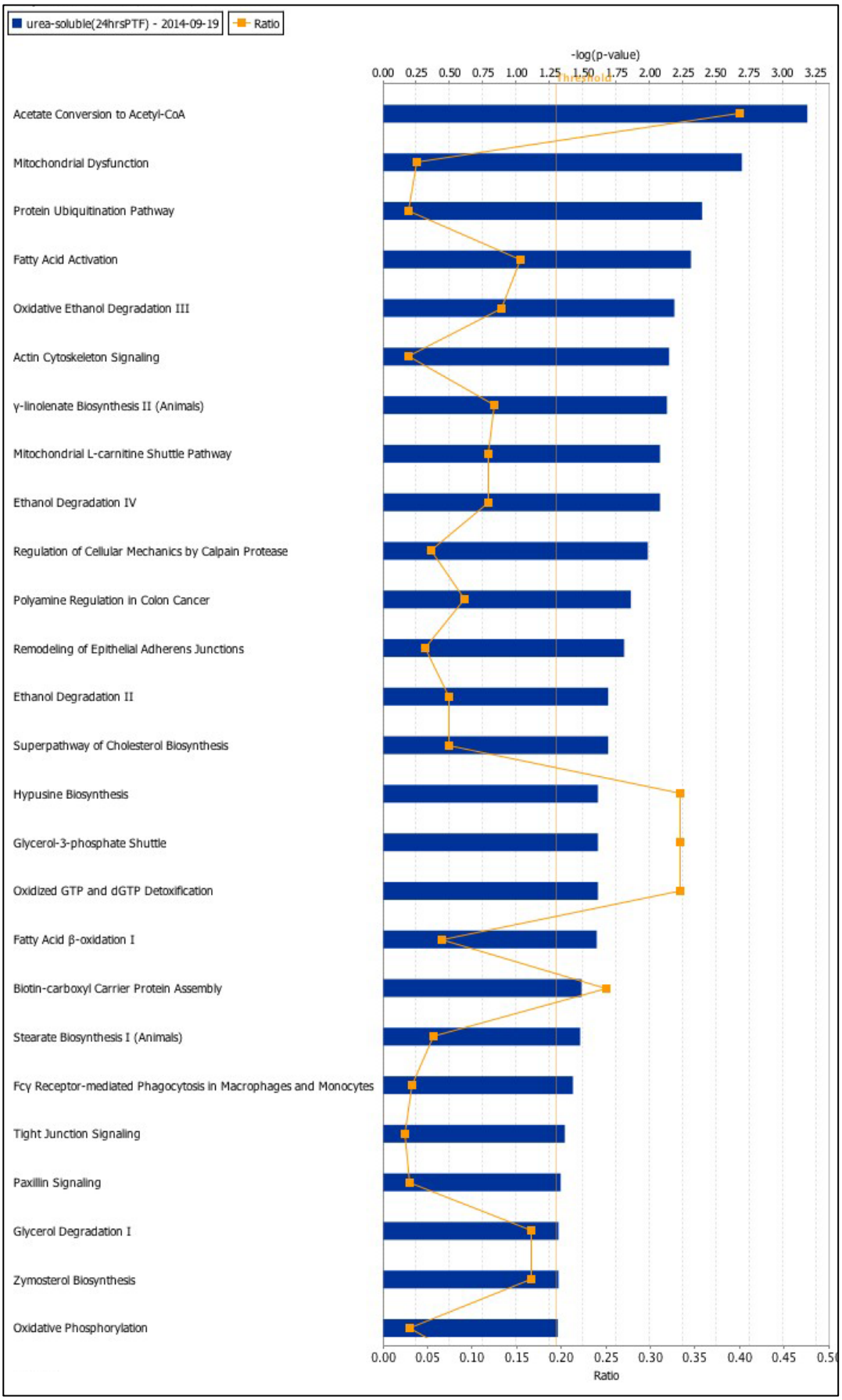

Figure 10. Ingenuity pathway analysis of the 190 urea-soluble proteins enriched in Cyclin F (S621G)-mCherry expressing cells.

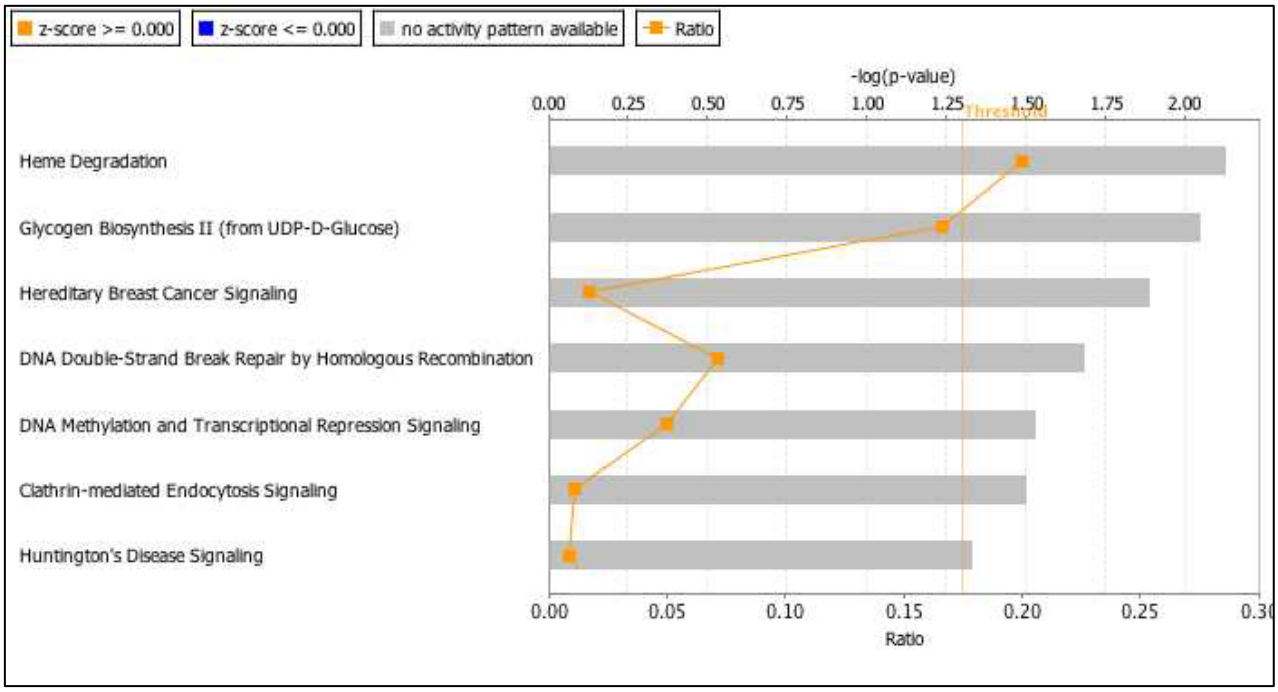

Figure 11. Ingenuity pathway analysis of the 30 urea-soluble proteins enriched in Cyclin F (WT)-mCherry expressing cells.

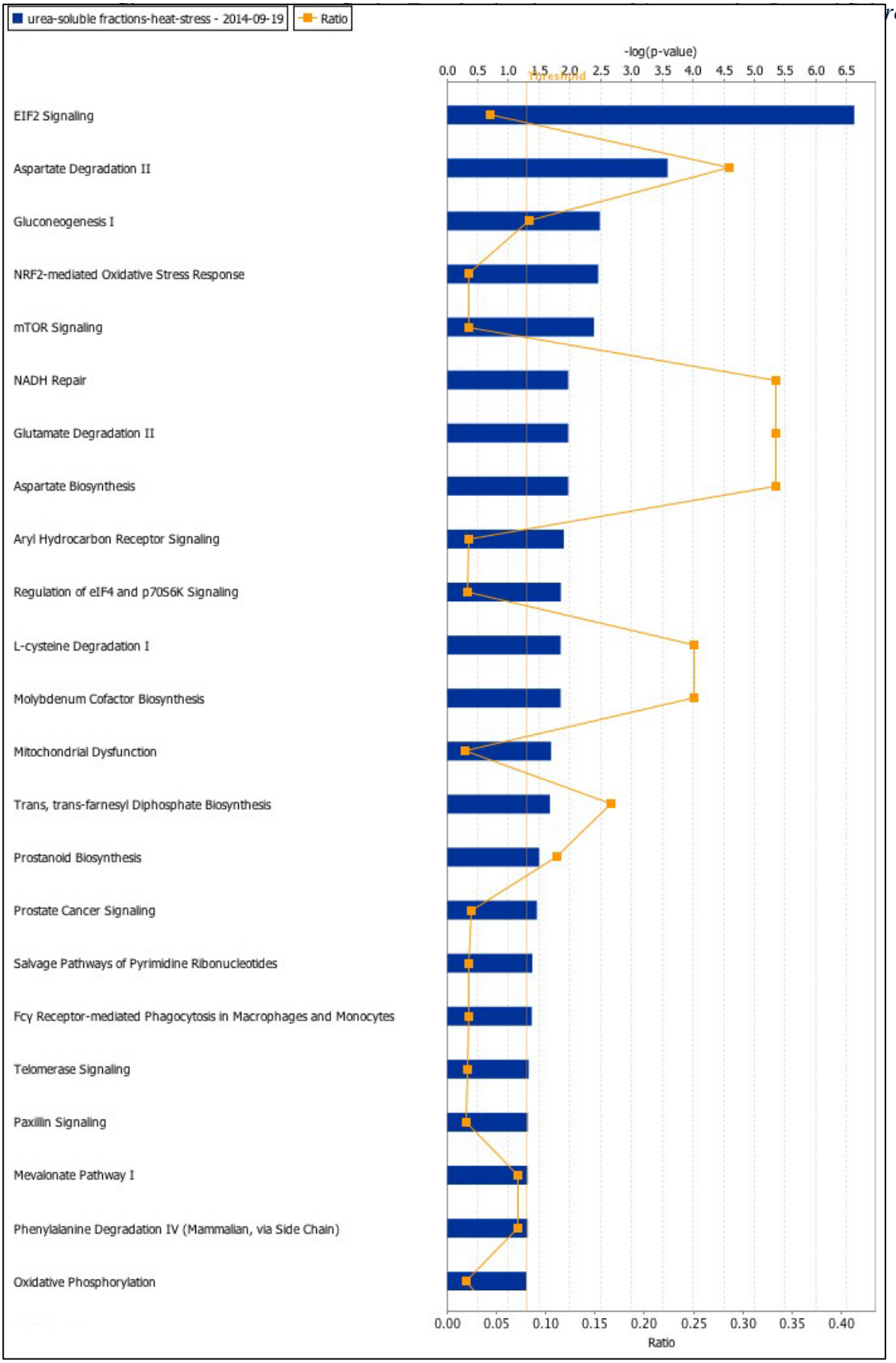

Figure 12. Ingenuity pathway analysis of the 64 urea-soluble proteins enriched in Cyclin F (S621G)-mCherry expressing cells also subject to heat shock.

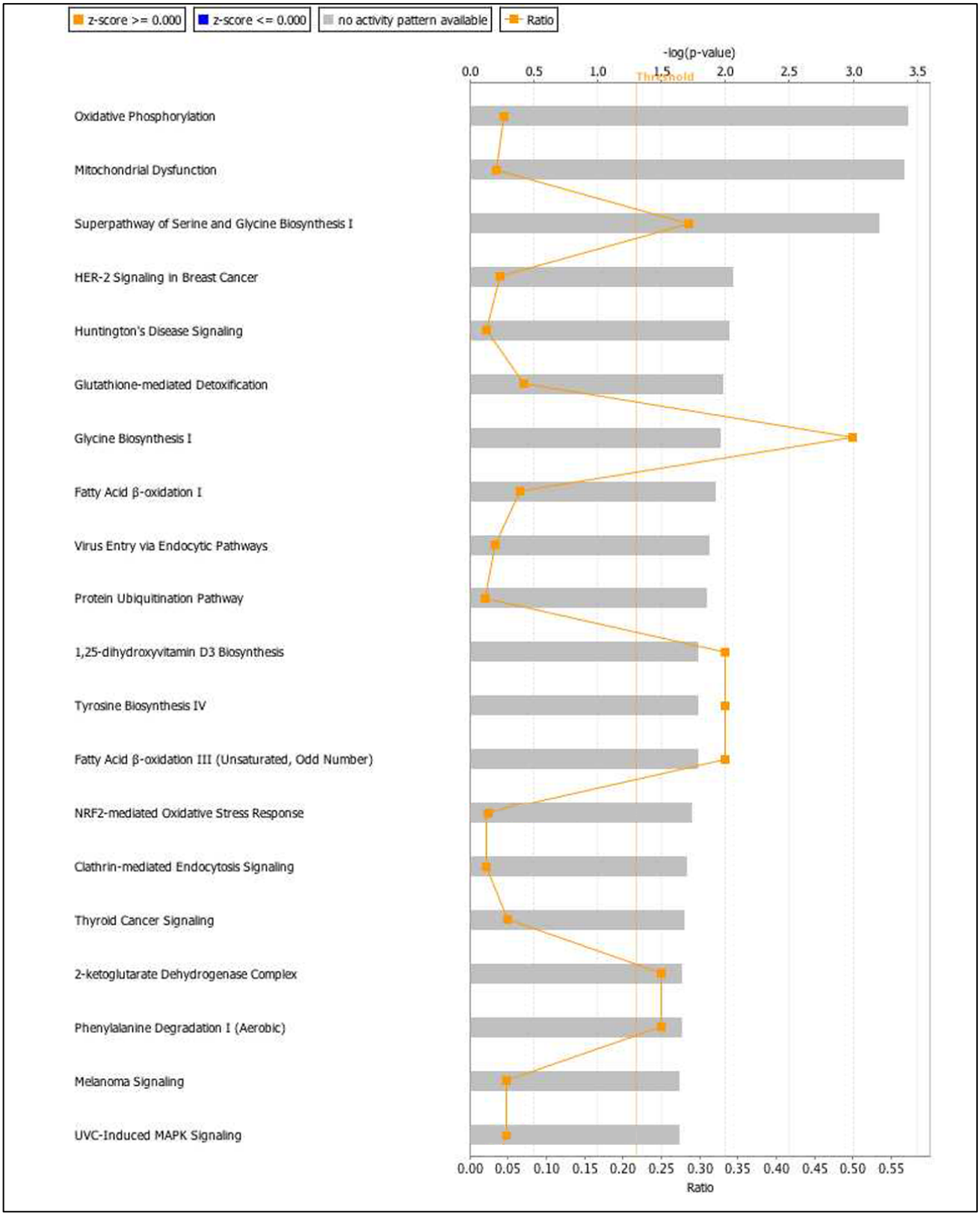

Figure 13. Ingenuity pathway analysis of the 121 urea-soluble proteins enriched in Cyclin F (WT)-mCherry expressing cells also subject to heat shock. The top 20 pathways are shown.

4 Discussion

The objective of this project was to investigate the effect of a novel missense mutation in the *CCNF* gene that is causative of familial ALS. Data obtained from biochemical studies as well as MS studies were designed to characterise the cellular proteome and urea-soluble fractions of transfected neuron-like cells. Data sets generated in these studies have been used to gain insight in to the biological processes influenced by *CCNF* (S621G).

4.1 Implications of Cyclin F-mCherry expression

The first aim was to determine the functional implications of the missense *CCNF* (S261G) mutation on the $SCF^{Cyclin\ F}$ complex. As mentioned earlier this complex plays essential roles in cell cycle progression as it ubiquitinates specific substrates for rapid proteolytic degradation in order to finely tune protein abundance required for cell cycle progression. At 24h, the abundance of mutant Cyclin F was lower than wild type Cyclin F in total cell lysates (Figure 5A). One possible explanation for the differences in expression could be unequal transfection efficiency. However, time course studies tracking the expression of wild type and mutant Cyclin F over 8, 24 and 48h showed that the abundance of wild type and mutant Cyclin F are equal at an early time point (8h) and only become significantly different after 24h (Figure 6A). This could indicate altered processing of Cyclin F at the protein level or altered mRNA stability. The serine to glycine missense mutation occurs within the PEST region of Cyclin F which makes the protein highly unstable [76]. The data generated for this thesis opens up the possibility that the mutation within the PEST sequence increases the instability of mutant Cyclin F-mCherry. It is unknown if Cyclin F abundance is also significantly lowered in the post-mortem tissue of ALS patients harbouring this mutation. If Cyclin F (S621G) was found to be increasingly unstable, it is possible that differences in Cyclin F (S621G) expression may also be observed in post-mortem tissue and may play a role in ALS pathogenesis. mRNA expression data would be useful for determining why the difference in abundance has occurred in experiments conducted for this thesis, especially because Cyclin F has a short half-life and a major determinant of protein abundance is transcriptional control and mRNA stability [76].

In these studies, flow cytometry revealed a transfection efficiency of around 73% (Figure 4A). This suggests that the majority of cells in these experiments express the construct of interest. At 24 and 48h however, the abundance of wild type and mutant Cyclin F-mCherry

vary. To account for these differences and obtain equal numbers of wild type and mutant Cyclin F-mCherry expressing cell populations, cells could first be sorted based on mCherry fluorescence using flow cytometry. This is achievable using the mCherry constructs used in this study as shown by the easy distinction between transfected and non-transfected cells (Figure 4A).

In this study, Cyclin F-mCherry is transiently over-expressed at 8 and 24h. Overexpression studies conducted by Fung *et al* show that elevated Cyclin F causes an accumulation of cells at the G_2/M stage of the cell cycle and this effect is increased in cells expressing Cyclin F without PEST sequences [76]. This suggests that the prolonged expression of Cyclin F interferes with cell cycle progression. In future studies it will be useful to determine cell cycle stages by flow cytometry and correlate this with the observation of lower Cyclin F abundance at 24h post-transfection (Figure 5A).

4.2 Human cyclin F-mCherry may regulate RRM2 abundance in the cytoplasm

Cyclin F is known to regulate the amount of RRM2 through ubiquitin-mediated proteolysis. When Cyclin F is expressed, RRM2 is degraded and abundance decreases. Conversely, when Cyclin F abundance decreases, RRM2 is allowed to accumulate in the cell [43]. This trend is seen in the cytoplasm of human Cyclin F (WT)-mCherry transfected Neuro-2A cells over time (Figure 6A). At 8 and 24h, both wild type and mutant Cyclin F-mCherry are overexpressed. During this time, RRM2 does not change in abundance nor is it affected by the differences between the overall abundance of wild type and mutant Cyclin F-mCherry. At 48h however, wild type and mutant Cyclin F-mCherry abundance drop and this is correlated with an increase in *cytoplasmic* RRM2 abundance (Figure 6A). Figure 6C demonstrates a significant increase in *cytoplasmic* RRM2 in cells expressing wild type Cyclin F-mCherry compared to the empty vector control. This was determined by densitometry of Figure 6A and suggests that human Cyclin F (WT)-mCherry expression may indeed influence the amount of endogenous RRM2 in the cytoplasm of Neuro-2A cells in a way consistent with the literature. It is important to note that during these experiments, endogenous Cyclin F is also expressed however, it is expressed at low levels compared to over-expressed human Cyclin F-mCherry.

The potential interaction between human wild type Cyclin F and RRM2 is not observed in the nucleus of transfected cells. The amount of *nuclear* RRM2 remains consistent throughout the time course (Figure 6A) suggesting fine control over subcellular localisation and abundance

of RRM2 in the nucleus where it is required to perform important roles in managing and protecting against DNA damage by keeping the pool of dNTPs balanced [43]. It is known that after a cell is subject to DNA damage, Cyclin F abundance decreases in order to allow a build up of RRM2 in the nucleus in order to manage DNA damage [41]. Data shown in this thesis however does not show this trend in the nucleus as the abundance of RRM2 is consistent throughout the time course even though *nuclear* wild type and mutant Cyclin F-mCherry abundance fluctuates over time and are differentially expressed at 24h. Together this data suggest that DNA damage has not occurred within cells transiently expressing mutant Cyclin F-mCherry over 48 hours and that fine control over RRM2 abundance in the nucleus is not affected by Cyclin F-mCherry over this time course. The idea that DNA damage had not occurred due to mutant Cyclin F-mCherry, as expected, is reiterated by the fact that RRM2 did not appear to translocate into the nucleus at any point [41].

To complement the trends seen in RRM2 and Cyclin F-mCherry abundance, data generated in collaboration with Dr. Albert Lee goes on to demonstrate that after pulling down ubiquitinated proteins from Neuro-2A whole cell lysates (generated from the studies mentioned in this thesis) there is a greater amount of RRM2 that was ubiquitinated or associated with ubiquitinated proteins in mutant Cyclin F-mCherry expressing cells at 24h. Together these results demonstrated that the mutation may not affect the abundance of RRM2 however increased ubiquitination implicates ubiquitin-ligase activity or degradation of ubiquitinated $SCF^{Cyclin\ F}$ substrates. Additional evidence for a change in ubiquitin ligase activity could be gained by using an E1-E2-E3 ubiquitin ligase activity kit to directly measure any differences in activity between wild type and mutant $SCF^{Cyclin\ F}$ complexes. Furthermore, other known substrates of $SCF^{Cyclin\ F}$ may be observed and checked for increased ubiquitination.

When looking at the expression patterns of upper and lower isoforms of Cyclin F-mCherry, it remains unclear if the smaller molecular weight Cyclin F isoform contributes toward $SCF^{Cyclin\ F}$ activity. At 8 and 24h, and in both cytoplasmic and nuclear fractions, the higher molecular weight isoform of wild type and mutant Cyclin F-mCherry are equal in abundance (Figure 6B). In contrast, the lower molecular weight isoform is less abundant in mutant Cyclin F-mCherry expressing cells after 24h (Figure 6A and 6B). It may be the case that the upper isoform of Cyclin F is responsible for maintaining levels of *cytoplasmic* RRM2 at 8 and 2h. This could explain the consistent abundance of *cytoplasmic* RRM2 at 8 and 24h post-transfection despite fluctuating levels of total Cyclin F-mCherry. In order to identify whether

both bands correspond to Cyclin F and to determine why Cyclin F-mCherry has an upper and lower isoform, pull-downs of Cyclin F could be conducted. Co-immunoprecipitating proteins may then be separated using SDS-PAGE and individual bands excised for analysis by MS. The two bands could also be individually excised from a gel and analysed by MS to identify reasons for their differing molecular weights.

Two E3-ligases are known to ubiquitinate RRM2; $SCF^{Cyclin\ F}$ and APC/C^{Cdh1}. Cell cycle analysis would be helpful in determining which E3-ligase is responsible for regulating RRM2 activity as APC/C^{Cdh1} is known to target RRM2 during G1 of the cell cycle whilst $SCF^{Cyclin\ F}$ targets RRM2 during G2 [45]. Unlike Cdh1, Cyclin F binds to RRM2 using a hydrophobic CY (RxL) motif. Prior to the formation of this protein-protein interaction RRM2 is phosphorylated at threonine 33 (Thr 33) in order to induce a conformational change that exposes this CY motif at residues 49-51 for binding [41]. Non-phosphorylated RRM2 (Thr33) on the other hand, prevents interaction between RRM2 and Cdh1. Thus, to confirm that $SCF^{Cyclin\ F}$ is responsible for the ubiquitination of RRM2, cell cycle analysis and immunoblotting for phosphorylated RRM2 (Thr 33) could be conducted.

4.3 TDP-43 did not translocate into the nucleus or become increasingly insoluble in mutant Cyclin F expressing cells

Translocation of TDP-43 from the nucleus into the cytoplasm is typical of ALS pathology and occurs prior to or during TDP-43 aggregation in the cytoplasm [48]. By immunoblotting for TDP-43 in nuclear and cytoplasmic fractions of transfect Neuro-2A cells, translocation events could be monitored. Over the time-course, the amount of TDP-43 decreased slightly in the nucleus and in the cytoplasm (Figure 6A) suggesting that it did not translocate but rather decreased in overall abundance. One possibility for the lack of TDP-43 translocation is due to the fact that this study monitors proteins over a relatively short time frame of up to 48h post-transfection. In future studies it may be necessary to examine TDP-43 translocation over extended time frames. A similar observation is seen in differentiated Neuro-2A and COS1 cells transfected with wild type and mutant *TARDBP*. Transient expression of these proteins for up to 72h reveal that all forms of TDP-43 remain nuclear even though the mutations of interest occurred in the aggregate-prone domain. In rare cases, diffuse cytosolic labelling of mutant and wild type TDP-43 were observed at 72h post-transfection [49]. In another study conducted using primary neurons, transient expression of wild type and mutant TDP-43 tagged with GFP revealed translocation of mutant forms of TDP-43 just after 24h post-

transfection. Under these conditions, TDP-43 aggregation was not observed suggesting that translocation occurs prior to aggregation in the cytoplasm [77]. Given that TDP-43 aggregates are observed in post-mortem tissue of ALS patients harbouring the *CCNF* (S621G) mutation (unpublished data), cell culture conditions can be optimised in order to observe the point at which translocation of TDP-43 occurs in mutant Cyclin F-mCherry expressing cells. This lack of TDP-43 translocation seen in this study suggests that changes in cellular functions are occurring prior to TDP-43 translocation and aggregation in the cytoplasm.

4.4 Investigating changes in the proteome occurring alongside wild type and mutant Cyclin F expression

In the second part of this study, two separate label free proteomics experiments were carried out using MS. This enabled (i) the identification of any changes in protein abundance that occurred alongside mutant Cyclin F expression, and (ii) identification of proteins enriched in urea-soluble aggregates of mutant Cyclin F expressing cells.

Proteome profiles as well as a list of differentially expressed proteins were obtained for Neuro-2A cells transfected with *CCNF* (WT)-mCherry, *CCNF* (S621G)-mCherry and an empty vector control 8 and 24h post-transfection. These were early time points at which Cyclin F-mCherry was clearly overexpressed in the cells (Figure 6A). This overarching and non-biased proteomics data provides valuable insight into some of the overall effects that occur alongside *CCNF* (S261G) expression. A second experiment exploring the detergent-insoluble aggregates of transfected cells is considered preliminary data (replicates are needed), but has proposed some interesting leads. Together, these experiments reveal some interesting biological events that occur alongside mutant Cyclin F-mCherry expression including altered RNA processing and changes in protein homeostasis. Based on the proteins identified in the insoluble fractions, attention has also been drawn to protein candidates that are potential aggregate-forming proteins during ALS pathogenesis.

4.5 RNA processing and protein translation were affected in mutant Cyclin F transfected cells

Altered RNA processing is an established mechanism involved in ALS pathogenesis. Differential expression studies and enriched urea-soluble protein data sets consistently hint at differences in RNA metabolism and protein processing in mutant Cyclin F-mCherry expressing cells.

4.5.1 Insight into altered RNA processing and protein translation provided by differential expression studies

Differential expression studies undertaken in this thesis revealed that <2% of proteins changed in expression at 8 and 24h using the criteria chosen. This indicates that samples were approximately identical at these time points. It is important to note that many of these are also low in abundance. In addition, some proteins that were differentially expressed were not detected in one condition, which means they were either not detected by the mass spectrometer or not present in the sample to begin with. However, GO annotations for differentially expressed proteins show statistically significant enrichment of GO annotations pertaining to translation initiation and RNA processing at 8 and 24h, respectively (Table 5 and 6). Given there was little change in protein levels at the examined time points, future studies would benefit by examining additional time points post-transfection to evaluate whether other proteins change in abundance.

At 8h post-transfection, differentially expressed proteins include eukaryotic translation initiation factor 3 subunit L (EIF3L), eukaryotic translation initiation factor 2 subunit 2 (IF2B), eukaryotic translation initiation factor 1A (IF1AX) and 39S ribosomal protein L46 (RM46). Eukaryotic translation initiation factors 1A, 2 and 3 are multi-unit complexes known to associate with the 40S ribosome and other factors to form the 43S translation pre-initiation complex. EIF2 complexes also assists in dissociating factors from the 43S complex to enable binding of the 60S ribosomal subunit [78]. Spectral counts for all of these proteins decreased modestly in mutant Cyclin F-mCherry expressing cells. In contrast 39S ribosomal protein increased by 1.5-fold in mutant Cyclin F-mCherry expressing cells. These results may have implications on the formation of the pre-initiation complex and ribosome function.

At 24h post-transfection, several proteins involved in pre-mRNA splicing were noted. These included pinin (PININ), polypyrimidine tract-binding protein 1 (PTBP1) and nuclease-sensitive element-binding protein 1 (YBOX1). Pinin decreased 1.7-fold in mutant Cyclin F expressing cells. Pinin is known to play a role in pre-mRNA splicing as it is a unit of the PSAP (Pinin, RNPS1 and SAP18) complex. PSAP has RNA and DNA-binding properties which facilitates RNA binding and precise regulation of intron excision within a subset of transcripts [79]. The formation and function of ribosomes was again implicated at this time point with a modest 1.4-fold decrease in ribosome biogenesis protein BOP1 (BOP1) and a 2.3-fold increase in 60S ribosomal protein L31 (RL31).

4.5.2 Insight into altered translational control provided by proteins enriched in urea-soluble fractions

IPA analysis of urea-soluble proteins that were enriched in mutant Cyclin F-mCherry expressing cells exposed to heat stress revealed a few canonical pathways related to translation initiation. The top-ranking pathway was EIF2 signaling (Figure 12). Although the ratio of proteins involved in this pathway was fairly low, it was complemented by pathways representing 'Regulation of eIF4 and p70S6K signaling' and 'mTOR signaling'. In contrast, there were no canonical pathways clearly involved in translation initiation in wild type Cyclin F-mCherry expressing cells. In both wild type and mutant Cyclin F-mCherry expressing cells, pathways involved in amino acid metabolism were found suggesting altered amino acid metabolism during heat-stress.

EIF2 signaling is a well-characterised canonical pathway. When the cell is under stress, this pathway regulates translation initiation [80]. It is interesting to see that this pathway is only implicated in mutant Cyclin F-mCherry expressing cells even though both wild type and mutant Cyclin F-mCherry expressing cells were subject to heat shock. mTOR signaling complements EIF2 signaling given that mTOR is a key regulatory protein that sits at the interface of several converging pathways to control a wide range of processes including protein translation, especially in response to stress [81]. Upon closer examination of urea-soluble proteins enriched in mutant Cyclin F-mCherry expressing cells, several initiation factors and ribosomal subunits were noted. In a study conducted by David *et al*, ribosomal units are prone to aggregate in models of *C. elegans* over the life-span of the organism. This suggested that ribosomal units are prone to aggregate, making it relevant to age-related diseases such as ALS. Furthermore, characterisation of TDP-43 aggregates undertaken by Dammer *et al* also showed increasing insolubility of several 60S ribosomal proteins within protein aggregates isolated in SOD1 ALS mice models.

In mutant Cyclin F-mCherry expressing cells that were not exposed to heat stress, there was a lack of canonical pathways involved with translational control. Instead, transcriptional repression and DNA methylation pathways were implicated. Together, this suggests that transcriptional control may be a processes affected during heat stress in mutant Cyclin F-mCherry expressing Neuro-2A cells.

4.6 Several components of the ubiquitin-proteasome pathway are regulated by mutant Cyclin F

Precise control of proteostasis is reliant on the function of both ubiquitin-conjugating systems, including the $SCF^{Cyclin\ F}$ complex, and the proteasome. Thus, changes in the expression or solubility of proteasome and ubiquitin-ligase components are of interest in this study.

4.6.1 Insight into altered proteostasis networks provided by differential expression studies

Overall, there was a decrease in spectral counts for proteins involved in proteostasis. At the earliest time point of 8h post-transfection, spectral counts for proteasome subunit alpha type-6 (PSA6) and 26S proteasome non-ATPase regulatory subunit 2 (PSMD2) decreased 2-fold in mutant Cyclin F-mCherry expressing cells. This could have implications on proteasome subunit assembly. In addition, spectral counts for S-phase kinase-associated protein 1 (SKP1), an integral component of SCF complexes decreased by 1.7-fold. SKP1 is responsible for attaching the F-box proteins, including Cyclin F, to other components of the SCF complex. Confirmed decreases in SKP1 abundance would therefore implicate the formation of several SCF complexes in the cell, including $SCF^{Cyclin\ F}$. Given that it also binds substrates to the SCF complex, decreased SKP1 abundance would also have implications on E3-ligase activity and control over substrate abundance.

At 24-hours post-transfection there was a 2-fold decrease in 26S proteasome non-ATPase regulatory subunit 8 (PSMD8) spectral counts. Overall, changes in proteasome subunit stoichiometry would have implications for subunit assembly and ultimately proteasome function.

4.6.2 Insight into altered proteostasis networks provided by proteins enriched in urea-soluble fractions

Observation of proteins in urea-soluble fractions revealed an increasing insolubility of several E2 and E3-ligases in mutant Cyclin F-mCherry expressing cells (Table 7). In addition, IPA revealed that the protein ubiquitination pathway is a statistically significant pathway represented in this data set and is not implicated in wild type Cyclin F-mCherry expressing cell (Figure 10 and 11). Literature-mining to determine the function of urea-soluble E3-ligases revealed their involvement in diverse biological processes from transcriptional control

to cytoskeleton remodelling. Two E3-ligases that stood out in the data set were E3-ligase HUWE and E3-ligase UBR4.

E3-ligase HUWE1 increased 4.53-fold when comparing mutant to wild type Cyclin F-mCherry expressing cells. Notably, it also increased 12.23-fold in respect to cells expressing the empty vector control. Like $SCF^{Cyclin\ F}$, HUWE1 can play a role in genome integrity, depending on the substrate ubiquitinated. HUWE1 is known to ubiquitinate DNA polymerase β (POLB) at Lys 41, Lys 61 and Lys 81 in order to facilitate degradation and maintain steady-state levels of base excision repair proteins. Knock down studies HUWE1 using siRNA leads to accumulation of POLB and increases DNA repair [82] This highlights its regulatory role in DNA damage and repair pathways. It is unclear why this E3-ligase has become increasingly insoluble in mutant Cyclin F-mCherry expressing cells. Perhaps co-localisation studies aimed at determining the spatial distribution of this protein in wild type and mutant Cyclin F-mCherry expressing cells would assist in understanding this.

E3-ligase UBR4 increased 4.92-fold when comparing mutant to wild type Cyclin F-mCherry expressing cells. It also increased 26.55-fold in respect to the empty vector control. UBR4 localises to the cytoplasm and nucleus where it perform different roles. In a study by Nakatani *et al*, immunolocalisation of UBR4 in the cytoplasm reveals cytoplasmic UBR4 concentration at cytoskeleton protrusion sites where is it required for ruffle formation, a process linked to cell-crawling activity. Within nuclear compartments, UBR4 is known to form a scaffold for chromatin assembly [83]. In terms of E3-ligase activity UBR4 is a N-recognin, which recognises N-degron degradation signals on substrate proteins. UBR4 E3-ligase activity has been implicated in neuronal excitability [84] and synaptic vesicle fusion [85]. It is unclear why UBR4 is increasingly insoluble in mutant Cyclin F-mCherry expressing cells. Again, co-localisation studies aimed at determining the spatial distribution of this protein in wild type and mutant Cyclin F-mCherry expressing cells would assist in understanding this.

Several proteasome subunits were also enriched in urea-soluble fractions of mutant Cyclin F-mCherry expressing cells (Table 7). In a study conducted by David *et al*, many proteasome subunits also became aggregate prone over the life span of *C. elegans*. One possible explanation for enriched proteasome subunits in mutant Cyclin F-mCherry expressing cells is an increasing association between proteasomes and ubiquitinated proteins. This would not indicate proteasome dysfunction however as the proteasome can remain functional even when

associated with ubiquitinated aggresomes [86]. Co-localisation studies between proteasomes and ubiquitinated proteins may shed light on this observation.

The ubiquitin-proteasome pathway and autophagy-lysosome pathways are functionally coupled and in the case of proteasome dysfunction, autophagy is known to manage protein degradation [87]. Autophagy is also known to clear away aggregated proteins in the cytosol [88]. Immunoblotting for classical markers of autophagy revealed a clear increase in the amount of LC3-I in urea-soluble fractions of mutant Cyclin F-mCherry expressing cells (Figure 9). Increased insolubility of LC3-I could affect the conjugation of this protein to phosphatidylethanolamine; a process that converts LC3-I to LC3-II during autophagy stimulation [87]. Studies conducted by Cherra *et al* have shown that LC3-I dephosphorylation enhances its recruitment to autophagosomes in SH-SY5Y cells and this is necessary for the formation of autophagosomes [89]. The inclusion of urea-soluble LC3-I in mutant-Cyclin F cells may suggest that the site of autophagosome formation may be close to insoluble cell components such as aggregates. LC3-II, which is a marker of autophagosome membranes, remained consistent in all conditions suggesting that there was no increase in the number of autophagosomes with insoluble aggregates under these conditions. Co-localisation studies showing the distribution of LC3-I, LC3-II and proteins that initiate autophagosome formation would provide more insight into this observation.

Overall, studies shown in this thesis reveal no clear indication of proteasome or lysosome dysfunction caused by mutant Cyclin F-mCherry. While total ubiquitin levels were unaffected by the missense mutation (Figure 5B), mutant Cyclin F expression occurred alongside increased insolubility of several E3-ligases and proteasome subunits. Taken together, mutant Cyclin F-mCherry may have an effect on the ubiquitin-proteasome network in general and may not only affect the function of $SCF^{Cyclin\ F}$. This raises the possibility that alterations to the ubiquitin-proteasome system could be detrimental over longer periods of time and be involved in the development of TDP-43 positive aggregates seen in the post-mortem tissue of patients carrying the $CCNF^{S621G}$ mutation.

4.7 Chaperones were not enriched in mutant Cyclin F expressing cells

Chaperone proteins play an important role in neurodegenerative diseases as they may refold or facilitate degradation of misfolded proteins in the cell.

4.7.1 Insight into chaperone function provided by differential expression studies

Overall there was an under-representation of heat shock proteins differentially expressed between wild type and mutant Cyclin F-mCherry expressing cells. At 8 hours however, the spectral counts for peptidyl-prolyl cis-trans isomerase (FKBP4) decreased 2-fold in mutant Cyclin F-mCherry expressing cells. FKBP proteins are known to play a role in several neurodegenerative diseases as they can dissociate aggregating proteins. For example, in prion-disease models, changes to Fkbp9 was found to play a key role in the process of prion propagation and clearance. mRNA knockdown of this protein, in cell lines susceptible to prion protein aggregation, caused a 21-fold increase of misfolded prion protein [90].

Spectral counts for DnaJ homolog subfamily B member 1 (DNJB) increased 4.3-fold in mutant Cyclin F-mCherry expressing cells after 24h post-transfection. DNJB is also known as heat-shock protein (Hsp) 40. When bound to Hsp 70 in yeast, Hsp 40 plays an important role in preventing aggregation of polyglutamine proteins into amyloid-like fibres [91].

4.7.2 Insight into chaperone function provided by proteins enriched in urea-soluble fractions

Data-sets in this study reveal an under-representation of molecular chaperones enriched in mutant Cyclin F-mCherry expressing cells. This under-representation occurred whether or not cells were exposed to heat-stress. It has been demonstrated previously however, that chaperones have transient interactions with substrates and do not form structural components of the refolded protein [92].

4.7.3 Proteasome and chaperone function in urea-soluble fractions

Cyclin F-mCherry expressing cells have been monitored over a short time frame. During this period, it may be the case that chaperones and the proteasome are effectively managing protein aggregation and abundance. This would help to explain why TDP-43 did not increase in urea-soluble fractions of mutant Cyclin F-mCherry expressing cells that were not exposed to heat-stress. To determine whether or not this is the case, proteasome inhibitor MG-132 could be used to prevent clearance of aggregating proteins. Comparison of urea-soluble TDP-43 abundance between wild type and mutant cells after this treatment could then be conducted using immunoblotting.

4.8 Changes to mitochondrial energy metabolism

Mitochondrial dysfunction has been established to be an early event and contributing factor to several motor neuron diseases including Parkinsons, Alzheimers disease and ALS with oxidative phosphorylation being essential for generating a large proportion of ATP in the cell [93]. It is not surprising that any changes to mitochondrial proteins could be catastrophic to the function of many cell types including neurons. In post-mortem tissue, the numbers of organelles can be reduced and reductions in respiratory chain activity have been noted. In this study we noted a few changes in protein abundances and biochemical properties that implicate cellular energy as a biological process that could be affected by mutant Cyclin F.

4.8.1 Insight into altered energy metabolism provided by differential expression studies

Inorganic pyrophosphatase 2 increased 2.5-fold in spectral counts after 24h post-transfection. This enzyme plays a role in several biochemical pathways including ATP synthesis. Therefore altered protein abundance could have implications for energy production within the cell. Another change was a 1.4-fold decrease in NADH dehydrogenase 1α subcomplex 8 (NDUA8) spectral counts. NDUA8 forms part of complex I of the mitochondrial electron transport chain. Decreases in abundance of this protein would affect assembly of the multi-subunit complex and ultimately influence the production of ATP within the cell.

4.8.2 Insight into altered energy metabolism provided by proteins enriched in urea-soluble fractions

In urea-soluble fractions, it was not surprising to see the presence of membrane-associated ATP synthase and cytochrome c oxidase subunits, however it was interesting to note enrichment of these subunits alongside Cyclin F-mCherry expression. Increasing insolubility of ATP synthase has not been seen in relevant studies. For instance, David *et al* found several units of ATP synthase in insoluble fractions of *C. elegans* but did not observe increasing insolubility with age. It has been shown however, that aggregating proteins in ALS can associate with mitochondria. For example, aggregated forms of TDP-43 increasingly associate with mitochondria. This correlates with altered mitochondrial morphology and density [94]. TDP-43 interaction with mitochondrial components is also demonstrated by Freibaum *et al* who have shown a few ATP synthase subunit are binding partners of TDP-43.

Although there was an enrichment of mitochondrial subunits in mutant Cyclin F-mCherry expressing cells, especially upon heat stress, it remains unclear whether or not these mitochondrial proteins associate with aggregating proteins in these experiments. To determine this, co-localisation studies in heat-stressed cells showing clear association between mitochondria and ubiquitinated aggregates could be conducted.

4.9 A closer look at aggregating proteins

There are two main groups of proteins that were of interest in this study and are potentially associating with aggregates. The first group of proteins of interest were the E3-ligases and proteasome subunits that were found enriched in mutant Cyclin F expressing cells. The second group of proteins are known to aggregate in other neurodegenerative diseases. As the E3-ligases have already been discussed, this next section will focus on proteins clearly involved in neurodegeneration.

4.9.1 Septins may be involved in ALS pathogenesis

Septin 2 and 8 represent strong candidates to follow up in validation studies. In the urea-fractions of heat-stressed cells, Septin 2 increased nearly 18-fold in mutant Cyclin F-mCherry expressing cells relative to the wild type control. Spectral counts indicated Septin 2 to be relatively abundant in the urea-soluble fractions of mutant Cyclin F expressing cells (Ranked 11 out of 63 proteins; Supplementary table 2). Within the urea-fractions of Neuro-2A cells that were not heat-stressed, Septin 8 increased 3.8-fold in mutant Cyclin F-mCherry expressing cells relative to the wild type control.

Septins are a family of evolutionarily conserved GTP-binding proteins of 30-65 kDa that form components of the cytoskeleton alongside actin and tubulin. In humans there are 13 different septins which assemble into heterohexamer and heterooctamer complexes to form large filaments, bundles and rings [95]. These higher-order structures can also associate with membranes, actin and microtubules to create large scaffolds that help carry out diverse biological processes. This is achieved by forming scaffolds for protein recruitment and forming barriers that create subcellular compartments. In relation to neuron functions, some septins have been found to promote dendrite and axon development and have an interaction with HDAC 6. For example, knock-down and knock-out studies of septin 7 in cerebrocortical neurons in mice result in impaired axon projections and production of dendrites. Furthermore,

septins have been shown to provide a scaffold that HDAC6 associates with in order to deacetylate microtubules [96].

Septins have been extensively associated with neurodegenerative disease including Alzheimers Disease and ALS. Septin 1, 2 and 4 are known to co-localise with neurofibrillary tangles in Alzheimers Disease [97]. Septin 11 has been previously enriched in urea-soluble fractions from FTLD-U post-mortem tissue. Characterisation of Septin 11 in FTLD-U tissue also revealed proteolytic cleavage at the N-terminal and co-localisation with stress fibres within affected brain regions of FTLD-U patients [98].

Structural studies of Septin 2 *in vitro* reveal that at increasing temperatures, Septin 2 undergoes conformational changes as it loses its helical structure (at 30°C) and takes on a β-sheet structure (at 45°C) [99]. This change may be involved in the aggregation of Septin 2 in ALS pathology as it has also been noted that in ageing *C. elegans*, aggregate prone proteins tend to have a significantly higher β asheet content than non-aggregated proteins. Given the involvement of septin aggregation in several motor neuron diseases, attention is also given to the increase in insoluble Septin 8 in mutant Cyclin F-mCherry expressing cells that were not subject to stress. Septin 8 is known to form part of the exocyst complex alongside septin 6. This exocyst complex is involved in vesicle targeting and docking events and is important for organising proteins on plasma membranes [95].

As mentioned earlier, *CCNF*(S621G) was associated with aberrant and truncated neuron phenotypes in zebrafish. Septins play an important role in the spatial organisation of filament networks and are involved in neuritogenesis. The increasing insolubility of these proteins in mutant Cyclin F-mCherry expressing cells could therefore alter filament and microtubule networks within the cell and contribute to aberrant neuron formation in zebrafish expressing mutant Cyclin F.

Overall, Septin 2 and 8 are likely to form aggregates in cells expressing mutant Cyclin F. Confirming the trend will involve repeating the experiment to obtain statistically relevant results followed by immunoblotting.

4.9.2 Cross-over with aggregating proteins identified in similar studies

There is limited cross-over between urea-soluble proteins identified in this study and similar studies in the literature. This may be due to differences in the cell models used or modes of stress. Studies conducted by David *et al* and Basso *et al* in ALS mouse models or *C. elegans* aging models however, also describe increasing insolubility of glycerol-3-phosphate dehydrogenase (GPDH) and glyceraldehyde-3-phosphate dehydrogenase (GAPDH). Within this study, both were enriched by 2.2-fold in Cyclin F-mCherry expressing cells. GAPDH is a particularly interesting candidate as it is known to also aggregate in Alzheimer's disease [100].

Unexpectedly, there was an under-representation of TDP-43 binding partners enriched in urea-soluble fractions of mutant Cyclin F-mCherry expressing cells. This may be due to the fact that equal amounts of TDP-43 aggregated under control conditions and less TDP-43 aggregated under heat shock conditions.

4.10 Limitations

One of the limitations to this work was the use of Neuro-2A cells. These neuron-like cells are immortalised, which means that they are dividing cells unlike neurons which are post-mitotic [101]. As a result, the changes we see during cell cycle progression may not be occurring in a primary neuron. The use of Neuro-2A cells is a pragmatic solution and represents a starting point for developing hypotheses. These will need to be tested in future studies using primary neurons, post-mitotic cells or animal models so that we can better understand the effect of the $SCF^{Cyclin\ F}$ within the brain.

Cyclin F and the various constructs were transiently expressed. On one hand, tracking the changes over periods longer than 48 hours would be ideal to see how the disease progresses over a longer time frame and leads to clear pathological features associated with ALS pathology. On the other hand, having over-expressed Cyclin F for a brief period highlights clearer relationships between Cyclin F-mCherry expression and changes in biological processes. This model therefore represents a useful starting point to identify key biological changes that are caused by mutant Cyclin F. Through the experiments conducted for this thesis, only subtle changes in protein abundance and solubility were observed in mutant cyclin F-mCherry expressing cells. Several possibilities exist including: CCNF plays only a minor role; our methods to detect changes had insufficient sensitivity; or the time points

examined were insufficient to allow sufficient protein expression. Therefore with the current data it is difficult to tell which groups and pathways are the most important players of ALS pathology.

When investigating contents of protein aggregates, the soluble fraction of lysates could also have been analysed by MS. This would reveal proteins that are being directed into the aggregates. This experiment would have been informative however it could not be done due to time limitations.

4.11 Future Directions

There are a couple of hypotheses that are developed from this work that could be explored in future studies. Firstly, the mutation occurring in the PEST sequence could increase mutant Cyclin F instability. Secondly, septin 2 and 8 are likely aggregating proteins in mutant Cyclin F expressing cells. Their increasing insolubility may lead to rearrangement of septin networks that ultimately alter neuron phenotypes.

It is unknown why wild type and mutant Cyclin F-mCherry abundance is significantly different at 24 hours post-transfection. The work carried out in this thesis raises the possibility that the stability of mutant Cyclin F or its mRNA transcript may be compromised. This has direct implications on the functionality of Cyclin F and cell cycle progression. It is therefore worth determining the reason for differing Cyclin F abundance in future experiments. As a start, mRNA transcripts for wild type and mutant Cyclin F-mCherry could be monitored over time and correlated with protein abundance data.

Septin 2 and 8 are high confidence candidates for follow up studies. Due to their integrated interactions with cytoskeletal components and synaptic vesicles, alterations that lead to the increased insolubility of these proteins is worth following up on. Co-localisation studies between Septin 2 or 8 with aggregates in heat-stressed cells or aggregates in ALS animal models would increase our confidence in this finding. Furthermore, inhibition and overexpression of septin 2 and 8 in animal models and consequent observation of neuron growth would also help to determine the role septin 2 or 8 plays in the phenotype seen in zebrafish.

4.12 Concluding remarks

In conclusion, this work has provided a framework for understanding how the novel S621G missense mutation may affect Cyclin F activity as well as its influence on cellular processes. This work has hinted at changes that are in agreement with ALS pathogenesis including alterations in RNA processing and proteostasis. In addition, characterising the urea-soluble fractions of transfected cells has shed light onto the pathogenesis of ALS in Cyclin F (S621G) expressing cells. In particular Septin 2 and 8 represent strong candidates that are likely involved in ALS pathogenesis and can be followed up in further studies.

5 References

[1] Boillée, S., Velde, C. V., Cleveland, D. W., ALS: A Disease of Motor Neurons and Their Nonneuronal Neighbors. *Neuron* 2006, *52*, 39-59.
[2] Cleveland, D. W., Rothstein, J. D., From Charcot to Lou Gehrig: deciphering selective motor neuron death in ALS. *Nat. Rev. Neurosci.* 2001, *2*, 806-819.
[3] A. Czaplinski, A. A. Yen, E. P. Simpson, Appel, S. H., Slower disease progression and prolonged survival in contemporary patients with amyotrophic lateral sclerosis: is the natural history of amyotrophic lateral sclerosis changing? *Arch. Neurol.* 2006, *8*, 1139-1143.
[4] Lillo, P., Hodges, J. R., Frontotemporal dementia and motor neurone disease: overlapping clinic-pathological disorders. *J. Clin. Neurosci.* 2009, *16*, 1131-1135.
[5] Chen, S., Sayana, P., Zhang, X., Le, W., Genetics of amyotrophic lateral sclerosis: an update. *Mol. Neurodegener.* 2013, *8*, 28.
[6] Turner, M. R., Hardiman, O., Benatar, M., Brooks, B. R.*, et al.*, Controversies and priorities in amyotrophic lateral sclerosis. *Lancer Neurol.* 2013, *12*, 310-322.
[7] Ling, S. C., Polymenidou, M., Cleveland, D. W., Converging mechanisms in ALS and FTD: disrupted RNA and protein homeostasis. *Neuron* 2013, *79*, 416-438.
[8] Verma, A., Altered RNA metabolism and amyotrophic lateral sclerosis. *Ann. Indian Acad. Neurol.* 2011, *14*, 239-244.
[9] Blokhuis, A. M., Groen, E. J., Koppers, M., van den Berg, L. H.*, et al.*, Protein aggregation in amyotrophic lateral sclerosis. *Acta Neuropathol.* 2013, *125*, 777-794.
[10] Leigh, P. N., Whitwell, H., Garofalo, O., Buller, J.*, et al.*, Ubiquitin-immunoreactive intraneuronal inclusions in amyotrophic lateral sclerosis. Morphology, distribution, and specificity. *Brain* 1991, *114 (Pt 2)*, 775-788.
[11] Ou, S. H., Wu, F., Harrich, D., Garcia-Martinez, L. F.*, et al.*, Cloning and characterization of a novel cellular protein, TDP-43, that binds to human immunodeficiency virus type 1 TAR DNA sequence motifs. *J. Virol.* 1995, *69*, 3584-3596.
[12] Ayala, Y. M., Zago, P., D'Ambrogio, A., Xu, Y. F.*, et al.*, Structural determinants of the cellular localization and shuttling of TDP-43. *J. Cell Sci.* 2008, *121*, 3778-3785.
[13] Maris, C., Dominguez, C., Allain, F. H., The RNA recognition motif, a plastic RNA-binding platform to regulate post-transcriptional gene expression. *FEBS J.* 2005, *272*, 2118-2131.
[14] Freibaum, B. D., Chitta, R. K., High, A. A., Taylor, J. P., Global analysis of TDP-43 interacting proteins reveals strong association with RNA splicing and translation machinery. *J. Proteome Res.* 2010, *9*, 1104-1120.
[15] Lagier-Tourenne, C., Cleveland, D. W., Rethinking ALS: the FUS about TDP-43. *Cell* 2009, *136*, 1001-1004.

[16] Rogelj, B., Easton, L. E., Bogu, G. K., Stanton, L. W.*, et al.*, Widespread binding of FUS along nascent RNA regulates alternative splicing in the brain. *Sci. Rep.* 2012, *2*, 603.
[17] Dewey, C. M., Cenik, B., Sephton, C. F., Johnson, B. A.*, et al.*, TDP-43 aggregation in neurodegeneration: are stress granules the key? *Brain Res.* 2012, *1462*, 16-25.
[18] Wolozin, B., Physiological protein aggregation run amuck: stress granules and the genesis of neurodegenerative disease. *Disc. Med.* 2014, *17*, 47-52.
[19] Newby, G. A., Lindquist, S., Blessings in disguise: biological benefits of prion-like mechanisms. *Trends Cell Biol.* 2013, *23*, 251-259.
[20] Li, Y. R., King, O. D., Shorter, J., Gitler, A. D., Stress granules as crucibles of ALS pathogenesis. *J. Cell Biol.* 2013, *201*, 361-372.
[21] Xie, W., Denman, R. B., Protein methylation and stress granules: posttranslational remodeler or innocent bystander? *Mol. Biol. Int.* 2011, *2011*, 137459.
[22] Sendtner, M., TDP-43: multiple targets, multiple disease mechanisms? *Nat. Neurosci.* 2011, *14*, 403-405.
[23] Barmada, S. J., Skibinski, G., Korb, E., Rao, E. J.*, et al.*, Cytoplasmic mislocalization of TDP-43 is toxic to neurons and enhanced by a mutation associated with familial amyotrophic lateral sclerosis. *J. Neurosci.* 2010, *30*, 639-649.
[24] Kabuta, T., Suzuki, Y., Wada, K., Degradation of amyotrophic lateral sclerosis-linked mutant Cu,Zn-superoxide dismutase proteins by macroautophagy and the proteasome. *J. Biol. Chem.* 2006, *281*, 30524-30533.
[25] Urushitani, M., Sato, T., Bamba, H., Hisa, Y.*, et al.*, Synergistic effect between proteasome and autophagosome in the clearance of polyubiquitinated TDP-43. *J. Neurosci. Res.* 2010, *88*, 784-797.
[26] Yamamoto, A., Simonsen, A., The elimination of accumulated and aggregated proteins: a role for aggrephagy in neurodegeneration. *Neurobiol. Dis.* 2011, *43*, 17-28.
[27] Adams, J., The proteasome: structure, function, and role in the cell. *Cancer Treat. Rev.* 2003, *29 Suppl 1*, 3-9.
[28] Kraft, C., Peter, M., Hofmann, K., Selective autophagy: ubiquitin-mediated recognition and beyond. *Nat. Cell Biol.* 2010, *12*, 836-841.
[29] Klionsky, D. J., Emr, S. D., Autophagy as a regulated pathway of cellular degradation. *Science* 2000, *290*, 1717-1721.
[30] Gal, J., Strom, A. L., Kilty, R., Zhang, F.*, et al.*, p62 accumulates and enhances aggregate formation in model systems of familial amyotrophic lateral sclerosis. *J. Biol. Chem.* 2007, *282*, 11068-11077.
[31] Hochstrasser, M., Ubiquitin signalling: what's in a chain? *Nat. Cell Biol.* 2004, *6*, 571-572.
[32] Lamark, T., Johansen, T., Aggrephagy: selective disposal of protein aggregates by macroautophagy. *Int. J. Cell Biol.* 2012, *2012*, 736905.
[33] Chin, L. S., Olzmann, J. A., Li, L., Parkin-mediated ubiquitin signalling in aggresome formation and autophagy. *Biochem. Soc. Trans.* 2010, *38*, 144-149.
[34] Garcia-Mata, R., Gao, Y. S., Sztul, E., Hassles with taking out the garbage: aggravating aggresomes. *Traffic* 2002, *3*, 388-396.
[35] Kong, M., Barnes, E. A., Ollendorff, V., Donoghue, D. J., Cyclin F regulates the nuclear localization of cyclin B1 through a cyclin-cyclin interaction. *EMBO J.* 2000, *19*, 1378-1388.
[36] Bai, C., Sen, P., Hofmann, K., Ma, L.*, et al.*, SKP1 connects cell cycle regulators to the ubiquitin proteolysis machinery through a novel motif, the F-box. *Cell* 1996, *86*, 263-274.
[37] Wei, D., Sun, Y., Small RING Finger Proteins RBX1 and RBX2 of SCF E3 Ubiquitin Ligases: The Role in Cancer and as Cancer Targets. *Genes Cancer* 2010, *1*, 700-707.

[38] D'Angiolella, V., Donato, V., Vijayakumar, S., Saraf, A.*, et al.*, SCF(Cyclin F) controls centrosome homeostasis and mitotic fidelity through CP110 degradation. *Nature* 2010, *466*, 138-142.
[39] Wu, K., Fuchs, S. Y., Chen, A., Tan, P.*, et al.*, The SCF(HOS/beta-TRCP)-ROC1 E3 ubiquitin ligase utilizes two distinct domains within CUL1 for substrate targeting and ubiquitin ligation. *Mol. Cell Biol.* 2000, *20*, 1382-1393.
[40] Wang, Z., Liu, P., Inuzuka, H., Wei, W., Roles of F-box proteins in cancer. *Nat. Rev. Cancer* 2014, *14*, 233-247.
[41] D'Angiolella, V., Esencay, M., Pagano, M., A cyclin without cyclin-dependent kinases: cyclin F controls genome stability through ubiquitin-mediated proteolysis. *Trends Cell Biol.* 2013, *23*, 135-140.
[42] Zheng, N., Schulman, B. A., Song, L., Miller, J. J.*, et al.*, Structure of the Cul1-Rbx1-Skp1-F boxSkp2 SCF ubiquitin ligase complex. *Nature* 2002, *416*, 703-709.
[43] D'Angiolella, V., Donato, V., Forrester, F. M., Jeong, Y. T.*, et al.*, Cyclin F-mediated degradation of ribonucleotide reductase M2 controls genome integrity and DNA repair. *Cell* 2012, *149*, 1023-1034.
[44] Emanuele, M. J., Elia, A. E., Xu, Q., Thoma, C. R.*, et al.*, Global identification of modular cullin-RING ligase substrates. *Cell* 2011, *147*, 459-474.
[45] D'Angiolella, V., Donato, V., Forrester, F. M., Jeong, Y.*, et al.*, The Cyclin F-Ribonucleotide Reductase M2 axis controls genome integrity and DNA repair. *Cell* 2012, *149*, 1023-1034.
[46] D'Angiolella, V., Donato, V., Vijayakumar, S., Saraf, A.*, et al.*, SCF(Cyclin F) controls centrosome homeostasis and mitotic fidelity through CP110 degradation. *Nature* 2010, *466*, 138-142.
[47] Raemaekers, T., Ribbeck, K., Beaudouin, J., Annaert, W.*, et al.*, NuSAP, a novel microtubule-associated protein involved in mitotic spindle organization. *J. Cell Biol.* 2003, *162*, 1017-1029.
[48] Xu, Z. S., Does a loss of TDP-43 function cause neurodegeneration? *Mol. Neurodegener.* 2012, *7*, 27.
[49] Kabashi, E., Lin, L., Tradewell, M. L., Dion, P. A.*, et al.*, Gain and loss of function of ALS-related mutations of TARDBP (TDP-43) cause motor deficits in vivo. *Hum. Mol. Genet.* 2010, *19*, 671-683.
[50] Yang, C., Wang, H., Qiao, T., Yang, B.*, et al.*, Partial loss of TDP-43 function causes phenotypes of amyotrophic lateral sclerosis. *Proc. Natl. Acad. Sci. U. S. A.* 2014, *111*, E1121-1129.
[51] Vanden Broeck, L., Callaerts, P., Dermaut, B., TDP-43-mediated neurodegeneration: towards a loss-of-function hypothesis? *Trends Mol. Med.* 2014, *20*, 66-71.
[52] Polymenidou, M., Cleveland, D. W., The seeds of neurodegeneration: prion-like spreading in ALS. *Cell* 2011, *147*, 498-508.
[53] Prusiner, S. B., Prions. *Proc. Natl. Acad. Sci. U. S. A.* 1998, *95*, 13363-13383.
[54] Udan-Johns, M., Bengoechea, R., Bell, S., Shao, J.*, et al.*, Prion-like nuclear aggregation of TDP-43 during heat shock is regulated by HSP40/70 chaperones. *Hum. Mol. Genet.* 2014, *1*, 157-170.
[55] Jucker, M., Walker, L. C., Self-propagation of pathogenic protein aggregates in neurodegenerative diseases. *Nature* 2013, *501*, 45-51.
[56] Nonaka, T., Masuda-Suzukake, M., Arai, T., Hasegawa, Y.*, et al.*, Prion-like properties of pathological TDP-43 aggregates from diseased brains. *Cell Rep.* 2013, *4*, 124-134.
[57] Neumann, M., Sampathu, D. M., Kwong, L. K., Truax, A. C.*, et al.*, Ubiquitinated TDP-43 in frontotemporal lobar degeneration and amyotrophic lateral sclerosis. *Science* 2006, *314*, 130-133.

[58] Farg, M. A., Soo, K. Y., Walker, A. K., Pham, H.*, et al.*, Mutant FUS induces endoplasmic reticulum stress in amyotrophic lateral sclerosis and interacts with protein disulfide-isomerase. *Neurobiol. Aging* 2012, *33*, 2855-2868.
[59] Liu, D., Liu, C., Li, J., Azadzoi, K.*, et al.*, Proteomic analysis reveals differentially regulated protein acetylation in human amyotrophic lateral sclerosis spinal cord. *PLoS One* 2013, *8*, e80779.
[60] Wang, J., Farr, G. W., Zeiss, C. J., Rodriguez-Gil, D. J.*, et al.*, Progressive aggregation despite chaperone associations of a mutant SOD1-YFP in transgenic mice that develop ALS. *Proc. Natl. Acad. Sci. U. S. A.* 2009, *106*, 1392-1397.
[61] Mori, K., Weng, S. M., Arzberger, T., May, S.*, et al.*, The C9orf72 GGGGCC repeat is translated into aggregating dipeptide-repeat proteins in FTLD/ALS. *Science* 2013, *339*, 1335-1338.
[62] Neumann, M., Mackenzie, I. R., Cairns, N. J., Boyer, P. J.*, et al.*, TDP-43 in the ubiquitin pathology of frontotemporal dementia with VCP gene mutations. *J. Neuropathol. Exp. Neurol.* 2007, *66*, 152-157.
[63] Farg, M. A., Soo, K. Y., Warraich, S. T., Sundaramoorthy, V.*, et al.*, Ataxin-2 interacts with FUS and intermediate-length polyglutamine expansions enhance FUS-related pathology in amyotrophic lateral sclerosis. *Hum. Mol. Genet.* 2013, *22*, 717-728.
[64] Williams, K. L., Warraich, S. T., Yang, S., Solski, J. A.*, et al.*, UBQLN2/ubiquilin 2 mutation and pathology in familial amyotrophic lateral sclerosis. *Neurobiol. Aging* 2012, *33*, 2527 e2523-2510.
[65] Collins, T. J., ImageJ for microscopy. *BioTechniques* 2007, *43*, 25-30.
[66] Shevchenko, A., Tomas, H., Havlis, J., Olsen, J. V.*, et al.*, In-gel digestion for mass spectrometric characterization of proteins and proteomes. *Nature Protoc.* 2006, *1*, 2856-2860.
[67] Perkins, D. N., Pappin, D. J., Creasy, D. M., Cottrell, J. S., Probability-based protein identification by searching sequence databases using mass spectrometry data. *Electrophoresis* 1999, *18*, 3551-3567.
[68] Zybailov, B., Mosley, A. L., Sardiu, M. E., Coleman, M. K.*, et al.*, Statistical analysis of membrane proteome expression changes in Saccharomyces cerevisiae. *J. Proteome Res.* 2006, *5*, 2339-2347.
[69] Huang, D. W., Sherman, B. T., Lempick, R. A., Systematic and integrative analysis of large gene lists using DAVID Bioinformatics Resources. *Nature Protoc.* 2009, *4*, 44-57.
[70] Cohen, T. J., Hwang, A. W., Unger, T., Trojanowski, J. Q.*, et al.*, Redox signalling directly regulates TDP-43 via cysteine oxidation and disulphide cross-linking. *EMBO J.* 2012, *31*, 1241-1252.
[71] Kirsh, O., Seeler, J. S., Pichler, A., Gast, A.*, et al.*, The SUMO E3 ligase RanBP2 promotes modification of the HDAC4 deacetylase. *EMBO J.* 2002, *21*, 2682-2691.
[72] Tan, N. G., Ardley, H. C., Scott, G. B., Rose, S. A.*, et al.*, Human homologue of ariadne promotes the ubiquitylation of translation initiation factor 4E homologous protein, 4EHP. *FEBS Lett.* 2003, *554*, 501-504.
[73] Hall, J. R., Kow, E., Nevis, K. R., Lu, C. K.*, et al.*, Cdc6 Stability Is Regulated by the Huwe1 Ubiquitin Ligase after DNA Damage. *Mol. Biol. Cell* 2007, *18*, 3340-3350.
[74] Zhao, X., D, D. A., Lim, W. K., Brahmachary, M.*, et al.*, The N-Myc-DLL3 cascade is suppressed by the ubiquitin ligase Huwe1 to inhibit proliferation and promote neurogenesis in the developing brain. *Develop. Cell* 2009, *17*, 210-221.
[75] Lin, R., Tao, R., Gao, X., Li, T.*, et al.*, Acetylation stabilizes ATP-citrate lyase to promote lipid biosynthesis and tumor growth. *Mol. Cell* 2013, *51*, 506-518.
[76] Fung, T. K., Siu, W. Y., Yam, C. H., Lau, A.*, et al.*, Cyclin F is degraded during G2-M by mechanisms fundamentally different from other cyclins. *J. Biol. Chem.* 2002, *277*, 35140-35149.

[77] Fallini, C., Bassell, G. J., Rossoll, W., The ALS disease protein TDP-43 is actively transported in motor neuron axons and regulates axon outgrowth. *Hum. Mol. Genet.* 2012, *21*, 3703-3718.
[78] Klann, E., Dever, T. E., Biochemical mechanisms for translational regulation in synaptic plasticity. *Nat. Rev. Neurosci.* 2004, *5*, 931-942.
[79] Murachelli, A. G., Ebert, J., Basquin, C., Le Hir, H.*, et al.*, The structure of the ASAP core complex reveals the existence of a Pinin-containing PSAP complex. *Nat. Struct. Mol. Biol.* 2012, *19*, 378-386.
[80] Anderson, P., Kedersha, N., Visibly stressed: the role of eIF2, TIA-1, and stress granules in protein translation. *Cell stress Chaperones* 2002, *7*, 213-221.
[81] Laplante, M., Sabatini, D. M., mTOR signaling in growth control and disease. *Cell* 2012, *149*, 274-293.
[82] Parsons, J. L., Tait, P. S., Finch, D., Dianova, II*, et al.*, Ubiquitin ligase ARF-BP1/Mule modulates base excision repair. *EMBO J.* 2009, *28*, 3207-3215.
[83] Nakatani, Y., Konishi, H., Vassilev, A., Kurooka, H.*, et al.*, p600, a unique protein required for membrane morphogenesis and cell survival. *Proc. Natl. Acad. Sci. U. S. A.* 2005, *102*, 15093-15098.
[84] Richards, S., Hillman, T., Stern, M., Mutations in the Drosophila pushover gene confer increased neuronal excitability and spontaneous synaptic vesicle fusion. *Genetics* 1996, *142*, 1215-1223.
[85] Yager, J., Richards, S., Hekmat-Scafe, D. S., Hurd, D. D.*, et al.*, Control of Drosophila perineurial glial growth by interacting neurotransmitter-mediated signaling pathways. *Proc. Natl. Acad. Sci. U. S. A.* 2001, *98*, 10445-10450.
[86] Fabunmi, R. P., Wigley, W. C., Thomas, P. J., DeMartino, G. N., Activity and regulation of the centrosome-associated proteasome. *J. Biol. Chem.* 2000, *275*, 409-413.
[87] Ding, W. X., Ni, H. M., Gao, W., Yoshimori, T.*, et al.*, Linking of autophagy to ubiquitin-proteasome system is important for the regulation of endoplasmic reticulum stress and cell viability. *Am. J. Pathol.* 2007, *171*, 513-524.
[88] Williams, A., Jahreiss, L., Sarkar, S., Saiki, S.*, et al.*, Aggregate-prone proteins are cleared from the cytosol by autophagy: therapeutic implications. *Curr. Top. Dev. Biol.* 2006, *76*, 89-101.
[89] Cherra, S. J., 3rd, Kulich, S. M., Uechi, G., Balasubramani, M.*, et al.*, Regulation of the autophagy protein LC3 by phosphorylation. *J. Cell Biol.* 2010, *190*, 533-539.
[90] Brown, C. A., Schmidt, C., Poulter, M., Hummerich, H.*, et al.*, In vitro screen of prion disease susceptibility genes using the scrapie cell assay. *Hum. Mol. Genet.* 2014.
[91] Muchowski, P. J., Schaffar, G., Sittler, A., Wanker, E. E.*, et al.*, Hsp70 and hsp40 chaperones can inhibit self-assembly of polyglutamine proteins into amyloid-like fibrils. *Proc. Natl. Acad. Sci. U. S. A.* 2000, *97*, 7841-7846.
[92] Fink, A. L., Chaperone-mediated protein folding. *Physiol. Rev.* 1999, *79*, 425-449.
[93] Senior, A. E., ATP synthesis by oxidative phosphorylation. *Physiol. Rev.*1988, *68*, 177-231.
[94] Wang, W., Li, L., Lin, W. L., Dickson, D. W.*, et al.*, The ALS disease-associated mutant TDP-43 impairs mitochondrial dynamics and function in motor neurons. *Hum. Mol. Genet.* 2013, *22*, 4706-4719.
[95] Mostowy, S., Cossart, P., Septins: the fourth component of the cytoskeleton. *Nature reviews. Mol. Cell Biol.* 2012, *13*, 183-194.
[96] Ageta-Ishihara, N., Miyata, T., Ohshima, C., Watanabe, M.*, et al.*, Septins promote dendrite and axon development by negatively regulating microtubule stability via HDAC6-mediated deacetylation. *Nat. Commun.* 2013, *4*, 2532.

[97] Kinoshita, A., Kinoshita, M., Akiyama, H., Tomimoto, H.*, et al.*, Identification of septins in neurofibrillary tangles in Alzheimer's disease. *Am. J. Pathol.* 1998, *153*, 1551-1560.
[98] Gozal, Y. M., Seyfried, N. T., Gearing, M., Glass, J. D.*, et al.*, Aberrant septin 11 is associated with sporadic frontotemporal lobar degeneration. *Mol. Neurodegener.* 2011, *6*, 82.
[99] Pissuti Damalio, J. C., Garcia, W., Alves Macedo, J. N., de Almeida Marques, I.*, et al.*, Self assembly of human septin 2 into amyloid filaments. *Biochimie* 2012, *94*, 628-636.
[100] Cumming, R. C., Schubert, D., Amyloid-beta induces disulfide bonding and aggregation of GAPDH in Alzheimer's disease. *FASEB J.* 2005, *19*, 2060-2062.
[101] Herrup, K., Yang, Y., Cell cycle regulation in the postmitotic neuron: oxymoron or new biology? *Nat. Rev. Neurosci.* 2007, *8*, 368-378.

6 Supplementary material

Supplementary Table 1. Proteins enriched in urea-soluble fractions in Cyclin F (S621G) expressing cells under control conditions; **M**: Mutant Cyclin F expressing cells; **W**: Wild type Cyclin F expressing cells; **E**: Empty vector control; **NSAF**: Normalised Spectral Abundance Factor; **SpC**: Spectral Count/s. Proteins are ranked in descending order based on M (SpC).

Rank	Accession Number	M (NSAF)	M (SpC)	E (NSAF)	E (SpC)	W (NSAF)	W (SpC)	M/W (NSAF)	M/E (NSAF)
1	H11_MOUSE	0.678	149	0.288	74	0.268	67	2.53	2.35
2	YBOX3_MOUSE	0.028	31	0.0125	16	0.0135	29	2.07	2.24
3	IF5A1_MOUSE	0.185	27	0.0645	11	0.0868	14	2.13	2.87
4	LAP2B_MOUSE	0.0203	26	0.00599	16	0.00807	13	2.52	3.39
5	TLN1_MOUSE	0.0101	25	0.00391	11	0.00478	13	2.11	2.58
6	UBR4_MOUSE	0.00462	23	0.000174	1	0.000939	5	4.92	26.55
7	ABCE1_MOUSE	0.0384	22	0.0136	9	0.0142	9	2.7	2.82
8	VAT1_MOUSE	0.0566	22	0.0222	10	0.024	10	2.36	2.55
9	RBP2_MOUSE	0.00723	21	0.000887	3	0.00159	5	4.55	8.15
10	ACACA_MOUSE	0.00941	21	0.00193	5	0.00467	12	2.01	4.88
11	USP9X_MOUSE	0.00827	20	0.00318	9	0.00238	6	3.47	2.6
12	PCKGM_MOUSE	0.0273	17	0.0127	9	0.0076	5	3.59	2.15
13	TPR_MOUSE	0.00719	17	0.00334	9	0.0035	9	2.05	2.15
14	ADNP_MOUSE	0.0211	17	0.00654	6	0.0103	9	2.05	3.23
15	DNLI1_MOUSE	0.0181	16	0.00394	4	0.00796	8	2.27	4.59
16	ZO1_MOUSE	0.00896	15	0.00362	7	0.00139	3	6.45	2.48
17	TPIS_MOUSE	0.0523	15	0.0181	6	0.0122	4	4.29	2.89
18	EZRI_MOUSE	0.011	15	0.00462	11	0.00415	10	2.65	2.38
19	PSA7_MOUSE	0.0631	15	0.0255	7	0.0245	6	2.58	2.47
20	CND1_MOUSE	0.0106	14	0.00389	6	0.00262	4	4.05	2.72
21	VAPA_MOUSE	0.0554	13	0.0181	5	0.00488	1	11.35	3.06
22	TMEDA_MOUSE	0.063	13	0.0206	5	0.0167	4	3.77	3.06
23	NASP_MOUSE	0.0155	12	0.00351	3	0.00157	1	9.87	4.42
24	IQGA2_MOUSE	0.00584	12	0.000573	4	0.000772	4	7.56	10.19
25	DHB12_MOUSE	0.0413	12	0.00579	2	0.00779	3	5.3	7.13
26	PSME3_MOUSE	0.0471	12	0.00711	2	0.00957	3	4.92	6.62
27	SAE2_MOUSE	0.0187	12	0.00425	3	0.00381	3	4.91	4.4
28	ATP5L_MOUSE	0.125	12	0.0263	3	0.0354	4	3.53	4.75
29	IF4G2_MOUSE	0.0142	12	0.00399	4	0.00403	4	3.52	3.56
30	AFAD_MOUSE	0.00657	12	0.00198	4	0.002	4	3.29	3.32
31	CLU_MOUSE	0.00909	12	0.00137	2	0.00277	4	3.28	6.64
32	GLYC_MOUSE	0.025	12	0.00945	5	0.00763	4	3.28	2.65
33	SURF4_MOUSE	0.0445	12	0.0201	6	0.0181	5	2.46	2.21
34	NU155_MOUSE	0.0086	12	0.00325	5	0.0035	5	2.46	2.65
35	STRBP_MOUSE	0.00411	12	0.00134	6	0.00181	14	2.27	3.07
36	VINC_MOUSE	0.0121	12	0.00339	4	0.0057	6	2.12	3.57
37	PIMT_MOUSE	0.0486	11	0.0119	3	0.0107	3	4.54	4.08
38	HUWE1_MOUSE	0.00252	11	0.000206	1	0.000556	3	4.53	12.23
39	IF4B_MOUSE	0.0181	11	0.00887	6	0.00597	4	3.03	2.04

40	XPP1_MOUSE	0.0177	11	0.00725	5	0.00781	5	2.27	2.44
41	CBR1_MOUSE	0.0365	10	0.013	4	0.00878	3	4.16	2.81
42	BAG6_MOUSE	0.00877	10	0.00313	4	0.00211	3	4.16	2.8
43	GTF2I_MOUSE	0.0101	10	0.00181	2	0.00244	3	4.14	5.58
44	ELYS_MOUSE	0.00451	10	0.00121	3	0.00163	4	2.77	3.73
45	RPAP3_MOUSE	0.0153	10	0.00411	3	0.00553	4	2.77	3.72
46	GNA13_MOUSE	0.0171	10	0.00719	6	0.00645	9	2.65	2.38
47	XPO5_MOUSE	0.0084	10	0.003	4	0.00404	5	2.08	2.8
48	GLU2B_MOUSE	0.0177	9	0.0052	3	0.00233	1	7.6	3.4
49	NAA25_MOUSE	0.00946	9	0.00465	5	0.00125	1	7.57	2.03
50	COX5A_MOUSE	0.063	9	0.0186	3	0.00833	1	7.56	3.39
51	NDUS2_MOUSE	0.0199	9	0.0078	4	0.00525	3	3.79	2.55
52	PGM1_MOUSE	0.0164	9	0.00803	5	0.00433	3	3.79	2.04
53	PSPC1_MOUSE	0.0176	9	0.00691	4	0.00465	3	3.78	2.55
54	HYEP_MOUSE	0.0202	9	0.00992	5	0.00534	3	3.78	2.04
55	UBP2L_MOUSE	0.00831	9	0.00163	2	0.0022	3	3.78	5.1
56	IPO9_MOUSE	0.00884	9	0.00434	5	0.0035	4	2.53	2.04
57	HEAT3_MOUSE	0.0122	8	0.00532	4	0.00179	1	6.82	2.29
58	DIEXF_MOUSE	0.0107	8	0.00468	4	0.00157	1	6.82	2.29
59	ECM29_MOUSE	0.0045	8	0.00196	4	0.000661	1	6.81	2.3
60	MARE1_MOUSE	0.0309	8	0.0135	4	0.00454	1	6.81	2.29
61	ACOC_MOUSE	0.00931	8	0.00102	1	0.00137	1	6.8	9.13
62	CUL5_MOUSE	0.0106	8	0.00232	2	0.00156	1	6.79	4.57
63	SC23A_MOUSE	0.0108	8	0.00472	4	0.00159	1	6.79	2.29
64	LETM1_MOUSE	0.0112	8	0.00245	2	0.00165	1	6.79	4.57
65	PRC2C_MOUSE	0.00291	8	0.000317	1	0.000854	3	3.41	9.18
66	MAP4_MOUSE	0.00736	8	0.00241	3	0.00216	3	3.41	3.05
67	AP3B1_MOUSE	0.00749	8	0.000817	1	0.0022	3	3.4	9.17
68	LMAN1_MOUSE	0.016	8	0.00349	2	0.0047	3	3.4	4.58
69	KDM1A_MOUSE	0.0097	8	0.00212	2	0.00285	3	3.4	4.58
70	DC1L1_MOUSE	0.0158	8	0.00691	4	0.00465	3	3.4	2.29
71	TNPO1_MOUSE	0.00922	8	0.00402	4	0.00406	4	2.27	2.29
72	PAXB1_MOUSE	0.00901	8	0.00393	4	0.00397	4	2.27	2.29
73	LARP4_MOUSE	0.0115	8	0.00502	4	0.00507	4	2.27	2.29
74	SC31A_MOUSE	0.00673	8	0.00294	4	0.00297	4	2.27	2.29
75	FAF2_MOUSE	0.0165	7	0.00812	4	0.00273	1	6.04	2.03
76	SNX2_MOUSE	0.0142	7	0.00348	2	0.00468	3	3.03	4.08
77	RS30_MOUSE	0.125	7	0.0306	2	0.0412	3	3.03	4.08
78	FA98A_MOUSE	0.0143	7	0.00351	2	0.00472	3	3.03	4.07
79	OPA1_MOUSE	0.00766	7	0.00188	2	0.00253	3	3.03	4.07
80	RAB10_MOUSE	0.0184	7	0.00452	5	0.00608	5	3.03	4.07
81	PCM1_MOUSE	0.00363	7	0.000892	2	0.0012	3	3.03	4.07
82	AP1G1_MOUSE	0.00895	7	0.00439	4	0.00296	3	3.02	2.04
83	MFAP1_MOUSE	0.0168	7	0.00411	2	0.00831	4	2.02	4.09
84	NOMO1_MOUSE	0.00606	7	0.00223	3	0.003	4	2.02	2.72
85	LYAR_MOUSE	0.0166	6	0.00698	3	0.00313	1	5.3	2.38

86	UBE2N_MOUSE	0.0424	6	0.0178	3	0.008	1	5.3	2.38
87	CNTFR_MOUSE	0.0173	6	0.00243	1	0.00327	1	5.29	7.12
88	PSME2_MOUSE	0.0269	6	0.00378	1	0.00509	1	5.28	7.12
89	CAND2_MOUSE	0.00447	6	0.00146	3	0.000984	1	4.54	3.06
90	SEPT8_MOUSE	0.0107	6	0.00211	2	0.00283	5	3.78	5.07
91	MPPB_MOUSE	0.0132	6	0.00554	3	0.00497	3	2.66	2.38
92	AL1L2_MOUSE	0.00698	6	0.00196	2	0.00263	3	2.65	3.56
93	CHRD1_MOUSE	0.0195	6	0.00819	3	0.00735	3	2.65	2.38
94	ENPP3_MOUSE	0.00737	6	0.0031	3	0.00278	3	2.65	2.38
95	NDUAD_MOUSE	0.0447	6	0.0125	2	0.0169	3	2.64	3.58
96	DDX6_MOUSE	0.0133	6	0.00561	3	0.00503	3	2.64	2.37
97	NCKP1_MOUSE	0.00571	6	0.0016	2	0.00216	3	2.64	3.57
98	TIA1_MOUSE	0.00715	6	0.00234	6	0.00315	4	2.27	3.06
99	CHIP_MOUSE	0.0182	5	0.00891	3	0.004	1	4.55	2.04
100	CCAR1_MOUSE	0.00482	5	0.00236	3	0.00106	1	4.55	2.04
101	RT02_MOUSE	0.019	5	0.00621	2	0.00418	1	4.55	3.06
102	NU160_MOUSE	0.00394	5	0.00129	2	0.000867	1	4.54	3.05
103	NDUV1_MOUSE	0.0119	5	0.00584	3	0.00262	1	4.54	2.04
104	CDC16_MOUSE	0.0089	5	0.00146	1	0.00196	1	4.54	6.1
105	ACSL1_MOUSE	0.0079	5	0.00258	2	0.00174	1	4.54	3.06
106	RTN3_MOUSE	0.00572	5	0.000937	1	0.00126	1	4.54	6.1
107	ARI1_MOUSE	0.00994	5	0.00325	2	0.00219	1	4.54	3.06
108	PA1B2_MOUSE	0.0241	5	0.0118	3	0.00531	1	4.54	2.04
109	UCHL3_MOUSE	0.024	5	0.0118	3	0.00529	1	4.54	2.03
110	THOC2_MOUSE	0.00346	5	0.000567	1	0.000763	1	4.53	6.1
111	AIFM1_MOUSE	0.00902	5	0.00443	3	0.00199	1	4.53	2.04
112	ACSL3_MOUSE	0.00766	5	0.00125	1	0.00169	1	4.53	6.13
113	NEUL_MOUSE	0.00784	5	0.00385	3	0.00173	1	4.53	2.04
114	CLPX_MOUSE	0.0087	5	0.00427	3	0.00192	1	4.53	2.04
115	NEST_MOUSE	0.00296	5	0.000485	1	0.0013	3	2.28	6.1
116	SPF30_MOUSE	0.0232	5	0.00379	1	0.0102	3	2.27	6.12
117	NUP62_MOUSE	0.0105	5	0.00343	2	0.00462	3	2.27	3.06
118	RT30_MOUSE	0.0125	5	0.00613	3	0.0055	3	2.27	2.04
119	KAD1_MOUSE	0.0284	5	0.014	3	0.0125	3	2.27	2.03
120	GTR3_MOUSE	0.0112	5	0.0055	3	0.00493	3	2.27	2.04
121	THIC_MOUSE	0.0139	5	0.00682	3	0.00612	3	2.27	2.04
122	TBC15_MOUSE	0.00822	5	0.00269	2	0.00362	3	2.27	3.06
123	ZN622_MOUSE	0.0116	5	0.0019	1	0.00511	3	2.27	6.11
124	PIGS_MOUSE	0.00994	5	0.00325	2	0.00438	3	2.27	3.06
125	ATX2L_MOUSE	0.00526	5	0.00258	3	0.00232	3	2.27	2.04
126	SRBD1_MOUSE	0.00544	5	0.00178	2	0.0024	3	2.27	3.06
127	NU107_MOUSE	0.00596	5	0.00195	2	0.00263	3	2.27	3.06
128	UBE2O_MOUSE	0.00428	5	0.000701	1	0.00189	3	2.26	6.11
129	PELP1_MOUSE	0.00491	5	0.00161	2	0.00217	3	2.26	3.05
130	HACD3_MOUSE	0.0152	5	0.00748	3	0.00672	3	2.26	2.03
131	NISCH_MOUSE	0.00346	5	0.000567	1	0.00153	3	2.26	6.1

132	HSP7E_MOUSE	0.0108	5	0.00532	3	0.00478	3	2.26	2.03
133	NUDC3_MOUSE	0.0127	4	0.00249	1	0.00335	1	3.79	5.1
134	UBP7_MOUSE	0.00417	4	0.000819	1	0.0011	1	3.79	5.09
135	CTR1_MOUSE	0.00739	4	0.00145	1	0.00195	1	3.79	5.1
136	RNZ2_MOUSE	0.00553	4	0.00109	1	0.00146	1	3.79	5.07
137	MANF_MOUSE	0.0257	4	0.00505	1	0.00679	1	3.78	5.09
138	ZMYM4_MOUSE	0.00297	4	0.000583	1	0.000785	1	3.78	5.09
139	SYIM_MOUSE	0.00454	4	0.00178	2	0.0012	1	3.78	2.55
140	DPOD1_MOUSE	0.00416	4	0.00163	2	0.0011	1	3.78	2.55
141	RSU1_MOUSE	0.0166	4	0.00652	2	0.00439	1	3.78	2.55
142	ASZ1_MOUSE	0.00968	4	0.0038	2	0.00256	1	3.78	2.55
143	YKT6_MOUSE	0.0232	4	0.00912	2	0.00614	1	3.78	2.54
144	PEPD_MOUSE	0.00933	4	0.00366	2	0.00247	1	3.78	2.55
145	SMC5_MOUSE	0.00334	4	0.00164	2	0.0011	1	3.04	2.04
146	IF4E_MOUSE	0.017	4	0.00832	2	0.0056	1	3.04	2.04
147	SNP25_MOUSE	0.0179	4	0.00877	2	0.0059	1	3.03	2.04
148	LTOR1_MOUSE	0.0229	4	0.00561	1	0.00755	1	3.03	4.08
149	TPX2_MOUSE	0.00494	4	0.00121	1	0.00163	1	3.03	4.08
150	NDUS3_MOUSE	0.014	4	0.00687	2	0.00462	1	3.03	2.04
151	ORC3_MOUSE	0.00515	4	0.00253	2	0.0017	1	3.03	2.04
152	TOIP1_MOUSE	0.00618	4	0.00152	1	0.00204	1	3.03	4.07
153	PBDC1_MOUSE	0.0186	4	0.00912	2	0.00614	1	3.03	2.04
154	WDR18_MOUSE	0.00854	4	0.00419	2	0.00282	1	3.03	2.04
155	ACADS_MOUSE	0.00893	4	0.00438	2	0.00295	1	3.03	2.04
156	M2OM_MOUSE	0.0117	4	0.00575	2	0.00387	1	3.02	2.03
157	RMD3_MOUSE	0.00783	4	0.00384	2	0.00259	1	3.02	2.04
158	SNR27_MOUSE	0.0237	4	0.0117	2	0.00784	1	3.02	2.03
159	VAS1_MOUSE	0.00795	4	0.00195	1	0.00263	1	3.02	4.08
160	CADM1_MOUSE	0.00807	4	0.00198	1	0.00267	1	3.02	4.08
161	ARF6_MOUSE	0.021	4	0.00516	1	0.00695	1	3.02	4.07
162	VAPB_MOUSE	0.0151	4	0.00372	2	0.005	3	3.02	4.06
163	PSB3_MOUSE	0.0179	4	0.00441	1	0.00593	1	3.02	4.06
164	CX023_MOUSE	0.00489	4	0.0012	1	0.00162	1	3.02	4.08
165	DPYL5_MOUSE	0.00652	4	0.0016	1	0.00216	1	3.02	4.08
166	SMC6_MOUSE	0.00335	4	0.000823	1	0.00111	1	3.02	4.07
167	SYNE3_MOUSE	0.00377	4	0.000926	1	0.00125	1	3.02	4.07
168	GPDM_MOUSE	0.0038	3	0.00124	1	0.00167	1	2.28	3.06
169	EMC3_MOUSE	0.0106	3	0.00346	1	0.00466	1	2.27	3.06
170	VATF_MOUSE	0.0232	3	0.00759	1	0.0102	1	2.27	3.06
171	COR2B_MOUSE	0.00575	3	0.00188	1	0.00253	1	2.27	3.06
172	DJB12_MOUSE	0.00734	3	0.0024	1	0.00323	1	2.27	3.06
173	PPIL4_MOUSE	0.00561	3	0.00184	1	0.00247	1	2.27	3.05
174	PA1B3_MOUSE	0.0119	3	0.00389	1	0.00524	1	2.27	3.06
175	COPZ1_MOUSE	0.0156	3	0.0051	1	0.00687	1	2.27	3.06
176	SHLB2_MOUSE	0.0069	3	0.00226	1	0.00304	1	2.27	3.05
177	FKBP2_MOUSE	0.0197	3	0.00645	1	0.00868	1	2.27	3.05

178	WDR6_MOUSE	0.00245	3	0.000803	1	0.00108	1	2.27	3.05
179	RM39_MOUSE	0.00821	3	0.00269	1	0.00362	1	2.27	3.05
180	NSDHL_MOUSE	0.00762	3	0.00249	1	0.00336	1	2.27	3.06
181	ALD1_MOUSE	0.00873	3	0.00286	2	0.00385	1	2.27	3.05
182	RDH11_MOUSE	0.00873	3	0.00286	1	0.00385	1	2.27	3.05
183	HGS_MOUSE	0.00356	3	0.00117	1	0.00157	1	2.27	3.04
184	MLKL_MOUSE	0.00585	3	0.00191	1	0.00258	1	2.27	3.06
185	CLPB_MOUSE	0.00408	3	0.00133	1	0.0018	1	2.27	3.07
186	LRWD1_MOUSE	0.00426	3	0.00139	1	0.00188	1	2.27	3.06
187	TIM13_MOUSE	0.029	3	0.00951	1	0.0128	1	2.27	3.05
188	TNPO3_MOUSE	0.00299	3	0.000978	1	0.00132	1	2.27	3.06
189	PSMD9_MOUSE	0.0124	3	0.00407	1	0.00548	1	2.26	3.05
190	PRDX5_MOUSE	0.0131	3	0.0043	1	0.00579	1	2.26	3.05

Supplementary Table 2. Proteins enriched in urea-soluble fractions in Cyclin F (S621G) expressing cells also subject to heat-shock; **M**: Mutant Cyclin F expressing cells; **W**: Wild type Cyclin F expressing cells; **E**: Empty vector control; **NSAF**: Normalised Spectral Abundance Factor; **SpC**: Spectral count/s. Proteins are ranked in descending order based on M (SpC).

Rank	Accession Number	M-HS (NSAF)	M-HS (SpC)	E-HS (NSAF)	E-HS (SpC)	W-HS (NSAF)	W-HS (SpC)	M/W (NSAF)	M/E (NSAF)
1	G3P_MOUSE	0.388	136	0.178	56	0.175	54	2.22	2.18
2	H12_MOUSE	0.197	103	0.0239	85	0.0857	68	2.3	8.24
3	AATM_MOUSE	0.133	60	0.057	23	0.0574	23	2.32	2.33
4	MDHC_MOUSE	0.102	36	0.0354	11	0.0428	13	2.38	2.88
5	ATPG_MOUSE	0.114	36	0.0312	9	0.0479	13	2.38	3.65
6	GDIR1_MOUSE	0.162	35	0.0497	10	0.0573	11	2.83	3.26
7	TCTP_MOUSE	0.181	33	0.059	10	0.0453	7	4	3.07
8	GSTP1_MOUSE	0.134	30	0.0241	5	0.0618	12	2.17	5.56
9	TEBP_MOUSE	0.164	28	0.0211	3	0.0649	10	2.53	7.77
10	RL19_MOUSE	0.134	28	0.0388	7	0.0596	11	2.25	3.45
11	SEPT2_MOUSE	0.0646	24	0.0234	8	0.0036	1	17.94	2.76
12	CLIC1_MOUSE	0.0847	21	0.0175	4	0.0323	7	2.62	4.84
13	PSB3_MOUSE	0.0948	20	0.0371	7	0.0253	5	3.75	2.56
14	ETFA_MOUSE	0.0583	20	0.0228	7	0.0273	8	2.14	2.56
15	HAP28_MOUSE	0.0966	18	0.00934	2	0.0359	6	2.69	10.34
16	MK01_MOUSE	0.0461	17	0.0142	5	0.0218	7	2.11	3.25
17	RL30_MOUSE	0.127	15	0.0441	5	0.0564	6	2.25	2.88
18	IF4B_MOUSE	0.0238	15	0.00968	6	0.0106	6	2.25	2.46
19	BAP31_MOUSE	0.0595	15	0.0241	6	0.0265	6	2.25	2.47
20	EIF3G_MOUSE	0.0455	15	0.0211	6	0.0203	6	2.24	2.16
21	RL35A_MOUSE	0.124	14	0.0154	2	0.0354	4	3.5	8.05
22	IDI1_MOUSE	0.0599	14	0.0223	5	0.0229	5	2.62	2.69
23	OST48_MOUSE	0.0308	14	0.0115	5	0.0147	6	2.1	2.68
24	BASP1_MOUSE	0.0559	13	0.0187	4	0.023	5	2.43	2.99
25	KAD1_MOUSE	0.0651	13	0.0174	3	0.0268	5	2.43	3.74
26	RS27_MOUSE	0.127	11	0.0201	2	0.0155	1	8.19	6.32

27	RL27A_MOUSE	0.0722	11	0.0343	5	0.0263	4	2.75	2.1
28	SSRA_MOUSE	0.034	10	0.0118	3	0.00908	2	3.74	2.88
29	IF4H_MOUSE	0.0392	10	0.0102	2	0.0157	4	2.5	3.84
30	S61A1_MOUSE	0.0204	10	0.00533	2	0.00818	4	2.49	3.83
31	SAP18_MOUSE	0.0571	9	0.011	2	0.00849	1	6.73	5.19
32	TOM22_MOUSE	0.0616	9	0.0238	3	0.0274	4	2.25	2.59
33	DEST_MOUSE	0.053	9	0.0154	2	0.0236	4	2.25	3.44
34	SRP14_MOUSE	0.0795	9	0.023	2	0.0354	4	2.25	3.46
35	CS010_MOUSE	0.0468	8	0.0102	2	0.00782	1	5.98	4.59
36	SAR1B_MOUSE	0.0393	8	0.00854	2	0.0131	2	3	4.6
37	TMX1_MOUSE	0.0245	7	0.00304	1	0.00934	2	2.62	8.06
38	TIM23_MOUSE	0.0325	7	0.00404	1	0.0124	2	2.62	8.04
39	CDC42_MOUSE	0.0356	7	0.00885	2	0.0136	2	2.62	4.02
40	UCRI_MOUSE	0.0213	6	0.00925	2	0.00474	1	4.49	2.3
41	HMGN1_MOUSE	0.0607	6	0.0088	1	0.027	2	2.25	6.9
42	VAMP3_MOUSE	0.0566	6	0.0082	1	0.0252	2	2.25	6.9
43	RL36A_MOUSE	0.055	6	0.00797	1	0.0245	2	2.24	6.9
44	DNJC8_MOUSE	0.023	6	0.00334	1	0.0103	2	2.23	6.89
45	RM39_MOUSE	0.0145	5	0.00252	1	0.00386	1	3.76	5.75
46	ATOX1_MOUSE	0.0714	5	0.0124	1	0.0191	1	3.74	5.76
47	IMA3_MOUSE	0.00559	5	0.00162	2	0.00249	4	2.24	3.45
48	RS27L_MOUSE	0.0347	5	0.0101	2	0.0155	2	2.24	3.44
49	LIMA1_MOUSE	0.00516	4	0.00112	1	0.00172	1	3	4.61
50	SPCS2_MOUSE	0.0172	4	0.00374	1	0.00574	1	3	4.6
51	SF3B4_MOUSE	0.00916	4	0.00399	2	0.00306	1	2.99	2.3
52	HINT1_MOUSE	0.0308	4	0.00671	1	0.0103	1	2.99	4.59
53	KPRA_MOUSE	0.0109	4	0.00237	1	0.00365	1	2.99	4.6
54	DRS7B_MOUSE	0.012	4	0.00262	1	0.00402	1	2.99	4.58
55	HACD3_MOUSE	0.0107	4	0.00467	2	0.00359	1	2.98	2.29
56	SYTC2_MOUSE	0.00369	4	0.00107	1	0.00164	2	2.25	3.45
57	FIS1_MOUSE	0.0192	3	0.00556	1	0.00854	1	2.25	3.45
58	PARVA_MOUSE	0.00783	3	0.00227	1	0.00349	1	2.24	3.45
59	GEPH_MOUSE	0.00379	3	0.0011	1	0.00169	1	2.24	3.45
60	MTMR2_MOUSE	0.00453	3	0.00131	1	0.00202	1	2.24	3.46
61	PSMD9_MOUSE	0.0131	3	0.00381	1	0.00585	1	2.24	3.44
62	APOO_MOUSE	0.0137	3	0.00399	1	0.00612	1	2.24	3.43
63	SPAG7_MOUSE	0.0128	3	0.00372	1	0.00572	1	2.24	3.44

Supplementary Table 3. Proteins enriched in urea-soluble fractions in Cyclin F (Wild Type) expressing cells under control conditions. **M**: Mutant Cyclin F expressing cells; **W**: Wild type Cyclin F expressing cells; **E**: Empty vector control; **NSAF**: Normalised Spectral Abundance Factor; **SpC**: Spectral count/s. Proteins are ranked in descending order based on M (SpC).

Rank	Accession Number	M (NSAF)	M (SpC)	E (NSAF)	E (SpC)	W (NSAF)	W (SpC)	W/M (NSAF)	W/E (NSAF)
1	UBB_MOUSE	0.268	79	0.275	91	0.55	179	2.05	2
2	ATRX_MOUSE	0.00632	15	0.0062	17	0.0152	40	2.41	2.45
3	CEBPZ_MOUSE	0.0131	13	0.00858	10	0.0266	30	2.03	3.1

4	RPB2_MOUSE	0.011	12	0.0115	15	0.0342	43	3.11	2.97
5	DNM3A_MOUSE	0.0142	12	0.0129	13	0.0308	30	2.17	2.39
6	ATAD2_MOUSE	0.0115	12	0.0104	12	0.0245	27	2.13	2.36
7	ELAV3_MOUSE	0.00501	11	0.00738	8	0.0166	18	3.31	2.25
8	TP53B_MOUSE	0.00564	11	0.00323	7	0.0118	25	2.09	3.65
9	SRSF4_MOUSE	0.00376	7	0.00554	9	0.0124	10	3.3	2.24
10	RL31_MOUSE	0.0589	7	0.0506	7	0.165	22	2.8	3.26
11	SNR40_MOUSE	0.018	6	0.0177	7	0.0509	19	2.83	2.88
12	TIF1A_MOUSE	0.00438	6	0.0043	5	0.00925	12	2.11	2.15
13	NOC2L_MOUSE	0.00739	5	0.00725	6	0.0163	13	2.21	2.25
14	BAZ2A_MOUSE	0.00292	5	0.00239	5	0.00644	13	2.21	2.69
15	GYS1_MOUSE	0.00623	4	0.00734	6	0.0165	13	2.65	2.25
16	AURKB_MOUSE	0.0133	4	0.0157	6	0.0317	12	2.38	2.02
17	WDR74_MOUSE	0.012	4	0.0118	5	0.0285	12	2.38	2.42
18	HDGR3_MOUSE	0.00455	3	0.00894	4	0.0241	6	5.3	2.7
19	MAGD1_MOUSE	0.00356	3	0.00466	4	0.00941	8	2.64	2.02
20	GPC1_MOUSE	0.0033	2	0.00162	1	0.00873	5	2.65	5.39
21	ERH_MOUSE	0.0177	2	0.00868	1	0.0468	5	2.64	5.39
22	CLIC4_MOUSE	0.00727	2	0.00357	1	0.0192	5	2.64	5.38
23	TRBP2_MOUSE	0.00504	2	0.00495	2	0.0133	5	2.64	2.69
24	LLPH_MOUSE	0.0142	2	0.00695	1	0.0374	5	2.63	5.38
25	CKAP2_MOUSE	0.00139	1	0.00136	1	0.00549	4	3.95	4.04
26	ARP5L_MOUSE	0.00601	1	0.0059	1	0.0159	3	2.65	2.69
27	CLPP_MOUSE	0.00338	1	0.00332	1	0.00894	3	2.64	2.69
28	BLVRB_MOUSE	0.00447	1	0.00438	1	0.0118	3	2.64	2.69
29	THEM6_MOUSE	0.00444	1	0.00436	1	0.0117	3	2.64	2.68
30	NAA10_MOUSE	0.00391	1	0.00384	1	0.0103	3	2.63	2.68

Supplementary Table 4. Proteins enriched in urea-soluble fractions in Cyclin F (Wild Type) expressing cells subject to heat-shock; **M**: Mutant Cyclin F expressing cells; **W**: Wild type Cyclin F expressing cells; **E**: Empty vector control; **NSAF**: Normalised Spectral Abundance Factor; **SpC**: Spectral count/s. Proteins are ranked in descending order based on M (SpC).

Rank	Accession Number	M-HS (NSAF)	M-HS (SpC)	E-HS (NSAF)	E-HS (SpC)	W-HS (NSAF)	W-HS (SpC)	W/M (NSAF)	W/E (NSAF)
1	SERA_MOUSE	0.0219	12	0.0206	10	0.0438	21	2	2.13
2	CBX5_MOUSE	0.0559	11	0.0398	7	0.156	27	2.79	3.92
3	UBR4_MOUSE	0.00188	10	0.00131	6	0.00451	21	2.4	3.44
4	FRIL1_MOUSE	0.0531	10	0.0554	10	0.114	19	2.15	2.06
5	PRS7_MOUSE	0.0224	10	0.0234	10	0.048	19	2.14	2.05
6	MOES_MOUSE	0.00337	9	0.00293	10	0.00675	11	2	2.3
7	SC23B_MOUSE	0.00633	8	0.00551	7	0.0135	11	2.13	2.45
8	SRPR_MOUSE	0.0122	8	0.00797	5	0.0245	14	2.01	3.07
9	NH2L1_MOUSE	0.0531	7	0.0594	7	0.223	26	4.2	3.75
10	NDUS1_MOUSE	0.00935	7	0.0116	8	0.0268	18	2.87	2.31
11	RAB3C_MOUSE	0.00428	7	0.00372	2	0.0114	5	2.66	3.06
12	TOM70_MOUSE	0.0111	7	0.00968	6	0.0276	16	2.49	2.85
13	ODO1_MOUSE	0.00665	7	0.00661	6	0.0152	14	2.29	2.3

14	PSA6_MOUSE	0.0276	7	0.024	6	0.0581	13	2.11	2.42
15	IDE_MOUSE	0.00572	6	0.00166	2	0.0178	17	3.11	10.72
16	MAOX_MOUSE	0.0102	6	0.00295	2	0.0227	12	2.23	7.69
17	UBP15_MOUSE	0.00594	6	0.00431	4	0.0132	12	2.22	3.06
18	KTN1_MOUSE	0.00439	6	0.00318	4	0.00881	11	2.01	2.77
19	IF4G3_MOUSE	0.00185	5	0.00161	6	0.00576	11	3.11	3.58
20	PSMD5_MOUSE	0.00964	5	0.00838	4	0.0258	12	2.68	3.08
21	GLYC_MOUSE	0.0102	5	0.00707	3	0.0272	12	2.67	3.85
22	RM12_MOUSE	0.0242	5	0.0042	1	0.0517	10	2.14	12.31
23	GSTM2_MOUSE	0.00446	4	0.0116	3	0.0238	5	5.34	2.05
24	MSH6_MOUSE	0.00286	4	0.00498	6	0.0115	14	4.02	2.31
25	GSTM1_MOUSE	0.00446	4	0.00775	3	0.0179	4	4.01	2.31
26	EHD1_MOUSE	0.00728	4	0.0111	6	0.0267	13	3.67	2.41
27	OGT1_MOUSE	0.00371	4	0.00485	5	0.0112	11	3.02	2.31
28	PFD5_MOUSE	0.0252	4	0.0165	2	0.059	8	2.34	3.58
29	PURA2_MOUSE	0.00852	4	0.00741	3	0.0171	7	2.01	2.31
30	ELOB_MOUSE	0.0329	4	0.0215	2	0.066	7	2.01	3.07
31	CLU_MOUSE	0.00296	4	0.00193	2	0.00592	7	2	3.07
32	TPD54_MOUSE	0.0177	4	0.0115	2	0.0354	7	2	3.08
33	SNP25_MOUSE	0.0189	4	0.0082	2	0.0378	7	2	4.61
34	IQGA2_MOUSE	0.000617	3	0.00107	3	0.00247	6	4	2.31
35	CPNE3_MOUSE	0.00547	3	0.00951	5	0.0195	10	3.56	2.05
36	PFD1_MOUSE	0.0239	3	0.0139	2	0.0745	8	3.12	5.36
37	DNPEP_MOUSE	0.00616	3	0.00715	3	0.0165	7	2.68	2.31
38	NCPR_MOUSE	0.0043	3	0.00499	3	0.0115	7	2.67	2.3
39	CBR3_MOUSE	0.00701	3	0.0061	2	0.0187	6	2.67	3.07
40	ERO1A_MOUSE	0.00628	3	0.00364	2	0.014	6	2.23	3.85
41	RTN3_MOUSE	0.00302	3	0.000877	1	0.00673	6	2.23	7.67
42	KRI1_MOUSE	0.00414	3	0.0024	2	0.00922	6	2.23	3.84
43	SNX1_MOUSE	0.00186	2	0.00486	4	0.0124	6	6.67	2.55
44	AMPD2_MOUSE	0.00243	2	0.00318	2	0.0114	8	4.69	3.58
45	TXLNA_MOUSE	0.00351	2	0.00153	1	0.0141	7	4.02	9.22
46	PRC2C_MOUSE	0.000683	2	0.00119	3	0.00274	7	4.01	2.3
47	PDXD1_MOUSE	0.00247	2	0.00215	2	0.0099	7	4.01	4.6
48	PPAC_MOUSE	0.0123	2	0.016	2	0.0411	6	3.34	2.57
49	DCTN3_MOUSE	0.0104	2	0.00454	1	0.0279	5	2.68	6.15
50	PSMG3_MOUSE	0.0159	2	0.0139	2	0.0426	5	2.68	3.06
51	STOM_MOUSE	0.00684	2	0.00595	2	0.0183	5	2.68	3.08
52	AFG31_MOUSE	0.00123	2	0.00107	1	0.00329	2	2.67	3.07
53	KLC1_MOUSE	0.00359	2	0.00312	2	0.0096	5	2.67	3.08
54	NEUL_MOUSE	0.00276	2	0.0024	2	0.00738	5	2.67	3.08
55	CLCA_MOUSE	0.00827	2	0.0036	1	0.0221	5	2.67	6.14
56	ABCF3_MOUSE	0.00274	2	0.00358	2	0.00732	5	2.67	2.04
57	MPPA_MOUSE	0.00371	2	0.00323	2	0.00991	5	2.67	3.07
58	NUDC1_MOUSE	0.00334	2	0.0029	2	0.00892	5	2.67	3.08
59	MPPB_MOUSE	0.00397	2	0.00173	1	0.0106	5	2.67	6.13

60	GSK3A_MOUSE	0.00397	2	0.00345	2	0.0106	5	2.67	3.07
61	VATD_MOUSE	0.00787	2	0.00684	2	0.021	5	2.67	3.07
62	RWDD4_MOUSE	0.0103	2	0.00449	1	0.0207	4	2.01	4.61
63	NDUS4_MOUSE	0.0111	2	0.00966	2	0.0223	4	2.01	2.31
64	ABT1_MOUSE	0.00722	2	0.00628	2	0.0145	4	2.01	2.31
65	ADAS_MOUSE	0.00301	2	0.00262	2	0.00604	4	2.01	2.31
66	SEC62_MOUSE	0.00488	2	0.00212	1	0.00979	4	2.01	4.62
67	NAB2_MOUSE	0.0037	2	0.00322	2	0.00742	4	2.01	2.3
68	MCES_MOUSE	0.00418	2	0.00363	2	0.00838	4	2	2.31
69	MD2L1_MOUSE	0.00948	2	0.00412	1	0.019	4	2	4.61
70	CLPT1_MOUSE	0.00293	2	0.00255	2	0.00587	4	2	2.3
71	ACADM_MOUSE	0.00462	2	0.00201	1	0.00925	4	2	4.6
72	LAMP1_MOUSE	0.00479	2	0.00416	2	0.00959	4	2	2.31
73	COPZ1_MOUSE	0.011	2	0.00477	1	0.022	4	2	4.61
74	VPS29_MOUSE	0.0107	2	0.00929	2	0.0214	4	2	2.3
75	GPSM1_MOUSE	0.00144	1	0.00753	5	0.0154	10	10.69	2.05
76	EHMT2_MOUSE	0.000769	1	0.00268	3	0.00617	7	8.02	2.3
77	DYN1_MOUSE	0.00112	1	0.00292	2	0.00599	5	5.35	2.05
78	WDR6_MOUSE	0.000864	1	0.00225	2	0.00462	5	5.35	2.05
79	XPO7_MOUSE	0.000894	1	0.00233	2	0.00478	5	5.35	2.05
80	NDUA8_MOUSE	0.00565	1	0.00491	1	0.0302	5	5.35	6.15
81	SP130_MOUSE	0.000919	1	0.0024	2	0.00491	5	5.34	2.05
82	AAAS_MOUSE	0.00178	1	0.00464	2	0.00951	5	5.34	2.05
83	RAD18_MOUSE	0.00191	1	0.00332	2	0.0102	5	5.34	3.07
84	ECI1_MOUSE	0.00336	1	0.00292	1	0.0135	4	4.02	4.62
85	AP1S1_MOUSE	0.00615	1	0.0107	2	0.0247	4	4.02	2.31
86	THUM3_MOUSE	0.00192	1	0.00167	1	0.00771	4	4.02	4.62
87	PMM2_MOUSE	0.00401	1	0.00349	1	0.0161	4	4.01	4.61
88	ATPD_MOUSE	0.00578	1	0.00503	1	0.0232	4	4.01	4.61
89	PBDC1_MOUSE	0.00491	1	0.00854	2	0.0197	4	4.01	2.31
90	NDUB5_MOUSE	0.00514	1	0.00894	2	0.0206	4	4.01	2.3
91	RASN_MOUSE	0.00514	1	0.00894	2	0.0206	4	4.01	2.3
92	SNX12_MOUSE	0.00589	1	0.0102	2	0.0236	4	4.01	2.31
93	MSTO1_MOUSE	0.00175	1	0.00152	1	0.00701	4	4.01	4.61
94	NIPA_MOUSE	0.00194	1	0.00337	2	0.00777	4	4.01	2.31
95	TIM9_MOUSE	0.0109	1	0.0095	1	0.0292	2	2.68	3.07
96	TR112_MOUSE	0.00777	1	0.00676	1	0.0208	2	2.68	3.08
97	PHS_MOUSE	0.00934	1	0.00813	1	0.025	2	2.68	3.08
98	MARC2_MOUSE	0.00287	1	0.0025	1	0.00768	2	2.68	3.07
99	EPS15_MOUSE	0.00108	1	0.000942	1	0.00289	2	2.68	3.07
100	GMFB_MOUSE	0.00684	1	0.00595	1	0.0183	2	2.68	3.08
101	IST1_MOUSE	0.00268	1	0.00233	1	0.00717	2	2.68	3.08
102	DHRS4_MOUSE	0.00348	1	0.00303	1	0.00931	2	2.68	3.07
103	ABRAL_MOUSE	0.012	1	0.0104	1	0.0321	2	2.68	3.09
104	P53_MOUSE	0.00251	1	0.00218	1	0.00671	2	2.67	3.08
105	HEM3_MOUSE	0.00269	1	0.00234	1	0.00719	2	2.67	3.07

106	TI17B_MOUSE	0.00565	1	0.00491	1	0.0151	2	2.67	3.08
107	CUED2_MOUSE	0.00342	1	0.00298	1	0.00914	2	2.67	3.07
108	STRN3_MOUSE	0.00122	1	0.00106	1	0.00326	2	2.67	3.08
109	CNOT7_MOUSE	0.00341	1	0.00297	1	0.00911	2	2.67	3.07
110	RPAC2_MOUSE	0.0073	1	0.00635	1	0.0195	2	2.67	3.07
111	NRM_MOUSE	0.00371	1	0.00323	1	0.00991	2	2.67	3.07
112	CHP1_MOUSE	0.00498	1	0.00433	1	0.0133	2	2.67	3.07
113	ODPX_MOUSE	0.00194	1	0.00169	1	0.00518	2	2.67	3.07
114	ADRO_MOUSE	0.00197	1	0.00171	1	0.00526	2	2.67	3.08
115	S38A2_MOUSE	0.00193	1	0.00168	1	0.00515	2	2.67	3.07
116	TPPC3_MOUSE	0.0054	1	0.00469	1	0.0144	2	2.67	3.07
117	SELB_MOUSE	0.00167	1	0.00145	1	0.00445	2	2.66	3.07
118	ARL1_MOUSE	0.00537	1	0.00467	1	0.0143	2	2.66	3.06
119	CHM1A_MOUSE	0.00496	1	0.00431	1	0.0132	2	2.66	3.06
120	UBE2S_MOUSE	0.00436	1	0.00379	1	0.0116	2	2.66	3.06
121	ARHG1_MOUSE	0.00106	1	0.000919	1	0.00282	2	2.66	3.07